frontiers | Research Topics

Prenatal genetic screening, diagnosis and treatment

Edited by
Aleksandra Jezela-Stanek, Sheela Nampoothiri, Przemysław Kosinski and Ting Hu

Published in
Frontiers in Genetics
Frontiers in Pediatrics

ISSN 1664-8714
ISBN 978-2-8325-3309-3
DOI 10.3389/978-2-8325-3309-3

About Frontiers

Frontiers is more than just an open access publisher of scholarly articles: it is a pioneering approach to the world of academia, radically improving the way scholarly research is managed. The grand vision of Frontiers is a world where all people have an equal opportunity to seek, share and generate knowledge. Frontiers provides immediate and permanent online open access to all its publications, but this alone is not enough to realize our grand goals.

Frontiers journal series

The Frontiers journal series is a multi-tier and interdisciplinary set of open-access, online journals, promising a paradigm shift from the current review, selection and dissemination processes in academic publishing. All Frontiers journals are driven by researchers for researchers; therefore, they constitute a service to the scholarly community. At the same time, the *Frontiers journal series* operates on a revolutionary invention, the tiered publishing system, initially addressing specific communities of scholars, and gradually climbing up to broader public understanding, thus serving the interests of the lay society, too.

Dedication to quality

Each Frontiers article is a landmark of the highest quality, thanks to genuinely collaborative interactions between authors and review editors, who include some of the world's best academicians. Research must be certified by peers before entering a stream of knowledge that may eventually reach the public - and shape society; therefore, Frontiers only applies the most rigorous and unbiased reviews. Frontiers revolutionizes research publishing by freely delivering the most outstanding research, evaluated with no bias from both the academic and social point of view. By applying the most advanced information technologies, Frontiers is catapulting scholarly publishing into a new generation.

What are Frontiers Research Topics?

Frontiers Research Topics are very popular trademarks of the *Frontiers journals series*: they are collections of at least ten articles, all centered on a particular subject. With their unique mix of varied contributions from Original Research to Review Articles, Frontiers Research Topics unify the most influential researchers, the latest key findings and historical advances in a hot research area.

Find out more on how to host your own Frontiers Research Topic or contribute to one as an author by contacting the Frontiers editorial office: frontiersin.org/about/contact

Prenatal genetic screening, diagnosis and treatment

Topic editors

Aleksandra Jezela-Stanek — National Institute of Tuberculosis and Lung Diseases, Poland

Sheela Nampoothiri — Amrita Vishwa Vidyapeetham University, India

Przemysław Kosinski — Medical University of Warsaw, Poland

Ting Hu — Sichuan University, China

Citation

Jezela-Stanek, A., Nampoothiri, S., Kosinski, P., Hu, T., eds. (2023). *Prenatal genetic screening, diagnosis and treatment*. Lausanne: Frontiers Media SA.

doi: 10.3389/978-2-8325-3309-3

Table of contents

frontiers | Frontiers in Pediatrics

CASE REPORT
published: 19 July 2022
doi: 10.3389/fped.2022.937668

Case Report: Prenatal Diagnosis of Nemaline Myopathy

*Dongmei Liu[1,2,3], Jiali Yu[1,2,3], Xin Wang[4], Yang Yang[1,2,3], Li Yu[1,2,3], Shi Zeng[1,2,3], Ming Zhang[1,2,3] and Ganqiong Xu[1,2,3]**

[1] Department of Ultrasound Diagnostic, The Second Xiangya Hospital, Central South University, Changsha, China, [2] Research Center of Ultrasound Diagnostic, The Second Xiangya Hospital, Central South University, Changsha, China, [3] Clinical Research Center for Medical Imaging in Hunan Province, Changsha, China, [4] Department of Obstetrics and Gynecology Prenatal Diagnosis Center, The Second Xiangya Hospital, Central South University, Changsha, China

Nemaline myopathy (NM) is a rare, hereditary heterogeneous myopathy. Fetal NM has a more severe disease course and a poorer prognosis and is usually lethal during the first few months of life. Hence, early prenatal diagnosis is especially important for clinical interventions and patient counseling. We report the case of a fetus with NM due to *KLHL40* gene variation leading to arthrogryposis multiplex congenita (AMC). The ultrasonography and histopathology results revealed an enhanced echo intensity and decreased muscle thickness, which may be novel features providing early clues for the prenatal diagnosis of NM. Moreover, to our knowledge, this article is the first report to describe a case of NM associated with complex congenital heart disease (CHD).

Keywords: nemaline myopathy, arthrogryposis multiplex congenita, *KLHL40* gene, amyoplasia, prenatal diagnosis

OPEN ACCESS

Edited by:
Aleksandra Jezela-Stanek, National Institute of Tuberculosis and Lung Diseases, Poland

Reviewed by:
Martin Lammens, Antwerp University Hospital, Belgium
Ankur Singh, Banaras Hindu University, India

***Correspondence:**
Ganqiong Xu
xuganqiong@csu.edu.cn

Specialty section:
This article was submitted to Genetics of Common and Rare Diseases, a section of the journal Frontiers in Pediatrics

Received: *06 May 2022*
Accepted: *22 June 2022*
Published: *19 July 2022*

Citation:
Liu D, Yu J, Wang X, Yang Y, Yu L, Zeng S, Zhang M and Xu G (2022) Case Report: Prenatal Diagnosis of Nemaline Myopathy. Front. Pediatr. 10:937668. doi: 10.3389/fped.2022.937668

INTRODUCTION

Nemaline myopathy (NM) is a rare congenital disease of skeletal muscle causing severe muscle weakness and other neuromuscular dysfunction manifestations. Shy first described it in 1963 (1) and Kaspersky first reported it as a prenatal diagnosis in 2008 (2). The incidence of NM is approximately 1:50,000 (3). Based on the time of onset and severity of symptoms, it can be classified into six forms ranging from severe congenital/neonatal onset to adult onset (4). The severe congenital subgroup accounts for 15% of all NM cases (5). NM is generally considered a hereditary disease, but its inheritance is heterogeneous, either dominant or recessive, and many loci are involved. Thus, NM causes various diseases. Variations in at least 12 genes including *ACTA1*, *CFL2*, *KBTBD13*, *KLHL40*, *KLHL41*, *LMOD3*, *MYPN*, *NEB*, *TNNT1*, *TNNT3*, *TPM2*, and *TPM3*, have been identified to be associated with the condition (6). Variations in the *KLHL40* gene have been recently identified as a cause of severe autosomal-recessive NM. The diagnosis of NM is mainly based on genetic and pathological features. The characteristic pathological change is the deposition of a large number of nemaline bodies in muscle fibers. Prenatal ultrasound diagnosis of NM is difficult and thus rarely performed. This study aimed to describe novel ultrasound findings for the lethal form of NM. Enhanced echo intensity and decreased muscle thickness demonstrate that amyoplasia seems to be an element of the poor prognosis of these patients. Thus, when ultrasonographic features such as polyhydramnios, decreased fetal movements and club feet are

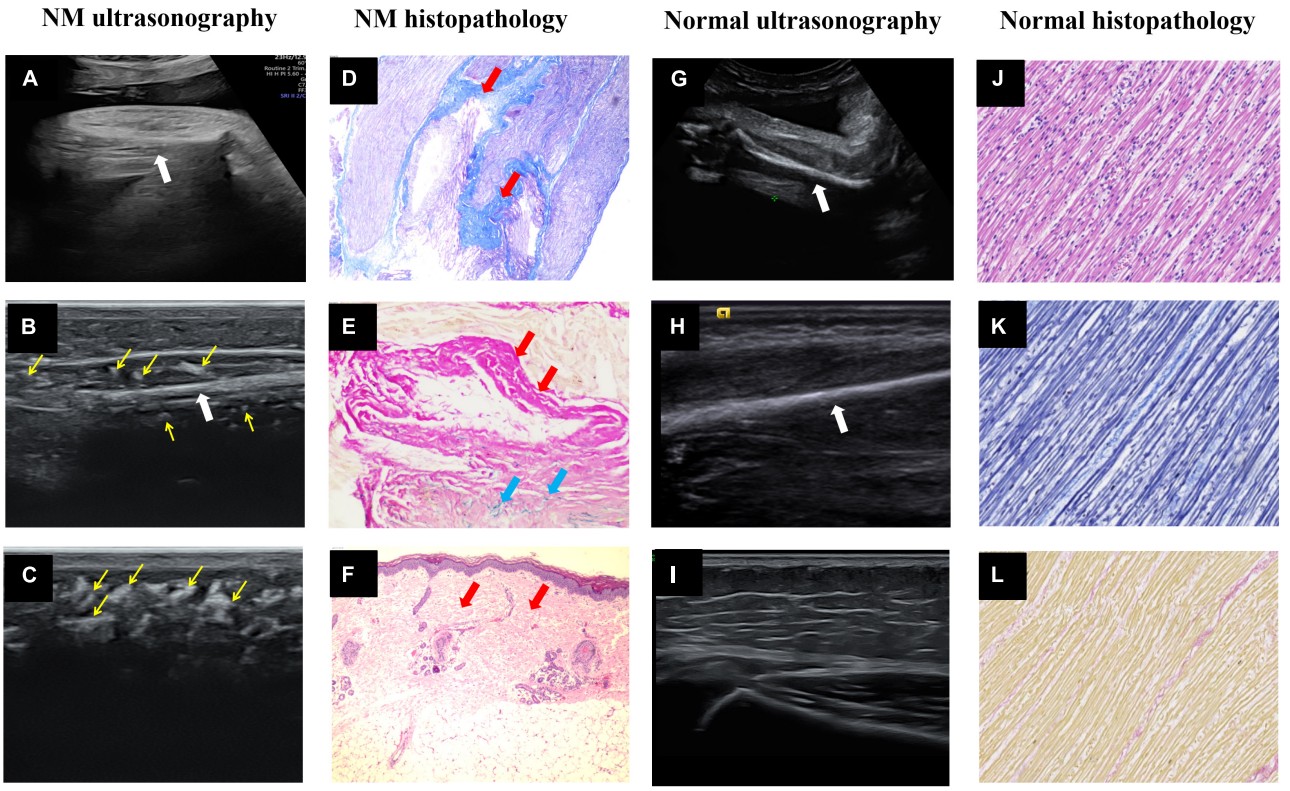

FIGURE 1 | Ultrasound images and histopathology of the prenatal and postnatal extremities. **(A)** Intrauterine ultrasound examination. **(B,C)** Postpartum high-frequency probe examination showed NM fetal upper limb muscle echo close to the humerus echo, and many hyperechoic regions (thin yellow arrows) in the muscle layer and subcutaneous tissue. **(D)** Right calf muscle Masson trichrome staining × 40 and **(E)** right calf muscle elastic fiber staining × 200. The muscle fiber fascicles were sparse and replaced by collagen fibers (thick red arrows) and elastic fibers (thick blue arrows). **(F)** Right calf skin H&E × 40 showed fibrous tissue (thick red arrows) proliferated in the dermis layer and subcutaneous tissue. **(G–I)** The normal fetal upper limb muscle echo was significantly lower than the humerus echo, and the subcutaneous tissue had low echo intensity with several echogenic septa of connective tissue. The thick white arrows point to the long bones of the fetal limbs. **(J–L)** The normal fetal right calf muscle H&E × 40, Masson trichrome staining × 40 and elastic fiber staining ×40.

noted during pregnancy, the echo and thickness of the muscle should be observed carefully to determine the potential existence of congenital neuromuscular disorders such as NM.

CASE REPORT

A 36-year-old Chinese woman, gravida 1, para 0, was referred to our hospital at 36 weeks of gestation because of multiple cardiac anomalies (right ventricular double outlet and aortic coarctation) and bilateral foot inversion observed in the fetus. At 18 weeks gestation, amniocentesis showed that the fetus was at high risk for trisomy 18 and trisomy 21. The chromosomal microarray of amniocytes was normal. No exposure to teratogenic substances or family history of congenital malformation was noted. The pregnancy was uncomplicated.

The first ultrasound examination conducted in our department showed polyhydramnios, and the fetus was in breech presentation with no obvious limb movements, bilateral clubfoot, or tilted fingers. The cardiac malformation was the same as before. Interestingly, we found that echoes of the skeletal muscles were significantly enhanced (close to or slightly weaker than the bone echo) and had posterior echo attenuation (**Figures 1A,B**). Serial scans were performed the following week, which confirmed limb stiffness (**Figures 2B,C**). In addition, it was found by comparison that limb muscles of this fetus were thinner than those in the control. Ultrasonographic findings led to the suspicion of AMC associated with amyoplasia, complex congenital heart disease (CHD) (**Figures 2E,F**), and polyhydramnios.

Whole-exome sequencing (WES) was then performed on fetal umbilical cord blood and revealed a homozygous variation in the *KLHL40* gene, NM_152393.2:c.1516A > C (p. Thr506Pro). Sanger sequencing verified that the patient was homozygous variation for c.1516A > C (p. Thr506Pro) (**Supplementary Figure 1**). According to ACMG guidelines, the variant was classified as pathogenic (PM1 + PM2 + PM3 + PP1 + PP4).

The pregnancy was selectively terminated after the patient received counseling. Postmortem radiological examination, necropsy (**Figures 2A,D**), and pathology confirmed all sonographic findings and revealed other malformations. X-rays showed pathological fractures. The autopsy revealed that the skin had increased hardness and decreased elasticity. The subcutaneous fat layer was significantly thickened, and

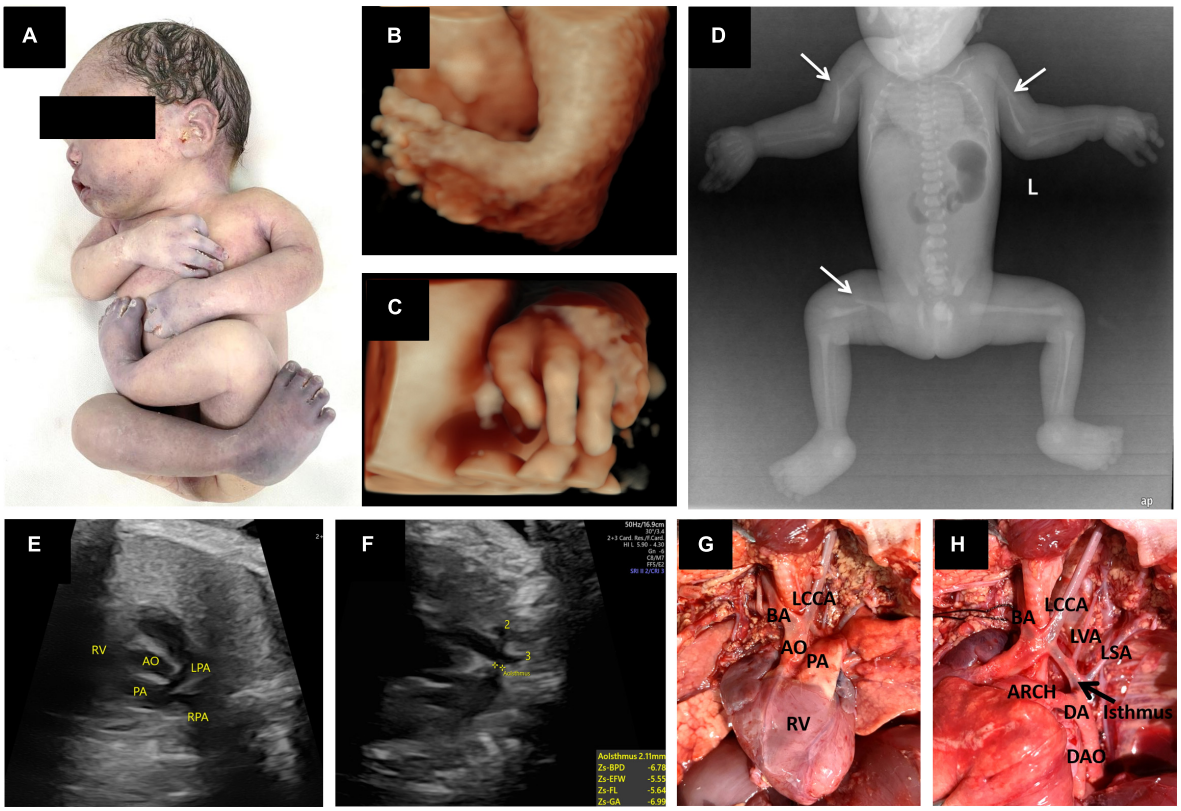

FIGURE 2 | Prenatal 3D ultrasound images and fetal echocardiography, postpartum gross anatomical specimens, X-ray photographs and cardiac anatomy. **(A)** Postmortem photo demonstrated multiple contractures of the upper and lower extremities. **(B,C)** Three-dimensional ultrasound showed fetal foot inversion and tilted fingers. **(D)** X-rays showed bilateral humerus and right femur fractures (thin white arrow). **(E,F)** Prenatal echocardiography showed a right ventricular double outlet with coarctation of the aortic arch. **(G,H)** Postpartum cardiac anatomy confirmed sonographic findings. In addition, there were four arteries of the aortic arch, from right to left: BA, the brachiocephalic artery; LCCA, the left common carotid artery; LVA, the left vertebral artery; and LSA, the left subclavian artery. RV, right ventricle; AO, aorta; PA, pulmonary artery; LPA, left pulmonary artery; RPA, right pulmonary artery; DA, ductus arteriosus; DAO, descending aorta; ARCH, aortic arch.

the muscle layer was significantly thinner (**Figures 3A,B**). In addition, there were four arteries in the aortic arch (**Figures 2G,H**).

Histopathological examination showed the following: (1) The muscle fibers were sparse, degenerated, and atrophied and were replaced by fatty-fibers (**Figures 3C–F**). (2) The dermis layer and subcutaneous tissue were thickened with fibrous tissue proliferation (**Figure 1F**); and (3) Nemaline bodies were positively stained with the anti-α-actinin antibody (**Figures 3E,F**). Unfortunately, we failed to perform electron microscopy. Altogether, the results of these examinations indicated a diagnosis of nemaline myopathy due to *KLHL40* gene variation leading to fetal AMC associated with CHD.

DISCUSSION

AMC is a heterogeneous disease characterized by multiple congenital joint contractures. This is the result of reduced fetal movement during development. AMC has been shown to be associated with more than 400 diseases and 350 known genes. AMC has been reported in association with neuromuscular disorders. NM is one of the congenital myopathies that leads to AMC (7). Fetal NM is a severe form of NM that carries a poor prognosis. Fetal NM due to variated *KLHL40* is one of the most severe subgroups characterized by fetal akinesia (8), contractures, severe muscle weakness, respiratory failure, dysphagia, and early perinatal death (average age of death is 5 months) (9, 10). Currently, there is no available cure for fetal NM, and it has an extremely poor prognosis. Thus, early prenatal diagnosis is especially important. Several studies have suggested that prenatal identification of NM is challenging and can only be achieved by WES or fetal muscle biopsy. However, less than half of the muscle histology results of suspected NM cases present with nemaline bodies (5, 11), and WES cannot be performed for all fetuses. Therefore, prenatal ultrasound is one of the best indicators of the need to perform further WES analyses of affected fetuses.

To date, 34 prenatally diagnosed cases of NM have been reported in the literature (**Table 1**). Decreased fetal movement (74%), polyhydramnios (65%), and arthrogryposis (47%) were common prenatal features on sonography. Other less frequent findings included fetal edema (32%), clubfoot (26%), facial abnormalities (15%), lung hypoplasia (6%), and

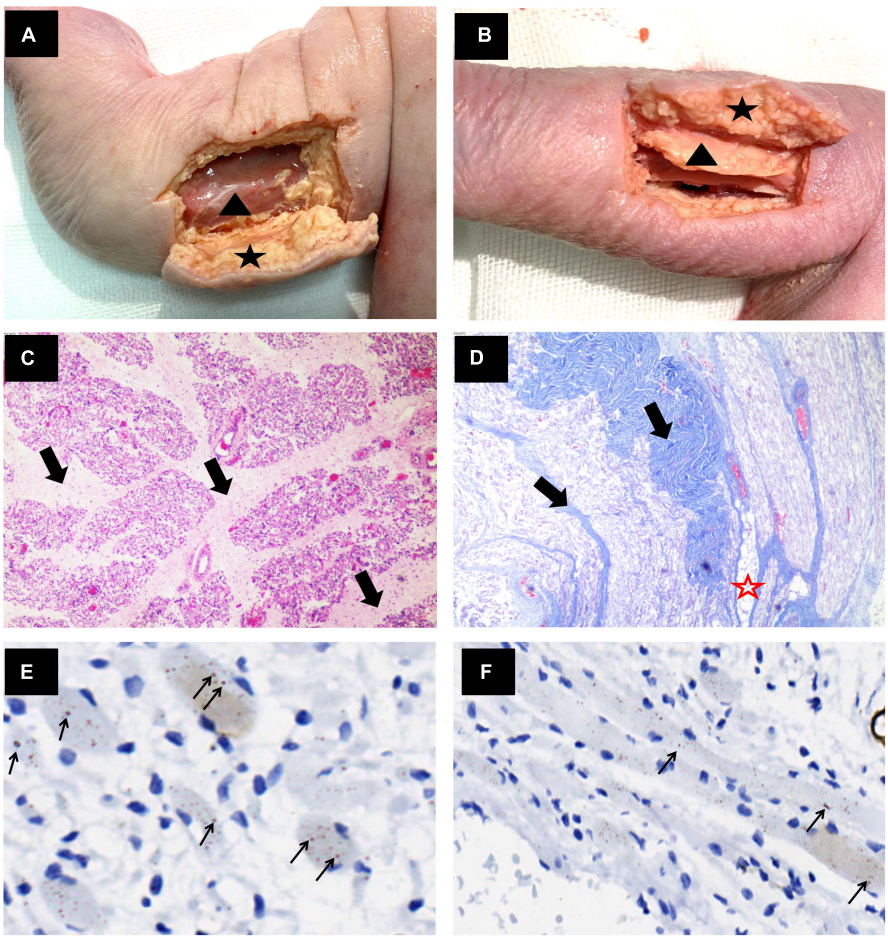

FIGURE 3 | Anatomical and pathological images of the limb muscles. **(A,B)** Gross anatomy showed thickened subcutaneous fat (black star) and a thin muscle layer (black triangle) in the lower limbs of the fetus. **(C)** Right thigh muscle cross section H&E × 40 and **(D)** Right forearm muscle longitudinal section Masson trichrome × 40. The muscle bundles showed marked variation in size, and muscle fibers were replaced by fibrous tissue (thick black arrows) and adipose tissue (red star). **(E,F)** Right calf muscle cross section and longitudinal section anti-α-actinin antibody stained × 400. The muscle fibers were sparse, degenerated, and atrophied. Lots of nemaline rods in muscle fibers were strongly stained with anti-α-actinin antibody (thin black arrow).

fractures (3%). Notably, our study is the first to describe the features of enhanced echo intensity and decreased thickness of skeletal muscle. In normal fetuses, muscle boundaries are clearly visible and the skeletal muscle echo is lower than or close to the liver echo. However, this fetus appeared to have unclear muscle boundaries. The muscle layer appeared thinned and had an enhanced echo (stronger than the liver echo and slightly weaker than or even approaching the bone echo, **Figures 1A,G**). Then, we used a high-frequency probe to compare the skin and muscle of this fetus to that of a normal infant (**Figures 1B,C,H,I**). Strikingly, the fetus demonstrated replacement of myofibers with connective tissue on ultrasonography (many hyperechoic regions in the muscles) and histopathology (**Figures 1D,E**). These were in stark contrast to the muscles of normal fetus (**Figures 1J–L**). Moreover, fibrous tissue proliferated in the dermis layer and subcutaneous tissue (**Figure 1F**), which exhibited several hyperechoic regions, replacing the several echogenic septa observed on ultrasonography (**Figures 1C,I**). Increased interstitial connective tissue is indicative of myopathy (12). In this case, the echo intensity increased because the muscular architecture was disrupted by muscle cell replacement with connective and fat tissue. These antenatal signs demonstrated that amyoplasia seemed to contribute to the poor prognosis. We recommend that decreased fetal movements combined with polyhydramnios should be used to observe the fetal joint activity and the echo and thickness of the skeletal muscle. Improving awareness and identification of abnormal ultrasound manifestations early alerts clinicians of the potential existence of neuromuscular disorders such as NM.

NM needs to be differentiated from other neuromuscular disease, such as congenital muscular dystrophy (13). It can also show decreased fetal movement, polyhydramnios, arthrogryposis on prenatal ultrasound. To the best of our knowledge, whether the enhanced echo intensity and decreased thickness of skeletal muscle also appear has not been reported in the literature. In the

TABLE 1 | Summary of prenatal ultrasound characteristics of nemaline myopathy.

Case	References	Gender	GA (weeks)	DFM	Poly	Arth	Fetal edema	Clubfoot	FA	LH	Fractures	MEE	MTT	Follow up
1	Vuopala et al. (13)	Male	INA	NS	NS	+	+	NS	NS	+	NS	NA	NA	Death (4 h)
2a	Vendittelli et al. (18)	Male	33	+	+	NS	NS	NS	NS	NS	NS	NA	NA	Death (6 days)
2b		Female	INA	+	+	–	–	–	–	–	–	NA	NA	Death (68 days)
3a	Lammens et al. (19)	Male	16	+	NS	+	NS	NS	NS	NS	NS	NA	NA	NS
3b		2 m 3F	INA	NS	NS	+	+	NS	+	NS	NS	NA	NA	NS
3c		Male	28	+	NS	+	+	NS	+	+	NS	NA	NA	Death (24 h)
4	Vardon et al. (7)	Male	32	+	+	+	+	+	NS	NS	NS	NA	NA	Death (5 h)
5a	Wallgren-Pettersson et al. (20)	Male	28	NS	+	NS	NS	NS	NS	NS	NS	NA	NA	Death (5 min)
5b		Female	30	NS	+	NS	NS	NS	NS	NS	NS	NA	NA	Death (19 months)
5c		Female	INA	+	NS	NS	NS	NS	NS	NS	NS	NA	NA	Death (5 months)
5d		Male	31	+	+	NS	NS	NS	NS	NS	NS	NA	NA	Death (30 min)
6	Kuwata et al. (21)	Female	36	+	+	+	NS	NS	NS	NS	NS	NA	NA	NS
7a	Lawlor et al. (22)	Male	31	+	+	NS	NS	NS	NS	NS	NS	NA	NA	Death (28 days)
7b		Male	INA	+	NS	+	NS	NS	NS	NS	NS	NA	NA	Death (1 day)
8a	Yonath et al. (23)	Female	36	+	+	NS	NS	NS	NS	NS	NS	NA	NA	TOP
8b		Female	23	+	+	NS	NS	+	NS	NS	NS	NA	NA	NA
8c		Unknown	30	+	+	+	NS	NS	NS	NS	NS	NA	NA	Death (5 min)
8d		Female	20	+	+	NS	NS	+	NS	NS	NS	NA	NA	Death (2 days)
9a	Ahmed et al. (24)	Female	19	NS	NS	+	+	+	+	NS	NS	NA	NA	TOP
9b		Male	20	+	NS	+	+	NS	NS	NS	NS	NA	NA	Intrauterine Fetal demise at 27 weeks

(Continued)

TABLE 1 | (Continued)

Case	References	Gender	GA (weeks)	DFM	Poly	Arth	Fetal edema	Clubfoot	FA	LH	Fractures	MEE	MTT	Follow up
9c		Male	21	NS	+	+	NS	+	NS	NS	NS	NA	NA	Death (8 min)
9d		Female	20	+	+	+	+	NS	NS	NS	NS	NA	NA	Intrauterine Fetal demise at 27 weeks
10	Berkenstadt et al. (12)	Female	26	+	+	+	NS	+	NS	NS	NS	NA	NA	TOP
11	Abbott et al. (25)	Female	31	NS	+	NS	+	NS	NS	NS	NS	NA	NA	Death (9 days)
12	Wang et al. (26)	Male	29	NS	+	NS	+	NS	NS	NS	NS	NA	NA	Death (2 days)
13	Avasthi et al. (10)	Unknown	INA	+	+	NS	+	NS	+	NS	NS	NA	NA	NS
14a	Yeung et al. (27)	Female	36	NS	+	NS	NS	NS	NS	NS	NS	NA	NA	Death (7 months)
14b		Male	32	+	+	NS	NS	NS	NS	NS	NS	NA	NA	Death (16 months)
14c		Female	INA	+	NS	NS	NS	+	NS	NS	NS	NA	NA	Death (49 days)
14d		Female	20	+	NS	+	NS	+	NS	NS	NS	NA	NA	TOP
15	Rocha et al. (28)	Male	13	+	NS	+	+	NS	+	NS	NS	NA	NA	TOP
16a	Zhang et al. (29)	Female	16	+	NS	+	NS	NS	NS	NS	NS	NA	NA	TOP
16b		Male	12	+	+	–	–	–	–	–	–	NA	NA	Death (3 months)
This study		Male	36	+	+	+	–	+	–	–	+	+	+	TOP
Total				25/34 (74%)	22/34 (65%)	16/34 (47%)	11/34 (32%)	9/34 (26%)	5/34 (15%)	2/34 (6%)	1/34 (3%)	1/34 (3%)	1/34 (3%)	

GA, Gestational age; DFM, Decreased fetal movement; Poly, Polyhydramnios; Arth, Arthrogryposis; FA, Facial abnormalities; LH, Lung hypoplasia; MEE, Muscle echo enhancement; MTT, Muscle thickness thinning; TOP, Termination of pregnancy; INA, Information not applicable; NS, Not specified; NA, Not assessed.

future, we will investigate whether other congenital myopathies also demonstrate this abnormal ultrasound performance. Congenital muscular dystrophy is associated with muscle enzymes significantly increased over 10 times, and some have white matter lesions (14). In addition, polymyositis, dermatomyositis, and mitochondrial encephalopathy also need to be distinguished from NM. Polymyositis is rare in the neonatal period. Dermatomyositis often has obvious skin lesions (15). Mitochondrial encephalomyopathy is a multisystem disease mainly involving the brain and muscle (16). Diagnosis can be further confirmed by histopathology. Congenital muscular dystrophy also show histological loss of muscle fibers and the replacement of muscle tissue by connective and adipose tissue (13). However, typical nemaline rods are characteristic of NM. Staining with Gomori trichrome or electron microscopy can substantiate the nemaline rods (17). Ultimately, WES provides a precise genetic diagnosis.

One limitation of our study was that electron microscopy was not performed because fresh specimens were not available. Another limitation is the small number of cases. We will evaluate more NM cases in the future to study the correlation between ultrasonography features and unfavorable outcomes.

CONCLUSION

The large size and complexity of the genome necessitates a costly and lengthy determination of presence of neuromuscular disorders. Therefore, early abnormal ultrasound findings (decreased fetal movements, polyhydramnios, enhanced echo intensity, and decreased muscle thickness) may prompt clinicians to suspect congenital neuromuscular disease. It may provide early clue of targeted genes to facilitate a prenatal diagnosis of NM, followed by WES and biopsy to confirm the diagnosis. This is important to offer parents informed choices regarding the subsequent course of the pregnancy and to alert physicians to plan appropriate investigations. Furthermore, NM can be associated with CHD. To the best of our knowledge, this is the first report of NM associated with complex CHD.

DATA AVAILABILITY STATEMENT

The original contributions presented in this study are included in the article/**Supplementary Material**, further inquiries can be directed to the corresponding author.

ETHICS STATEMENT

The studies involving human participants were reviewed and approved by Medical Ethics Committee, the Second Xiangya Hospital, Central South University. The patients/participants provided their written informed consent to participate in this study.

AUTHOR CONTRIBUTIONS

DL and GX contributed to conception and design of the study. DL completed the data collection and wrote the first draft of the manuscript. DL, JY, XW, YY, LY, SZ, and MZ wrote sections of the manuscript. All authors contributed to manuscript revision and read and approved the submitted version.

FUNDING

This study was supported by the National Natural Science Foundation of China (No. 81801721) and the Natural Science Foundation of Hunan Province (No. 2019JJ50880).

SUPPLEMENTARY MATERIAL

The Supplementary Material for this article can be found online at: https://www.frontiersin.org/articles/10.3389/fped.2022.937668/full#supplementary-material

Supplementary Figure 1 | Variant identification by Sanger sequencing. The red arrow represented the variant site (c.1516A > C).

REFERENCES

1. Shy GM, Engel WK, Somers JE, Wanko T. Nemaline myopathy. A new congenital myopathy. Brain. (1963) 86:793–810.
2. Kasperski SB, Brennan AM, Corteville JE, Finkel RS, Golden J, Johnson MP, et al. Utility of fetal muscle biopsy for diagnosis of nemaline myopathy. *Fetal Diagn Ther.* (2008) 24:400–4. doi: 10.1159/000170095
3. North KN, Laing NG, Wallgren-Pettersson C. Nemaline myopathy: current concepts. The ENMC International consortium and nemaline myopathy. *J Med Genet.* (1997) 34:705–13. doi: 10.1136/jmg.34.9.705
4. Lehtokari V-L, Kiiski K, Sandaradura SA, Laporte J, Repo P, Frey JA, et al. Mutation update: the spectra of nebulin variants and associated myopathies. *Hum Mutat.* (2014) 35:1418–26. doi: 10.1002/humu.22693
5. Feingold-Zadok M, Chitayat D, Chong K, Injeyan M, Shannon P, Chapmann D, et al. Mutations in the NEB gene cause fetal akinesia/arthrogryposis multiplex congenita. *Prenat Diagn.* (2017) 37:144–50. doi: 10.1002/pd.4977
6. Sewry CA, Laitila JM, Wallgren-Pettersson C. Nemaline myopathies: a current view. *J Muscle Res Cell Motil.* (2019) 40:111–26. doi: 10.1007/s10974-019-09519-9
7. Vardon D, Chau C, Sigodi S, Figarella-Branger D, Boubli L. Congenital rapidly fatal form of nemaline myopathy with fetal hydrops and arthrogryposis. A case report and review. *Fetal Diagn Ther.* (1998) 13:244–9. doi: 10.1159/000020847
8. Chen T-H, Tian X, Kuo P-L, Pan H-P, Wong L-JC, Jong Y-J. Identification of KLHL40 mutations by targeted next-generation sequencing facilitated a prenatal diagnosis in a family with three consecutive affected fetuses with fetal akinesia deformation sequence. *Prenat Diagn.* (2016) 36:1135–8. doi: 10.1002/pd.4949
9. Yi S, Zhang Y, Qin Z, Yi S, Zheng H, Luo J, et al. A novel and recurrent KLHL40 pathogenic variants in a Chinese family of multiple affected neonates with nemaline myopathy 8. *Mol Genet Genomic Med.* (2021) 9:e1683. doi: 10.1002/mgg3.1683
10. Avasthi KK, Agarwal S, Panigrahi I. Mutation associated with severe nemaline myopathy, fetal akinesia, and cleft palate. *J Pediatr Neurosci.* (2019) 14:222–4. doi: 10.4103/jpn.JPN_60_19
11. Malfatti E, Lehtokari VL, Bohm J, De Winter JM, Schaffer U, Estournet B, et al. Muscle histopathology in nebulin-related nemaline myopathy: ultrastrastructural findings correlated to disease severity and genotype. *Acta Neuropathol Commun.* (2014) 2:44. doi: 10.1186/2051-5960-2-44

12. Berkenstadt M, Pode-Shakked B, Barel O, Barash H, Achiron R, Gilboa Y, et al. LMOD3-associated nemaline myopathy: prenatal ultrasonographic, pathologic, and molecular findings. *J Ultrasound Med.* (2018) 37:1827–33. doi: 10.1002/jum.14520
13. Vuopala K, Leisti J, Herva R. Lethal arthrogryposis in Finland–a clinico-pathological study of 83 cases during thirteen years. *Neuropediatrics.* (1994) 25:308–15. doi: 10.1055/s-2008-1073045
14. Mary P, Servais L, Vialle R. Neuromuscular diseases: diagnosis and management. *Orthop Traumatol Surg Res.* (2018) 104:S89–95. doi: 10.1016/j.otsr.2017.04.019
15. Findlay AR, Goyal NA, Mozaffar T. An overview of polymyositis and dermatomyositis. *Muscle Nerve.* (2015) 51:638–56. doi: 10.1002/mus.24566
16. Scarpelli M, Todeschini A, Volonghi I, Padovani A, Filosto M. Mitochondrial diseases: advances and issues. *Appl Clin Genet.* (2017) 10:21–6. doi: 10.2147/TACG.S94267
17. Zhao B, Dai T, Zhao D, Ma X, Zhao C, Li L, et al. Clinicopathologic profiles of sporadic late-onset nemaline myopathy: practical importance of anti-α-actinin immunostaining. *Neurol Neuroimmunol Neuroinflamm.* (2022) 9:e1184. doi: 10.1212/NXI.0000000000001184
18. Vendittelli F, Manciet-Labarchède C, Gilbert-Dussardier B. Nemaline myopathy in the neonate: two case reports. *Eur J Pediatr.* (1996) 155:502–5.
19. Lammens M, Moerman P, Fryns JP, Lemmens F, van de Kamp GM, Goemans N, et al. Fetal akinesia sequence caused by nemaline myopathy. *Neuropediatrics.* (1997) 28:116–9. doi: 10.1055/s-2007-973683
20. Wallgren-Pettersson C, Donner K, Sewry C, Bijlsma E, Lammens M, Bushby K, et al. Mutations in the nebulin gene can cause severe congenital nemaline myopathy. *Neuromuscul Disord.* (2002) 12:674–9.
21. Kuwata T, Matsubara S, Ohkusa T, Yada Y, Suzuki M. Decreased fetal movement prompts investigation of prenatal/neonatal nemaline myopathy: the possible merit of fetal movement count. *J Obstet Gynaecol Res.* (2011) 37:921–5. doi: 10.1111/j.1447-0756.2010.01438.x
22. Lawlor MW, Ottenheijm CA, Lehtokari V-L, Cho K, Pelin K, Wallgren-Pettersson C, et al. Novel mutations in NEB cause abnormal nebulin expression and markedly impaired muscle force generation in severe nemaline myopathy. *Skelet Muscle.* (2011) 1:23. doi: 10.1186/2044-5040-1-23
23. Yonath H, Reznik-Wolf H, Berkenstadt M, Eisenberg-Barzilai S, Lehtokari V-L, Wallgren-Pettersson C, et al. Carrier state for the nebulin exon 55 deletion and abnormal prenatal ultrasound findings as potential signs of nemaline myopathy. *Prenat Diagn.* (2012) 32:70–4. doi: 10.1002/pd.2905
24. Ahmed AA, Skaria P, Safina NP, Thiffault I, Kats A, Taboada E, et al. Arthrogryposis and pterygia as lethal end manifestations of genetically defined congenital myopathies. *Am J Med Genet A.* (2018) 176:359–67. doi: 10.1002/ajmg.a.38577
25. Abbott M, Jain M, Pferdehirt R, Chen Y, Tran A, Duz MB, et al. Neonatal fractures as a presenting feature of LMOD3-associated congenital myopathy. *Am J Med Genet A.* (2017) 173:2789–94. doi: 10.1002/ajmg.a.38383
26. Wang Y, Zhu C, Du L, Li Q, Lin M-F, Férec C, et al. Compound heterozygosity for novel truncating variants in the gene as the cause of polyhydramnios in two successive fetuses. *Front Genet.* (2019) 10:835. doi: 10.3389/fgene.2019.00835
27. Yeung KS, Yu FNY, Fung CW, Wong S, Lee HHC, Fung STH, et al. The KLHL40 c.1516A>C is a Chinese-specific founder mutation causing nemaline myopathy 8: report of six patients with pre- and postnatal phenotypes. *Mol Genet Genomic Med.* (2020) 8:e1229. doi: 10.1002/mgg3.1229
28. Rocha ML, Dittmayer C, Uruha A, Korinth D, Chaoui R, Schlembach D, et al. A novel mutation in NEB causing foetal nemaline myopathy with arthrogryposis during early gestation. *Neuromuscul Disord.* (2021) 31:239–45. doi: 10.1016/j.nmd.2020.11.014
29. Zhang Y-L, Zhen L, Xu L-L, Li D-Z. Fetal akinesia: the need for clinical vigilance in first trimester with decreased fetal movements. *Taiwan J Obstet Gynecol.* (2021) 60:559–62. doi: 10.1016/j.tjog.2021.03.032

Conflict of Interest: The authors declare that the research was conducted in the absence of any commercial or financial relationships that could be construed as a potential conflict of interest.

Publisher's Note: All claims expressed in this article are solely those of the authors and do not necessarily represent those of their affiliated organizations, or those of the publisher, the editors and the reviewers. Any product that may be evaluated in this article, or claim that may be made by its manufacturer, is not guaranteed or endorsed by the publisher.

frontiers | Frontiers in Genetics

TYPE Mini Review
PUBLISHED 26 July 2022
DOI 10.3389/fgene.2022.938183

OPEN ACCESS

EDITED BY
Habiba Alsafar,
Khalifa University, United Arab Emirates

REVIEWED BY
Hoh Boon-Peng,
UCSI University, Malaysia

*CORRESPONDENCE
Ting Hu,
huting4123@163.com

SPECIALTY SECTION
This article was submitted to Genetics of Common and Rare Diseases, a section of the journal Frontiers in Genetics

RECEIVED 07 May 2022
ACCEPTED 11 July 2022
PUBLISHED 26 July 2022

CITATION
Liu X, Liu S, Wang H and Hu T (2022), Potentials and challenges of chromosomal microarray analysis in prenatal diagnosis.
Front. Genet. 13:938183.
doi: 10.3389/fgene.2022.938183

Potentials and challenges of chromosomal microarray analysis in prenatal diagnosis

Xijing Liu[1,2,3], Shanling Liu[1,2,3], He Wang[1,2,3] and Ting Hu[1,2,3]*

[1]Department of Medical Genetics, West China Second University Hospital, Sichuan University, Chengdu, China, [2]Department of Obstetrics and Gynecology, West China Second University Hospital, Sichuan University, Chengdu, China, [3]Key Laboratory of Birth Defects and Related Diseases of Women and Children (Sichuan University), Ministry of Education, Chengdu, China

Introduction: For decades, conventional karyotyping analysis has been the gold standard for detecting chromosomal abnormalities during prenatal diagnosis. With the development of molecular cytogenetic methods, this situation has dramatically changed. Chromosomal microarray analysis (CMA), a method of genome-wide detection with high resolution, has been recommended as a first-tier test for prenatal diagnosis, especially for fetuses with structural abnormalities.

Methods: Based on the primary literature, this review provides an updated summary of the application of CMA for prenatal diagnosis. In addition, this review addresses the challenges that CMA faces with the emergence of genome sequencing techniques, such as copy number variation sequencing, genome-wide cell-free DNA testing, and whole exome sequencing.

Conclusion: The CMA platform is still suggested as priority testing methodology in the prenatal setting currently. However, pregnant women may benefit from genome sequencing, which enables the simultaneous detection of copy number variations, regions of homozygosity and single-nucleotide variations, in near future.

KEYWORDS

chromosomal abnormalities, conventional karyotyping analysis, chromosomal microarray analysis, copy number variants, genome sequencing, prenatal diagnosis

Introduction

During the past decade, chromosomal microarray analysis (CMA) has been gaining popularity in prenatal diagnosis, especially in the detection of chromosomal abnormalities. Chromosomal abnormalities are responsible for more than 300 types of human syndromes, spanning a wide range of genomic imbalances from polyploidies and aneuploidies (abnormalities in chromosome number) to submicroscopic deletions and duplications (losses or gains of a small portion of chromosomes, known as copy number variants [CNVs]) (Peters et al., 2015). Chromosomal abnormalities occur in approximately 1 in 150 live births and appear in approximately 25% of all

miscarriages and stillbirths and in 50–60% of first-trimester miscarriages (Nussbaum et al., 2016).

Generally, the incidence of fetal aneuploidies increases with maternal age (Rose et al., 2020). In contrast, CNVs, which can also lead to unfavorable fetal prognosis, are independent of maternal age and occur in approximately 0.4% of pregnancies (Carvalho et al., 2010). Caused by chromosomal rearrangements resulting in the loss or gain of the dosage-sensitive gene(s)/region(s), CNVs can be categorized into recurrent and non-recurrent aberrations. Recurrent rearrangements, commonly interstitial deletions and duplications, are mediated by nonallelic homologous recombination between flanking sequences with DNA sequence homology (Carvalho et al., 2010). These chromosomal rearrangements, mediated by genomic architecture, generate hotspots for recurrent deletions or duplications that contain unique regions of genomic imbalance, shared among individuals (Carvalho et al., 2010). In contrast, non-recurrent aberrations have varied sizes and breakpoints for each individual and are generated by various molecular mechanisms (Rose et al., 2020). CNVs can directly influence phenotypes and cause diseases by altering gene dosage and/or disrupting gene (Redon et al., 2006). Moreover, CNVs can affect gene expression indirectly through position effects: by changing the regulatory landscape and thus altering crosstalk between alleles or by disclosing recessive mutations (Mikhail, 2014). According to the American College of Medical Genetics and Genomics (ACMG) and Clinical Genome Resource (ClinGen) five-tiered system, CNVs can be divided into the following categories: pathogenic (P), likely pathogenic (LP), variants of uncertain significance (VUS), likely benign (LB), or benign (B) (Riggs et al., 2020).

Trends in chromosomal testing techniques

Conventional karyotyping has historically been the gold standard for detecting genome-wide chromosomal abnormalities during the prenatal period (Steele and Breg, 1966; Vermeesch et al., 2007). Karyotyping can detect numerical chromosomal abnormalities (polyploidies or aneuploidies), relatively large structural abnormalities microscopically visible to a resolution of approximately 5–10 Mb, balanced or unbalanced translocations, and inversions (Vermeesch et al., 2007). Nevertheless, it has several inherent limitations, such as a relatively long turnaround time owing to the cell culture, the requirement of skilled technicians to perform the analysis, and the inability to detect submicroscopic chromosomal aberrations (Steele and Breg, 1966; Vermeesch et al., 2007).

In addition to karyotyping, various molecular cytogenetic methods have been developed to understand genome architecture in recent decades. For example, fluorescence *in situ* hybridization (FISH) bridges the gap between cytogenetic and molecular approaches. FISH can detect clinically significant chromosomal aberrations in cells during metaphase or interphase (Speicher and Carter, 2005). The major advantage of FISH is the rapid turnaround for the visualization of the physical location of target probe in individual cells (Speicher and Carter, 2005). However, the disadvantage of FISH-based tests is that they cannot balance the detection range and resolution. Chromosome paint-based FISH techniques, for instance, allow the rapid assessment of large chromosomal alterations in the entire genome, but the resolution of the method is limited. DNA probe-based FISH tests are targeted and can only screen individual DNA targets rather than the entire genome (Speicher and Carter, 2005).

With the introduction of CMA, genome-wide detection of CNVs has become possible. CMA can not only identify most chromosomal imbalances detected by conventional cytogenetic analysis but also CNVs with high resolution (Dugoff et al., 2016). Two major microarray platforms are employed in prenatal settings: array comparative genomic hybridization (aCGH) and single-nucleotide polymorphism (SNP) arrays (Schwartz, 2011; Dugoff et al., 2016). In aCGH, chromosomes are represented by large numbers of mapped probes spotted onto standard glass slides (Carvalho et al., 2010). These microarray probes span the whole genome, with particularly dense coverage of clinically relevant genes and regions (Dugoff et al., 2016). Following the hybridization of the fetal DNA sample and normal reference genomic DNA to the target sequences on the microarray, the slide is scanned to measure the fluorescence intensities at each target on the array (Dugoff et al., 2016). The relative intensities of the different fluorescence signals are compared using bioinformatic tools. Cases with duplications had a higher hybridization signal, whereas those with deletions had a lower hybridization signal than the reference sample (Carvalho et al., 2010). In SNP arrays, CNVs are measured using probe signal intensities, as used in the aCGH approach (Schwartz, 2011). SNP probes offer additional advantages. For instance, SNP probes allow for the detection of copy number neutral chromosome abnormalities, such as long stretches of homozygosity that occur owing to uniparental disomy (UPD), consanguinity and maternal cell contamination (MCC) (Schwartz, 2011).

Microarray application in prenatal diagnosis

CMA is recommended as the first-tier test in the postnatal evaluation of individuals with intellectual disability, developmental delay, autism spectrum disorder, and/or multiple congenital anomalies (Miller et al., 2010). In the prenatal setting, with multiple advantages over conventional karyotyping, CMA is the first-tier recommendation for a

prenatal evaluation of fetuses with structural anomalies (American College of Obstetricians and Gynecologists Committee on Genetics, 2013; Dugoff et al., 2016). CMA reliably detects CNVs as small as 50–100 kb in size, which provides better resolution than cytogenetic analysis (Peters et al., 2015). In addition, CMA can be performed on direct fetal samples (uncultured cells), including those obtained from chorionic villus sampling, amniocentesis, or fetal blood sampling, which may lead to a shorter turnaround time (usually within 3–5 days) than karyotyping.

Diagnostic yield of CMA

Several large-scale studies have compared the diagnostic yield of karyotyping with that of genome-wide CMA for prenatal diagnosis and have shown that a significant proportion of clinically relevant chromosomal aberrations are missed by karyotyping alone (Wapner et al., 2012; Hay et al., 2018; Srebniak et al., 2018). Wapner et al. (2012) reported a prospective study of 4,282 fetal samples for prenatal diagnosis and concluded that chromosomal microarray analysis identified all aneuploidies and unbalanced rearrangements detected by karyotyping. In samples with a normal karyotype, CMA revealed clinically relevant deletions or duplications in 6.0% of patients with a structural anomaly and 1.7% of those with advanced maternal age or positive screening results (Wapner et al., 2012). In a study by Hay et al. (2018) which included 1,475 fetuses with at least one structural anomaly, chromosomal aberrations were detected in 257 pregnancies (17%), of which 12% were karyotype-detectable, 0.7% were possibly partially detectable, and the remaining 4.7% could not be detected by karyotyping (Hay et al., 2018). When assessing the relationship between ultrasonographic soft markers and chromosomal aberrations, it was demonstrated that the overall prevalence of chromosomal aberrations in fetuses with soft markers was 4.3% (107/2,466), comprising 40.2% with numerical chromosomal abnormalities, 48.6% with P CNVs, and 11.2% with LP CNVs (Hu et al., 2021). Various ultrasound results of the fetus, such as ventriculomegaly, short femur, and thickened nuchal translucency, have been evaluated separately, and the advantages of CMA in prenatal diagnosis have been established (Zhang et al., 2019; Wang J et al., 2020; Li et al., 2021).

CMA also has the advantage of detecting chromosomal aberrations in general pregnancy. A meta-analysis assessed CMA in 10,614 fetuses from 10 large studies, reporting pathogenic, clinically significant CNVs in 0.84% (1:119) of cases referred for advanced maternal age or parental anxiety (Srebniak et al., 2018). In 0.34% of normal karyotype fetuses, submicroscopic CNVs associated with developmental delay/intellectual disability were detected; those CNVs may be missed by prenatal ultrasound (Srebniak et al., 2018).

Limitations of CMA

These results demonstrate that the diagnostic yield of CMA is much higher than that of karyotyping. It has been debated for years whether CMA should be recommended as a first-tier prenatal diagnosis approach to replace the previous recommendations (i.e., either CMA or karyotyping in pregnant women with no positive ultrasound findings). It is worth noting that, currently, karyotyping cannot be completely replaced. Firstly, as CMA cannot detect translocations and inversions, karyotyping should be performed in some situations. For example, CMA can detect trisomy 21 in a prenatal sample, but cannot identify its origin from a non-disjunction event or an unbalanced Robertsonian translocation. In cases of aneuploidies involving Group D/G chromosomes, karyotyping of these fetuses and their parents is essential to determine reproductive risks for future offspring. Secondly, VUS are uncommon genetic alterations with relatively little clinical evidence to evaluate potential pathogenicity effectively. However, their detection by CMA may cause stress and anxiety for the parents, who may need to consider terminating the pregnancy (Levy and Wapner, 2018). Thirdly, CMA is difficult to detect low-level mosaicism due to unbalanced rearrangements and aneuploidy. The copy number, DNA quality, data quality, and size of imbalance, as well as analytical methods, all influence CMA's sensitivity to detecting mosaicism. The mechanism underlying some genetic imbalances may necessitate the use of karyotyping or FISH. In addition, the fact that karyotyping is much more affordable compared to CMA should be taken into consideration in clinical practice. However, there is a lack of evidence to weigh the potential benefit of higher CMA yields in general pregnancy versus the extra cost of CMA. Lastly, the aCGH cannot identify MCC. In clinical application, quantitative fluorescent polymerase chain reaction (QF-PCR) with short tandem repeat (STR) markers is always performed.

Crisis and challenge on CMA

Currently, genome sequencing (GS) challenges the status of CMA in prenatal settings; for example, copy number variation sequencing (CNV-seq), genome-wide cell-free DNA (cfDNA), and whole exome sequencing (WES) have been developed in prenatal setting (Table 1).

Copy number variation sequencing

CNV-seq is uniform, low-coverage genome sequencing based on next-generation sequencing (NGS) at a relatively low price. It seems to be a useful tool for assessing CNVs and has recently been suggested for application in prenatal diagnosis (Dong et al.,

TABLE 1 Summary of prenatal diagnosis/screening methods.

Method	What is detected	Advantage	Disadvantage	Prenatal application
Karyotyping	• Numerical chromosomal abnormalities (polyploidies or aneuploidies)	• Detect chromosomal structure abnormalities	• Relatively long turnaround time	• General population with no positive ultrasound findings
	• Chromosomal abnormalities above 5–10 Mb	• Spend less	• Undetectable submicroscopic chromosomal aberrations	—
CMA	• Numerical chromosomal abnormalities (polyploidies or aneuploidies)	• Detect chromosomal abnormalities not detectable by karyotyping	• Inability to detect molecularly balanced chromosomal rearrangements	• First-tier test when fetal structural anomalies detected
	• CNVs	• Better define and characterize abnormalities identified by karyotyping	• Limitations in the detection of low-level mosaicism	• Fetal with a high risk of UPD
	• ROH	—	• Relatively Expensive	—
CNV-seq	• Numerical chromosomal abnormalities (aneuploidies)	• Detect chromosomal abnormalities not detectable by karyotyping	• Inability to detect molecularly balanced chromosomal rearrangements	• General population with no positive ultrasound findings
	• CNVs	• Relatively cheap	• Inability to detect polyploidies and ROHs	—
			• Less stability, reproducibility, and accuracy	—
NIPT	• Assess the risk of aneuploidies and CNVs	• Non-invasive	• Screening not a diagnostic method	• Screening in the general population
WES	• Exons and flanking sequence of target genes	• All sequence-able exons analyzed	• Only coding sequences, not all genes are equally captured	• Second-tier test when fetal structural anomalies detected
			• Inability to detect CNVs beyond the WES target regions, within poorly covered regions, associated with intragenic regions, or involving single-exon changes	• Situations when a single gene disorder is highly suspected
			• Expensive	—

Abbreviations: CMA, chromosomal microarray analysis; CNVs, Copy number variants; ROHs, Regions of homozygosity; CNV-seq, Copy number variation sequencing; NIPT, Non-invasive prenatal testing; WES, whole exome sequencing.

2021; Zhang et al., 2021). Zhang et al. (2021), reported that a combination of karyotyping and CNV-seq with an average sequencing depth of 0.08-fold detected an extra 63 cases (0.7%) of pathogenic CNVs in 8,705 cases in populations with a normal karyotype, polymorphism, mutual translocation, or marker chromosome (Zhang et al., 2021). Because of the detection limitations of CNV-seq, two cases of triploids were neglected. The study concluded that the combination of karyotyping and CNV-seq significantly improves the detection rate of fetal pathogenic CNVs (Zhang et al., 2021). Wang H et al. (2020) conducted a consecutive, prospective study to evaluate the yields of CNV-seq compared to CMA. A total of 1,023 women were recruited and CNV-seq identified 124 numerical disorders. CMA detected P/LP CNVs in 121 cases (11.8%) and 17 additional and clinically relevant P/LP CNVs in 17 cases (1.7%). Meanwhile, four cases with regions of homozygosity (ROHs) were missed by CNV-seq. QF-PCR with STR markers was used to exclude MCC and determine polyploidy. The study employed two CMA platforms, namely the 44 K Fetal DNA Chip v1.0 aCGH-based test and an updated 8 × 60 K Fetal DNA Chip v2.0 including SNP probes. The read depth used for CNV-seq was 0.25-fold (Wang H et al., 2020).

The idea that CNV-seq is equivalent or superior to routine CMA has recently been proposed. However, the current situation is insufficient. One of the major considerations for validating an NGS-based test is the read length, the average coverage and depths needed across the genome remain unclear. Short NGS read lengths prevent the detection of variations in repetitive regions with comparable sensitivities (Treangen and Salzberg, 2011). Repetitive DNA sequences are abundantly present in the human genome. Although some repeats appear non-functional, others may play a critical role in human physical development (Treangen and Salzberg, 2011). When repeats are longer than the length of a read, methods must rely on the depth of coverage or paired-end data to determine whether the repeat region is a variant (Treangen and Salzberg, 2011). For instance, suppose that a genome of interest is sequenced to an average depth of 30-fold coverage but a particular tandem repeat with two copies in the reference genome has a 60-fold coverage (Treangen and Salzberg, 2011), under such circumstances, some algorithms incorporating both read-depth and paired-end data for accurate CNVs detection have been employed to improve the estimation of the true copy number of each repeat (Hormozdiari et al., 2009; He et al., 2011; Treangen and Salzberg, 2011). In CNV-

seq, relatively shallow average coverage makes it difficult to identify repetitive regions related to specific diseases. For example, the Leri-Weill dyschondrosteosis (LWD)-SHOX deletion is a pseudoautosomal dominant disorder characterized by short stature, mesomelic limb shortening, and a characteristic "Madelung" deformity of the forearms. There are two types of genetic bases: one encompasses the *SHOX* gene deletion, whereas the others are centromeric to *SHOX* within the pseudoautosomal region, and the latter is undetectable by CNV-seq. In addition, although several studies have demonstrated that CNV-seq has a much higher diagnostic yield than CMA, the results should be interpreted cautiously for two reasons: one is that the CMA platforms are varied and have low resolution across different studies; another is the reproducibility of CNV-seq is poor, due to the short read lengths and low sequencing depth. A large, blinded comparative study should be conducted to verify the detection accuracy and stability of CNV-seq and CMA.

It is of great significance to detect UPD in the prenatal setting, as the prevalence of UPD associated with a clinical presentation due to imprinting disorders or recessive diseases ranges from 1 in 3500 to 1 in 5000 (Robinson, 2000). A recent study showed that UPD for all chromosomes occurs with an overall prevalence of 1 in 2000 births, but this can be as high as 1 in 176 among individuals with developmental delay (King et al., 2014; Nakka et al., 2019). UPD cases can be ascertained by testing for copy number abnormalities using CMA platforms with SNP probes. However, assessing ROH can be difficult using low-pass genome sequencing methods. Recently, Dong et al. (2021) demonstrated that all ROHs ascertained by CMA were revealed by low-coverage genome sequencing (4-fold) in 17 clinical samples. In another part of the study, among 1,639 samples (data available from the 1000 Genomes Project), genome sequencing not only consistently detected ROHs but also reported 60 terminal ROHs in 44 cases, including four mosaic ROHs at a level ranging from 50 to 75% (Dong et al., 2021). The authors suggested that for fetuses with a suspected genetic etiology of imprinting disorders or consanguineous mating, low-coverage genome sequencing (4-fold) with ROH detection would be applicable (Dong et al., 2021). However, this view is difficult in the clinical setting. Although the sample size from the 1000 Genomes Project satisfies a comparison study, the heterogeneity (different genome sequencing coverage and CMA density in the two parts of the study) and a very small clinical sample size affected the reliability of the study. Additionally, the coverage and depth of the current CNV-seq are not sufficiently close to satisfying the demand for and rising costs associated with increased sequencing depth. Notably, UPD for specific chromosomes associated with imprinting results in abnormal phenotypes either present or absent in fetal ultrasound (Del Gaudio et al., 2020). Currently, it is better to use CMA (SNP probes contained) rather than other methods for fetuses with structural anomalies, such as growth restriction, overgrowth, and large omphalocele, and for women with positive non-invasive prenatal testing associated with imprinting chromosomes.

Genome-wide cfDNA testing

Non-invasive prenatal testing (NIPT) has been shown to be a highly sensitive screening test for major fetal trisomies in the last decade. Recently, expanding NIPT covering the entire genome, called genome-wide cfDNA testing, has been applied to detect CNVs beyond major trisomies.

A meta-analysis conducted by Familiari *et al.* demonstrated that the positive predictive value (PPV) was 44.1% in detecting microdeletion and microduplication syndromes by expanding NIPT. However, the small number of cases in each study, the lack of standardized diagnostic confirmation, and different DNA sequencing methods make the results unclear (Familiari et al., 2021). Very recently, a study conducted by Rafalko *et al.* indicated that genome-wide cfDNA testing can provide patients with more clinically relevant information with a PPV of approximately 74.2% (95% CI: 68.1–79.5%) and 71.8% (95% CI: 65.5–77.4%) for "fetal-only" events (Rafalko et al., 2021). However, the opinion on genome-wide cfDNA testing in prenatal setting is controversies. Firstly, it is important to understand that the PPV of NIPT varies depending on the patient's prior risk of a chromosomal abnormality. Other-than-common benign CNVs are found in approximately 6.7% of fetuses with isolated ultrasound-detected abnormalities (Donnelly et al., 2014). The frequency of other-than-common benign CNVs increased to 13.6% when multiple organ system ultrasound anomalies were observed (Donnelly et al., 2014). All the above studies failed to distinguish the presence or absence of ultrasound anomalies among the true positive population. Stephanie Guseh et al (2021). Assessed the concordance of genome-wide screening and diagnostic testing, indicating that the major limitation of genome-wide screening compared with diagnostic testing is in the population with abnormal ultrasound with κ = 0.38 (95% CI, 0.08–0.67), including 5 concordant positives, 4 false positives, 7 false negatives, and 48 concordant negative results, indicating a high residual risk in a false negative population. For patients with a fetal anatomic abnormality, CMA on fetal samples is optimally recommended, whereas NIPT is a choice for low-risk populations. Second, all authorities recommend that a positive NIPT result should be confirmed by an invasive procedure. Although genome-wide cfDNA screening testing has a PPV of approximately 74.2%, the population that requires invasive procedures increases with the emergence of false-positive results. The initial purpose of NIPT was to decrease the need for invasive testing; however, the current situation is contrary to that intention.

As P/LP CNVs occur in approximately 1.7% of patients with a normal ultrasound examination (Wapner et al., 2012), the

concordance between genome-wide screening and diagnostic testing in a population without abnormal ultrasound findings is worthwhile. Further is required to comprehensively estimate the clinical implementation of genome-wide cfDNA testing.

Whole exome sequencing

WES is a technology used to interrogate the genome at the nucleotide level to identify variants in a single-gene disorder, and is empirically proposed to be more informative than CMA. WES sequences exons and flanking intron sequences with high coverage. Although WES provides more genomic information, the current best practices for CNV detection still require CMA. Studies have been conducted to assess the performance of WES data in CNV detection and have identified several potential blind spots: CNVs beyond the WES target regions, or within poorly covered regions, as well as CNVs associated with intragenic regions, or involving single-exon changes (Retterer et al., 2015; Royer-Bertrand et al., 2021).

Emerging evidence supports the benefits of WES when fetal structural anomalies are detected. Mellis et al. (2022) conducted a meta-analysis to determine the diagnostic yield of WES for prenatal diagnosis of fetal structural anomalies. The study summarized that the pooled incremental yield of WES over CMA/karyotype from all studies was 31% (95% CI 26-36%, $p < 0.0001$). An updated statement released by the International Society for Prenatal Diagnosis recommends using genome-wide sequencing for prenatal diagnosis, which suggested that the use of WES should follow indications in prenatal clinical diagnosis. For those with no genetic diagnosis found after CMA, pregnancy with a fetus having a single major anomaly or multiple organ system anomalies will benefit from WES or other genome sequencing methods (Van den Veyver et al., 2022). There is currently no evidence supporting WES as a routine test for indications other than fetal anomalies or a single gene disorder being highly suspected. It should also be noted that the interpretation of WES results is challenging in prenatal diagnosis settings. For instance, reporting uncertain results hinders clinical interpretation, and there is no universal consensus on the management of incidental and secondary findings. Currently, CMA is still the first step for a fetus with structural anomalies, and WES could be a further step when normal chromosomes are detected after detailed genetic counseling (Monaghan et al., 2020; Van den Veyver et al., 2022).

Conclusion

CMA is recommended when fetal structural anomalies are detected. Whether this is a first-tier recommendation in general pregnancy is disputable. Genome sequencing, which provides the ultimate genetic test for the detection of more informative genomic variation in a single assay, challenges the status of CMA in the prenatal setting, but until now, in a practical context, it has been insufficient to replace CMA. CMA platforms with SNP probes are currently superior to CNV-seq in detecting chromosomal abnormalities, such as the combined detection of CNVs, MCC, and ROHs, which are common and significant in prenatal settings. Moreover, the stability, reproducibility, and accuracy of CNV-seq remain unclear. The prenatal use of CNV-seq is at risk, especially in cases with positive ultrasound findings or positive noninvasive prenatal testing associated with imprinting chromosomes. Genome-wide cfDNA testing with non-invasive features has attracted the attention of researchers for assessing the utility of CNV detection. However, the application of genome-wide cfDNA testing in the prenatal setting is controversial because of its low concordance with diagnostic results, especially in fetuses with structural anomalies. WES with a scope at the nucleotide level is recommended as a second-line test when fetal structural anomalies are detected, as some CNVs may be missed by the method.

In conclusion, the development of molecular tests has changed prenatal diagnosis, and the CMA platform with SNP probes has been suggested in the prenatal setting. However, the trend toward GS, which is used to identify CNVs along with SNVs and ROHs simultaneously in a single assay, is unstoppable and will be of great benefit to pregnant women in the future by providing more useful information with rapid turnaround times and at acceptable prices.

Author contributions

XL collected and analyzed the data and was a major contributor in writing the manuscript. HW and SL edited the manuscript. TH was a major contributor in formatting and editing the manuscript. All authors reviewed the manuscript.

Funding

This work was supported by National Key Research and Development Program of China (2021YFC1005304) and Sichuan Province Science and Technology Support Program (2021YFS0078 and 2022YFS0078).

Conflict of interest

The authors declare that the research was conducted in the absence of any commercial or financial relationships that could be construed as a potential conflict of interest.

Publisher's note

References

American College of Obstetricians and Gynecologists Committee on Genetics (2013). Committee opinion no. 581: the use of chromosomal microarray analysis in prenatal diagnosis. *Obstet. Gynecol.* 122, 1374–1377. doi:10.1097/01.AOG.0000438962.16108.d1

Carvalho, C. M., Zhang, F., and Lupski, J. R. (2010). Evolution in health and medicine sackler colloquium: enomic disorders: a window into human gene and genome evolution. *Proc. Natl. Acad. Sci. U. S. A.* 107 (1), 1765–1771. doi:10.1073/pnas.0906222107

Del Gaudio, D., Shinawi, M., Astbury, C., Tayeh, M. K., Deak, K. L., and Raca, G. (2020). Diagnostic testing for uniparental disomy: a points to consider statement from the American College of medical genetics and genomics (ACMG). *Genet. Med.* 22, 1133–1141. doi:10.1038/s41436-020-0782-9

Dong, Z., Chau, M. H. K., Zhang, Y., Yang, Z., Shi, M., Wah, Y. M., et al. (2021). Low-pass genome sequencing-based detection of absence of heterozygosity: validation in clinical cytogenetics. *Genet. Med.* 23, 1225–1233. doi:10.1038/s41436-021-01128-7

Donnelly, J. C., Platt, L. D., Rebarber, A., Zachary, J., Grobman, W. A., Wapner, R. J., et al. (2014). Association of copy number variants with specific ultrasonographically detected fetal anomalies. *Obstet. Gynecol.* 124, 83–90. doi:10.1097/aog.0000000000000336

Dugoff, L., Norton, M. E., and Kuller, J. A. (2016). The use of chromosomal microarray for prenatal diagnosis. *Am. J. Obstet. Gynecol.* 215, B2–B9. doi:10.1016/j.ajog.2016.07.016

Familiari, A., Boito, S., Rembouskos, G., Ischia, B., Accurti, V., Fabietti, I., et al. (2021). Cell-free DNA analysis of maternal blood in prenatal screening for chromosomal microdeletions and microduplications: a systematic review. *Prenat. Diagn.* 41, 1324–1331. doi:10.1002/pd.5928

Guseh, S., Wilkins-Haug, L., Kaimal, A., Dunn-Albanese, L., Adams, S., Carroll, S., et al. (2021). Utility of noninvasive genome-wide screening: a prospective cohort of obstetric patients undergoing diagnostic testing. *Genet. Med.* 23, 1341–1348. doi:10.1038/s41436-021-01147-4

Hay, S. B., Sahoo, T., Travis, M. K., Hovanes, K., Dzidic, N., Doherty, C., et al. (2018). ACOG and SMFM guidelines for prenatal diagnosis: is karyotyping really sufficient? *Prenat. Diagn.* 38, 184–189. doi:10.1002/pd.5212

He, D., Hormozdiari, F., Furlotte, N., and Eskin, E. (2011). Efficient algorithms for tandem copy number variation reconstruction in repeat-rich regions. *Bioinformatics* 27, 1513–1520. doi:10.1093/bioinformatics/btr169

Hormozdiari, F., Alkan, C., Eichler, E. E., and Sahinalp, S. C. (2009). Combinatorial algorithms for structural variation detection in high-throughput sequenced genomes. *Genome Res.* 19, 1270–1278. doi:10.1101/gr.088633.108

Hu, T., Tian, T., Zhang, Z., Wang, J., Hu, R., Xiao, L., et al. (2021). Prenatal chromosomal microarray analysis in 2466 fetuses with ultrasonographic soft markers: a prospective cohort study. *Am. J. Obstet. Gynecol.* 224, 516. doi:10.1016/j.ajog.2020.10.039

King, D. A., Fitzgerald, T. W., Miller, R., Canham, N., Clayton-Smith, J., Johnson, D., et al. (2014). A novel method for detecting uniparental disomy from trio genotypes identifies a significant excess in children with developmental disorders. *Genome Res.* 24, 673–687. doi:10.1101/gr.160465.113

Levy, B., and Wapner, R. (2018). Prenatal diagnosis by chromosomal microarray analysis. *Fertil. Steril.* 109, 201–212. doi:10.1016/j.fertnstert.2018.01.005

Li, Q., Zhang, Z., Wang, J., Zhang, H., Zhu, H., Lai, Y., et al. (2021). Prenatal diagnosis of genetic aberrations in fetuses with short femur detected by ultrasound: a prospective cohort study. *Prenat. Diagn.* 41, 1153–1163. doi:10.1002/pd.6006

Mellis, R., Oprych, K., Scotchman, E., Hill, M., and Chitty, L. S. (2022). Diagnostic yield of exome sequencing for prenatal diagnosis of fetal structural anomalies: a systematic review and meta-analysis. *Prenat. Diagn.* 42, 662–685. doi:10.1002/pd.6115

Mikhail, F. M. (2014). Copy number variations and human genetic disease. *Curr. Opin. Pediatr.* 26, 646–652. doi:10.1097/mop.0000000000000142

Miller, D. T., Adam, M. P., Aradhya, S., Biesecker, L. G., Brothman, A. R., Carter, N. P., et al. (2010). Consensus statement: chromosomal microarray is a first-tier clinical diagnostic test for individuals with developmental disabilities or congenital anomalies. *Am. J. Hum. Genet.* 86, 749–764. doi:10.1016/j.ajhg.2010.04.006

Monaghan, K. G., Leach, N. T., Pekarek, D., Prasad, P., and Rose, N. C. (2020). The use of fetal exome sequencing in prenatal diagnosis: a points to consider document of the American College of medical genetics and genomics (ACMG). *Genet. Med.* 22, 675–680. doi:10.1038/s41436-019-0731-7

Nakka, P., Pattillo Smith, S., O'Donnell-Luria, A. H., McManus, K. F., Mountain, J. L., Ramachandran, S., et al. (2019). Characterization of prevalence and health consequences of uniparental disomy in four million individuals from the general population. *Am. J. Hum. Genet.* 105, 921–932. doi:10.1016/j.ajhg.2019.09.016

Nussbaum, R., McInnes, R., and Willard, H. (2016). *Thompson & Thompson genetics in medicine*. 8th ed. Philadelphia, PA: Elsevier, 57–74.

Peters, D. G., Yatsenko, S. A., Surti, U., and Rajkovic, A. (2015). Recent advances of genomic testing in perinatal medicine. *Semin. Perinatol.* 39, 44–54. doi:10.1053/j.semperi.2014.10.009

Rafalko, J., Soster, E., Caldwell, S., Almasri, E., Westover, T., Weinblatt, V., et al. (2021). Genome-wide cell-free DNA screening: a focus on copy-number variants. *Genet. Med.* 23, 1847–1853. doi:10.1038/s41436-021-01227-5

Redon, R., Ishikawa, S., Fitch, K. R., Feuk, L., Perry, G. H., Andrews, T. D., et al. (2006). Global variation in copy number in the human genome. *Nature* 444, 444–454. doi:10.1038/nature05329

Retterer, K., Scuffins, J., Schmidt, D., Lewis, R., Pineda-Alvarez, D., Stafford, A., et al. (2015). Assessing copy number from exome sequencing and exome array CGH based on CNV spectrum in a large clinical cohort. *Genet. Med.* 17, 623–629. doi:10.1038/gim.2014.160

Riggs, E. R., Andersen, E. F., Cherry, A. M., Kantarci, S., Kearney, H., Patel, A., et al. (2020). Technical standards for the interpretation and reporting of constitutional copy-number variants: a joint consensus recommendation of the American College of medical genetics and genomics (ACMG) and the clinical genome Resource (ClinGen). *Genet. Med.* 22, 245–257. doi:10.1038/s41436-019-0686-8

Robinson, W. P. (2000). Mechanisms leading to uniparental disomy and their clinical consequences. *Bioessays* 22, 452–459. doi:10.1002/(SICI)1521-1878(200005)22:5<452::AID-BIES7>3.0.CO;2-K

Rose, N. C., Kaimal, A. J., Dugoff, L., and Norton, M. E. (2020). Screening for fetal chromosomal abnormalities: ACOG practice bulletin, number 226. *Obstet. Gynecol.* 136, e48–e69. doi:10.1097/aog.0000000000004084

Royer-Bertrand, B., Cisarova, K., Niel-Butschi, F., Mittaz-Crettol, L., Fodstad, H., Superti-Furga, A., et al. (2021). CNV detection from exome sequencing data in routine diagnostics of Rare genetic disorders: opportunities and limitations. *Genes* 12, 1427. doi:10.3390/genes12091427

Schwartz, S. (2011). Clinical utility of single nucleotide polymorphism arrays. *Clin. Lab. Med.* 31, 581–594. doi:10.1016/j.cll.2011.09.002

Speicher, M. R., and Carter, N. P. (2005). The new cytogenetics: blurring the boundaries with molecular biology. *Nat. Rev. Genet.* 6, 782–792. doi:10.1038/nrg1692

Srebniak, M. I., Joosten, M., Knapen, M., Arends, L. R., Polak, M., van Veen, S., et al. (2018). Frequency of submicroscopic chromosomal aberrations in pregnancies without increased risk for structural chromosomal aberrations: systematic review and meta-analysis. *Ultrasound Obstet. Gynecol.* 51, 445–452. doi:10.1002/uog.17533

Steele, M. W., and Breg, W. R. (1966). Chromosome analysis of human amniotic-fluid cells. *Lancet* 1, 383–385. doi:10.1016/s0140-6736(66)91387-0

Treangen, T. J., and Salzberg, S. L. (2011). Repetitive DNA and next-generation sequencing: computational challenges and solutions. *Nat. Rev. Genet.* 13, 36–46. doi:10.1038/nrg3117

Van den Veyver, I. B., Chandler, N., Wilkins-Haug, L. E., Wapner, R. J., Chitty, L. S., and ISPD Board of Directors (2022). International society for prenatal diagnosis updated position statement on the use of genome-wide sequencing for prenatal diagnosis. *Prenat. Diagn.* 42, 796–803. doi:10.1002/pd.6157

Vermeesch, J. R., Fiegler, H., de Leeuw, N., Szuhai, K., Schoumans, J., Ciccone, R., et al. (2007). Guidelines for molecular karyotyping in constitutional genetic diagnosis. *Eur. J. Hum. Genet.* 15, 1105–1114. doi:10.1038/sj.ejhg.5201896

Wang J, J., Zhang, Z., Li, Q., Zhu, H., Lai, Y., Luo, W., et al. (2020). Prenatal diagnosis of chromosomal aberrations by chromosomal microarray analysis in foetuses with ventriculomegaly. *Sci. Rep.* 10, 20765. doi:10.1038/s41598-020-77400-8

Wang H, H., Dong, Z., Zhang, R., Chau, M. H. K., Yang, Z., Tsang, K. Y. C., et al. (2020). Low-pass genome sequencing versus chromosomal microarray analysis: implementation in prenatal diagnosis. *Genet. Med.* 22, 500–510. doi:10.1038/s41436-019-0634-7

Wapner, R. J., Martin, C. L., Levy, B., Ballif, B. C., Eng, C. M., Zachary, J. M., et al. (2012). Chromosomal microarray versus karyotyping for prenatal diagnosis. *N. Engl. J. Med.* 367, 2175–2184. doi:10.1056/NEJMoa1203382

Zhang, Z., Hu, T., Wang, J., Li, Q., Wang, H., Liu, S., et al. (2019). Prenatal diagnostic value of chromosomal microarray in fetuses with nuchal translucency greater than 2.5 mm. *Biomed. Res. Int.* 2019, 6504159. doi:10.1155/2019/6504159

Zhang, J., Tang, X., Hu, J., He, G., Wang, J., Zhu, Y., et al. (2021). Investigation on combined copy number variation sequencing and cytogenetic karyotyping for prenatal diagnosis. *BMC Pregnancy Childbirth* 21, 496. doi:10.1186/s12884-021-03918-y

frontiers | Frontiers in Genetics

TYPE Case Report
PUBLISHED 29 August 2022
DOI 10.3389/fgene.2022.950271

OPEN ACCESS

EDITED BY
Walter Erwin Kaufmann,
Emory University, United States

REVIEWED BY
Xiaofan Zhu,
First Affiliated Hospital of Zhengzhou University, China
Min Pan,
Guangzhou Medical University, China

*CORRESPONDENCE
Tian Tian,
158163921@qq.com
Ting Hu,
huting4123@163.com

†These authors have contributed equally to this work

SPECIALTY SECTION
This article was submitted to Genetics of Common and Rare Diseases, a section of the journal Frontiers in Genetics

RECEIVED 22 May 2022
ACCEPTED 29 July 2022
PUBLISHED 29 August 2022

CITATION
Liu X, Wang J, Yang M, Tian T and Hu T (2022), Case report: Cystic hygroma accompanied with campomelic dysplasia in the first trimester caused by haploinsufficiency with SOX9 deletion. *Front. Genet.* 13:950271. doi: 10.3389/fgene.2022.950271

Case report: Cystic hygroma accompanied with campomelic dysplasia in the first trimester caused by haploinsufficiency with *SOX9* deletion

Xijing Liu[1,2,3], Jianmin Wang[1,2,3], Mei Yang[1,2,3], Tian Tian[3,4]*† and Ting Hu[1,2,3]*†

[1]Department of Medical Genetics, West China Second University Hospital, Sichuan University, Chengdu, China, [2]Department of Obstetrics and Gynecology, West China Second University Hospital, Sichuan University, Chengdu, China, [3]Key Laboratory of Birth Defects and Related Diseases of Women and Children (Sichuan University), Ministry of Education, Chengdu, China, [4]Department of Diagnostic Ultrasound, West China Second University Hospital, Sichuan University, Chengdu, China

Introduction: Campomelic dysplasia (CD) is a rare autosomal dominant skeletal malformation syndrome characterized by shortness and bowing of the lower extremities with or without XY sex reversal. Diagnosis using ultrasonography is most often made in the latter half of pregnancy. Intragenic heterozygous mutations in SOX9 are responsible for most cases of CD. CD caused by SOX9 deletion is a rare condition.

Case presentation: We present a single case report of an individual with cystic hygroma accompanied by CD, which was detected by ultrasound in the first trimester. Chromosomal microarray analysis (CMA) was performed to determine copy number variants, whereas whole exome sequencing (WES) was performed to elucidate single-nucleotide variants. Chorionic villus sampling was performed to enable such analyses. Ultimately, CMA detected a 606 kb deletion in the 17q24.3 region with only one protein-coding gene (SOX9). However, no mutation in the SOX9 protein-coding sequence was detected by WES.

Conclusion: When cystic hygroma is detected, prenatal diagnoses for skeletal dysplasia by ultrasound are likely to be confirmed in the first trimester. We propose a comprehensive prenatal diagnostic strategy that combines CMA and WES to diagnose fetuses with cystic hygroma accompanied by skeletal dysplasia.

KEYWORDS

campomelic dysplasia, cystic hygroma, SOX9, ultrasound, chromosomal microarray analysis

Introduction

Campomelic dysplasia (CD, MIM: #114290) is a rare autosomal dominant skeletal malformation syndrome characterized by an under-mineralized skeleton with shortness and bowing of lower extremities and hypoplasia of scapular and pelvic bones. Moreover, other notable anatomical characteristics include a small chest, 11 pairs of ribs, clubfeet, a cleft palate, and micrognathia (Mansour et al., 1995; Jain and Sen, 2014). Two-thirds of affected males showed XY sex reversal or a lesser degree of genital defects (Mansour et al., 1995). CD is a semi-lethal disorder because most patients die during the neonatal period secondary to respiratory distress (Mansour et al., 2002).

SOX9 (SRY-related HMG-box gene 9, OMIM:608160), located in chromosome 17q24.3, is a transcription factor that plays a critical role in the development of skeletal and reproductive systems by inducing chondrocyte differentiation and anti-Mullerian hormone expression (Wagner et al., 1994; Olney et al., 1999). Most cases of CD are caused by intragenic heterozygous mutations in *SOX9*, including missense, nonsense, frameshift, and splice mutations (Unger et al., 1993). A second mechanism for CD is balanced chromosomal rearrangements, including translocations, inversions, and deletions, which do not affect *SOX9* but cause interruptions upstream or downstream of *SOX9* (Unger et al., 1993; Gordon et al., 2009; Lecointre et al., 2009). Additionally, a few CDs are caused by large deletions covering *SOX9* (Olney et al., 1999; Pop et al., 2004; Smyk et al., 2007; Kayhan et al., 2019).

CD might be suspected after shortened lower limbs and femoral angulation are detected by prenatal ultrasonography, although

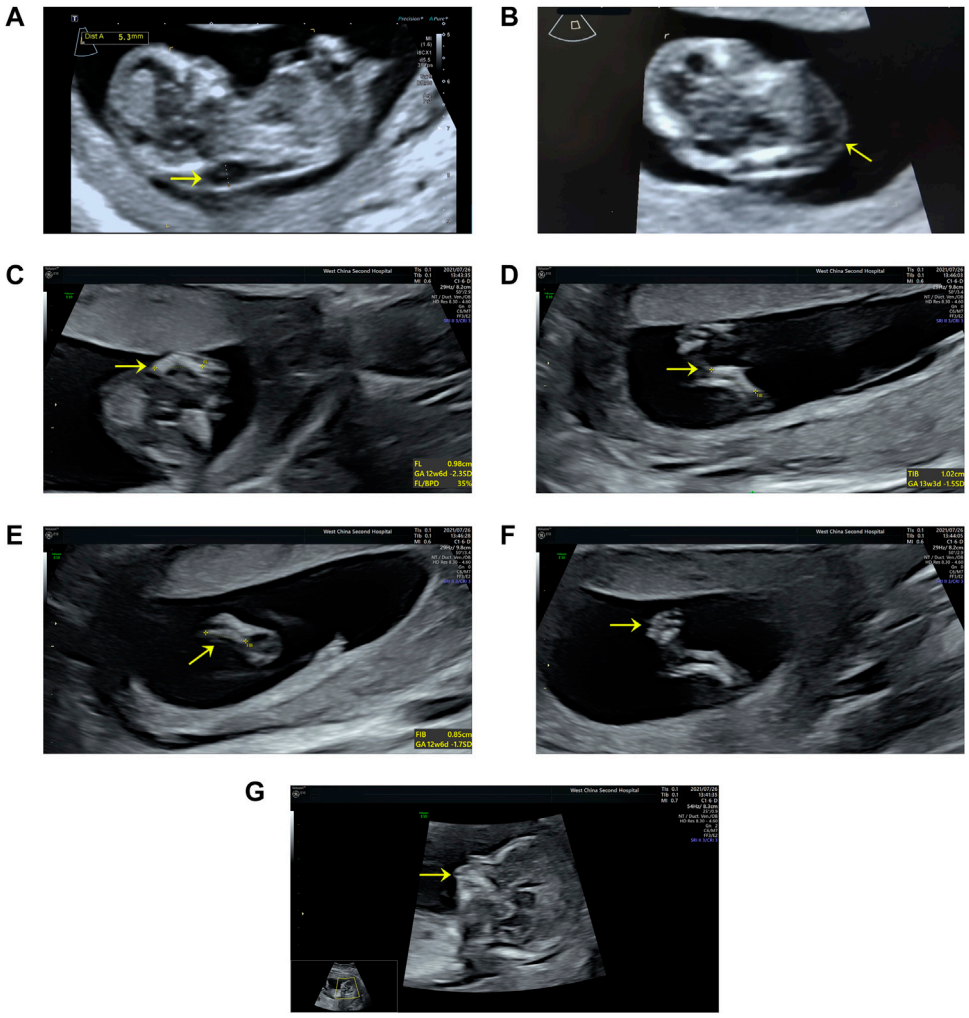

FIGURE 1
Ultrasound findings: **(A)** Cystic hygroma measuring 18 × 6 × 14 mm (CRL:60.9 mm) at the mid-sagittal plane. **(B)** Cystic hygroma in a transverse view. **(C)** Short and bowed femurs (<first centile). **(D)** Sagittal anterior angulated tibiae (fifth centile). **(E)** Sagittal anterior angulated fibula (fifth centile). **(F)** Unilateral equinovarus clubfoot. **(G)** Micrognathia.

observations are often made in the latter half of pregnancy. Thus, antenatal diagnosis of CD is difficult during the first trimester (Tongsong et al., 2000). We report an individual with cystic hygroma accompanied by CD in the first trimester and confirm that such a phenotype resulted from *SOX9* deletion.

Case description

A 27-year-old nulliparous woman was referred to the Prenatal Diagnosis Center of West China Second University Hospital of Sichuan University (a tertiary referral center) for consultation and sonography concerning a cystic hygroma discovered at 13 weeks and 4 days. The crown-rump length was 60.9 mm and a cystic hygroma measuring 18 × 6 × 14 mm was confirmed (Figures 1A,B). The couple has no history of consanguinity. At 14 weeks and 6 days, a detailed fetal anomaly scan revealed severe short and bowed femurs (<first centile), sagittal anterior-angulated tibiae and fibula (fifth centile), unilateral equinovarus clubfoot, and micrognathia (Figures 1C–G). The biparietal diameter was 27.9 mm, while the thorax and upper limbs appeared normal. The fetus was found to have female external genitalia. A presumptive diagnosis of skeletal dysplasia was made. However, a precise diagnosis was difficult to achieve based on limited ultrasound findings. Chorionic villus sampling was performed to enable chromosomal microarray analysis (CMA) and whole exome sequencing (WES).

The study was approved by the Medical Ethics Committee of the West China Second University Hospital of Sichuan University in China.

Diagnostic assessment

Methods

Chromosomal microarray analysis

We conducted the chromosomal microarray analysis using CytoScan 750 K Array (Affymetrix, Santa Clara, CA, United States). The samples were prepared according to the manufacturer's instructions. The array scan data were visualized using the Chromosome Analysis Suite v4.1 software. The GRCh38 genome was used for annotation. The pathogenicity of copy number variants (CNVs) was based on the technical standards of the American College of Medical Genetics and Genomics (ACMG) and the Clinical Genome Resource (ClinGen) (Riggs et al., 2020).

Whole exome sequencing

The Nano WES Human Exome V1 (Berry Genomics, Beijing, China) was used to capture the sequences. The enriched library was sequenced on a NovaSeq 6,000 with 150 paired-end reads. The reads were mapped to a human reference genome (GRCh38) using BWA (v0.7.15). Variant calling was performed using the Verita Trekker (v1.2.0.2). After filtering the variants with the classic population frequency databases, we rated the pathogenicity of the remaining mutations according to the ACMG guidelines, as previously described (Chen et al., 2022).

Methods

CMA was performed following chorionic villus sampling, which revealed a 606 kb deletion [arr [GRCh38] 17q24.3 (71,620,225_72,226,459)x1] in the 17q24.3 region (Figure 2A). The deletion contained one protein-coding gene (*SOX9*) and five other genes (*LINC01152*, *LINC02097*, *MYL6P5*, *ROCR*, and *SOX9-AS1*), which extended from 501 kb upstream to 100 kb downstream of *SOX9* (Figure 2B). The deletion overlapped only 9.3% of the *SOX9* upstream enhancer region, which is identified as a haploinsufficiency (HI) genomic region (ClinGen database (http://www.ncbi.nlm.nih.gov/projects/dbvar/clingen/)). The sex chromosome of the fetus was XX. This deletion was not detected in the couple, suggesting that a *de novo* event had occurred. The CNVs were classified as "Pathogenic" according to ACMG and ClinGen Technical standards (Riggs et al., 2020). Sequentially, a trio-WES was performed for genetic factors of skeletal dysplasia in addition to *SOX9* deletion, and yet the analysis yielded negative results.

The diagnosis of CD was confirmed based on the SNP-array results and fetal ultrasound findings.

Discussion

We report a case of CD with cystic hygroma detected in the first trimester by ultrasonography, and in which further testing confirmed the presence of *SOX9* deletion. Commonly, prenatal diagnosis of skeletal dysplasia is performed by ultrasonography during the second trimester. Recently, Kayhan et al. (2019) reported a 46, XY prenatal case of CD with *SOX9* deletion, characterized by micrognathia, bowed limbs, clubfeet, and female genitalia in the second trimester. However, ultrasound in the first trimester appeared normal, and no apparent anomalies, such as cystic hygroma or increased nuchal translucency, were observed. However, a cystic hygroma or increased nuchal translucency during the first 3 months has been reported to be a relatively frequent sign in fetuses subsequently diagnosed with skeletal dysplasia (Massardier et al., 2008; Zhen et al., 2015). As in our case, a detailed fetal anomaly scan was performed sequentially when cystic hygroma was detected, and skeletal dysplasia was confirmed. Kenkhuis et al. (2018) concluded that it is possible to detect approximately half of the prenatally detectable structural anomalies with an early scan performed in the first trimester by competent fetal sonographers. Thus, a detailed ultrasonography should be immediately performed when cystic hygroma or increased nuchal translucency is detected in the first trimester.

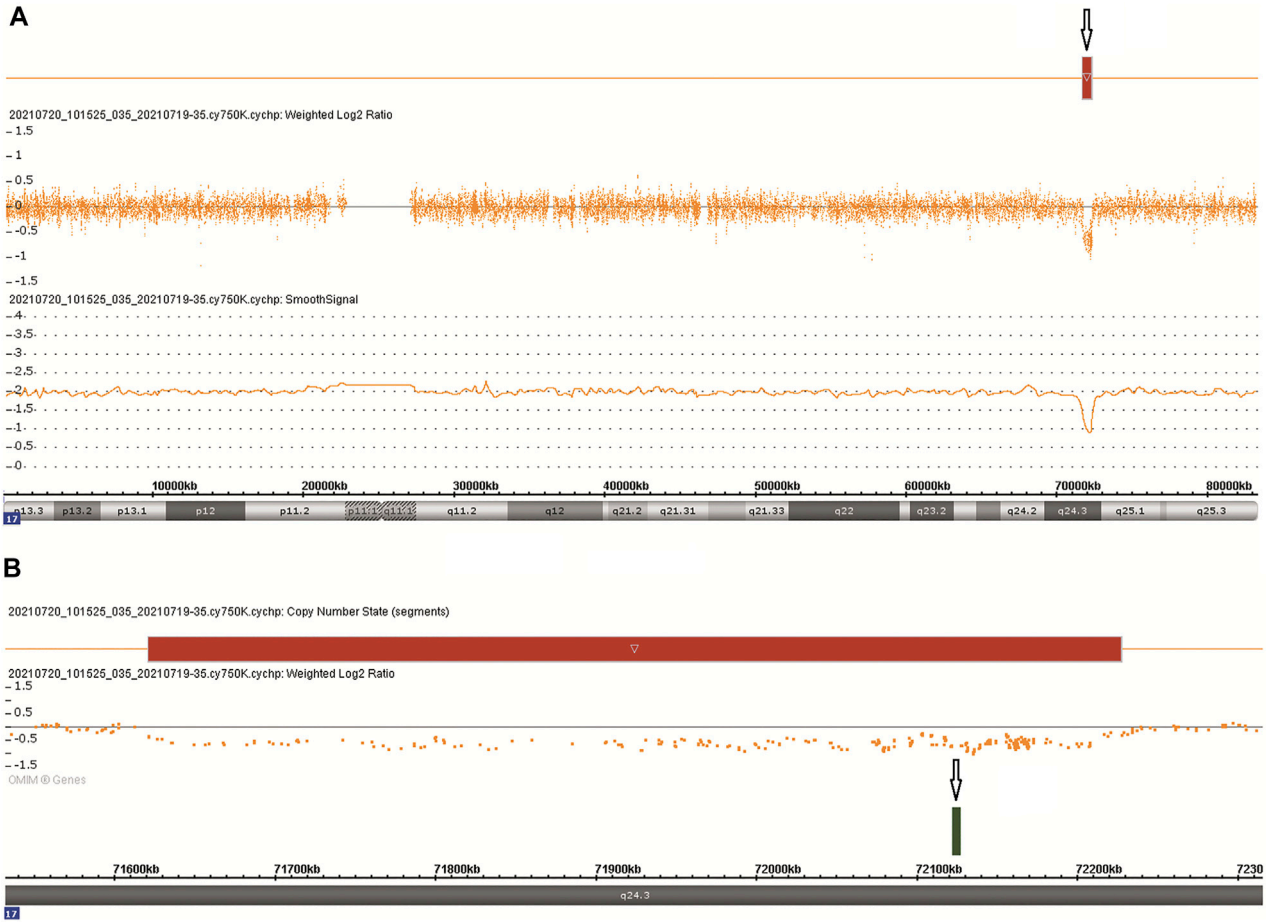

FIGURE 2
Chromosomal microarray findings: **(A)** A 606 kb deletion in the 17q24.3 region. **(B)** The deletion contains one OMIM gene SOX9.

CD is an autosomal dominant disease usually caused by a heterozygous pathogenic variant of *SOX9* (Unger et al., 1993). Most CD cases show heterozygous *de novo* mutations in the coding region of *SOX9*. A small number of cases have a heterozygous interstitial deletion or reciprocal translocation of 17q24.3-q25.1, which involves *SOX9* or its regulatory region (Unger et al., 1993; Gordon et al., 2009; Lecointre et al., 2009). Currently, the haploinsufficiency of *SOX9* is disputable. In the last few decades, loss-of-function mutations in one of the three *SOX9* exons have been identified in CD. Therefore, it has been assumed that the disease results from the haploinsufficiency of *SOX9* (Unger et al., 1993; Ninomiya et al., 2000). However, the research conducted by Csukasi et al. (2019) suggested a dominant-negative nature to *SOX9* mutations in CD. As isolated *SOX9* deletion is rare, the evidence for *SOX9* haploinsufficiency is insufficient.

Currently, only four CD cases have been reported with the complete deletion of the *SOX9* gene (Olney et al., 1999; Pop et al., 2004; Smyk et al., 2007; Kayhan et al., 2019). Olney et al. (1999) first reported an infant with CD who has an interstitial deletion from 17q23.3 to q24.3 by karyotyping, whereas Pop et al. (2004) reported a male CD patient with a *de novo* deletion of at least 4.0 Mb, and Smyk et al. (2007) reported a female CD patient with a paternally inherited deletion of ~4.7 Mb in size. Interestingly, all the three cases completely overlapped the *SOX9* upstream enhancer region that is positioned 2 Mb 5' to *SOX9*, and which is associated with the Pierre Robin sequence (PRS, MIM #261800). PRS, a partial phenotype of CD, is characterized by micrognathia, cleft palate, and glossoptosis (Lecointre et al., 2009). Thus, the evidence of haploinsufficiency in *SOX9* deletion-induced CD remains elusive. Kayhan et al. (2019) performed a prenatal array comparative genomic hybridization on a 46, XY CD fetus and revealed an 886 kb deletion in the 17q24.3 region, which included the entire *SOX9* gene. Although the deletion also overlapped approximately 29.3% of the *SOX9* upstream enhancer region, it is difficult to confirm that *SOX9* deletion is solely responsible for the CD phenotype.

The genotype–phenotype correlation of *SOX9* remains unclear. Although loss-of-function mutations have been identified in some CD cases, functional studies suggest a dominant-negative phenotype (Wagner et al., 1994; Ninomiya et al., 2000; Jain and Sen, 2014; Csukasi et al., 2019). The advent of CMA has revealed CNVs, including both the coding and regulatory regions of *SOX9* (Croft et al., 2018). The utility of WES elucidated single-nucleotide variants of genetic disorders that were not detectable by CMA. However, deletions or duplications associated with cis-regulatory elements upstream of *SOX9* were not detected by the algorithms (Mansour et al., 2002). Therefore, we performed CMA combined with WES as an unbiased approach when cystic hygroma and skeletal dysplasia were detected. In our case, the phenotype of the fetus revealed by ultrasonography was consistent with the loss of *SOX9*, providing an increasing evidence of *SOX9* haploinsufficiency.

With the advancements in molecular detection technology, the prenatal diagnosis of fetuses at risk for genetic disorders has rapidly increased in recent years. The choice of application of CMA and WES deserves consideration. When a fetal anomaly is observed, we support the recommendations released by the International Society for Prenatal Diagnosis (Van den Veyver et al., 2022), which contends that, if no genetic diagnosis is found after CMA, a fetus with a major single anomaly or multiple organ system anomalies will benefit from WES or other genome sequencing methods. If the anomaly "pattern" strongly suggests a single genetic disorder with no prior genetic testing, CMA should be run before or parallel to WES. In this case, a cystic hygroma was first observed, and CMA was the prior genetic test. After a detailed ultrasonography, CD was highly suspected, and whether WES could have been a prior genetic test is worth considering, as CD is a disorder mainly caused by *SOX9* heterozygous *de novo* mutations.

In clinical practice, when a cystic hygroma or increased nuchal translucency is detected using a detailed ultrasonography, prenatal diagnoses for skeletal dysplasia are likely to be confirmed in the first trimester. Since a meta-analysis has found that the highest exome sequencing diagnostic yields occurred in fetuses with skeletal abnormalities (53% [95% CI 42–63%], $p < 0.0001$) (Mellis et al., 2022), the prenatal diagnostic strategy for fetuses with cystic hygroma accompanied by skeletal dysplasia requires more clinical experience.

Patient perspective

After receiving the genetic and ultrasound reports, diagnosis was established, and the couple decided to terminate the pregnancy. The couple provided written informed consent to participate in this study. Written informed consent was obtained from each individual for the publication of potentially identifiable images or data included in this article.

Data availability statement

The datasets presented in this study can be found in online repositories. The names of the repository/repositories and accession number(s) can be found in the article.

Ethics statement

The studies involving human participants were reviewed and approved by the Medical Ethics Committee of the West China Second University Hospital, Sichuan University, China. The patients/participants provided their written informed consent to participate in this study. Written informed consent was obtained from the individual(s) for the publication of any potentially identifiable images or data included in this article.

Author contributions

XL wrote the manuscript and analyzed the CMA data. JW collected the information of the patient and performed the CMA experiment. MY performed the WES experiment and analyzed the WES data. TT performed the ultrasound examination and revised the manuscript. TH designed the research and revised the manuscript.

Funding

This work was supported by the National Key Research and Development Program of China (2021YFC1005304) and Sichuan Province Science and Technology Support Program (2022YFS0078).

Conflict of interest

The authors declare that the research was conducted in the absence of any commercial or financial relationships that could be construed as a potential conflict of interest.

Publisher's note

References

Chen, J., Xiang, Q., Xiao, X., Xu, B., Xie, H., Wang, H., et al. (2022). Carrying both COL1A2 and FBN2 gene heterozygous mutations results in a severe skeletal clinical phenotype: an affected family. *BMC Med. Genomics* 15 (1), 154. Epub 2022/07/09 PubMed PMID: 35804365; PubMed Central PMCID: PMCPMC9270787. doi:10.1186/s12920-022-01296-8

Croft, B., Ohnesorg, T., and Sinclair, A. H. (2018). The role of copy number variants in disorders of sex development. Sexual development : genetics, molecular biology, evolution, endocrinology, embryology, and pathology of sex determination and differentiation. *Sex. Dev.* 12 (1-3), 19–29. Epub 2017/11/18 PubMed PMID: 29145200. doi:10.1159/000481896

Csukasi, F., Duran, I., Zhang, W., Martin, J. H., Barad, M., Bamshad, M., et al. (2019). Dominant-negative SOX9 mutations in campomelic dysplasia. *Hum. Mutat.* 40 (12), 2344–2352. Epub 2019/08/08 PubMed PMID: 31389106; PubMed Central PMCID: PMCPMC7608528. doi:10.1002/humu.23888

Gordon, C. T., Tan, T. Y., Benko, S., Fitzpatrick, D., Lyonnet, S., and Farlie, P. G. (2009). Long-range regulation at the SOX9 locus in development and disease. *J. Med. Genet.* 46 (10), 649–656. Epub 2009/05/29 PubMed PMID: 19473998. doi:10.1136/jmg.2009.068361

Jain, V., and Sen, B. (2014). Campomelic dysplasia. *J. Pediatr. Orthop. B* 23 (5), 485–488. Epub 2014/05/08 PubMed PMID: 24800790. doi:10.1097/bpb.0000000000000058

Kayhan, G., Calis, P., Karcaaltincaba, D., and Tug, E. (2019). Prenatal diagnosis of campomelic dysplasia due to SOX9 deletion. *J. Obstet. Gynaecol.* 39 (8), 1175–1176. Epub 2019/06/27 PubMed PMID: 31234679. doi:10.1080/01443615.2019.1601165

Kenkhuis, M. J. A., Bakker, M., Bardi, F., Fontanella, F., Bakker, M. K., Fleurke-Rozema, J. H., et al. (2018). Effectiveness of 12-13-week scan for early diagnosis of fetal congenital anomalies in the cell-free DNA era. *Ultrasound Obstet. Gynecol.* 51 (4), 463–469. Epub 2017/04/12 PubMed PMID: 28397377. doi:10.1002/uog.17487

Lecointre, C., Pichon, O., Hamel, A., Heloury, Y., Michel-Calemard, L., Morel, Y., et al. (2009). Familial acampomelic form of campomelic dysplasia caused by a 960 kb deletion upstream of SOX9. *Am. J. Med. Genet. A* 149a (6), 1183–1189. Epub 2009/05/19 PubMed PMID: 19449405. doi:10.1002/ajmg.a.32830

Mansour, S., Hall, C. M., Pembrey, M. E., and Young, I. D. (1995). A clinical and genetic study of campomelic dysplasia. *J. Med. Genet.* 32 (6), 415–420. Epub 1995/06/01 PubMed PMID: 7666392; PubMed Central PMCID: PMCPMC1050480. doi:10.1136/jmg.32.6.415

Mansour, S., Offiah, A. C., McDowall, S., Sim, P., Tolmie, J., and Hall, C. (2002). The phenotype of survivors of campomelic dysplasia. *J. Med. Genet.* 39 (8), 597–602. PubMed PMID: 12161603; PubMed Central PMCID: PMCPMC1735206. doi:10.1136/jmg.39.8.597

Massardier, J., Roth, P., Michel-Calemard, L., Rudigoz, R. C., Bouvier, R., Dijoud, F., et al. (2008). Campomelic dysplasia: echographic suspicion in the first trimester of pregnancy and final diagnosis of two cases. *Fetal diagn. Ther.* 24 (4), 452–457. Epub 2008/11/27 PubMed PMID: 19033726. doi:10.1159/000176299

Mellis, R., Oprych, K., Scotchman, E., Hill, M., and Chitty, L. S. (2022). Diagnostic yield of exome sequencing for prenatal diagnosis of fetal structural anomalies: A systematic review and meta-analysis. *Prenat. Diagn.* 42 (6), 662–685. Epub 2022/02/17 PubMed PMID: 35170059. doi:10.1002/pd.6115

Ninomiya, S., Yokoyama, Y., Teraoka, M., Mori, R., Inoue, C., Yamashita, S., et al. (2000). A novel mutation (296 del G) of the SOX90 gene in a patient with campomelic syndrome and sex reversal. *Clin. Genet.* 58 (3), 224–227. Epub 2000/11/15 PubMed PMID: 11076045. doi:10.1034/j.1399-0004.2000.580310.x

Olney, P. N., Kean, L. S., Graham, D., Elsas, L. J., and May, K. M. (1999). Campomelic syndrome and deletion of SOX9. *Am. J. Med. Genet.* 84 (1), 20–24. Epub 1999/04/23. PubMed PMID: 10213041. doi:10.1002/(sici)1096-8628(19990507)84:1<20::aid-ajmg5>3.0.co;2-n

Pop, R., Conz, C., Lindenberg, K. S., Blesson, S., Schmalenberger, B., Briault, S., et al. (2004). Screening of the 1 Mb SOX9 5' control region by array CGH identifies a large deletion in a case of campomelic dysplasia with XY sex reversal. *J. Med. Genet.* 41 (4), e47. Epub 2004/04/03 PubMed PMID: 15060123; PubMed Central PMCID: PMCPMC1735745. doi:10.1136/jmg.2003.013185

Riggs, E. R., Andersen, E. F., Cherry, A. M., Kantarci, S., Kearney, H., Patel, A., et al. (2020). Technical standards for the interpretation and reporting of constitutional copy-number variants: a joint consensus recommendation of the American College of medical genetics and genomics (ACMG) and the clinical genome Resource (ClinGen). *Genet. Med.* 22 (2), 245–257. Epub 2019/11/07 PubMed PMID: 31690835; PubMed Central PMCID: PMCPMC7313390. doi:10.1038/s41436-019-0686-8

Smyk, M., Obersztyn, E., Nowakowska, B., Bocian, E., Cheung, S. W., Mazurczak, T., et al. (2007). Recurrent SOX9 deletion campomelic dysplasia due to somatic mosaicism in the father. *Am. J. Med. Genet. A* 143a (8), 866–870. Epub 2007/03/14 PubMed PMID: 17352389. doi:10.1002/ajmg.a.31631

Tongsong, T., Wanapirak, C., and Pongsatha, S. (2000). Prenatal diagnosis of campomelic dysplasia. *Ultrasound Obstet. Gynecol.* 15 (5), 428–430. Epub 2000/09/08 PubMed PMID: 10976487. doi:10.1046/j.1469-0705.2000.00126.x

Unger, S., Scherer, G., and Superti-Furga, A. (1993). "Campomelic dysplasia," in *GeneReviews(®)*. M. P. Adam, H. H. Ardinger, R. A. Pagon, S. E. Wallace, L. J. H. Bean, and G. Mirzaa. Editors (Seattle (WA): University of Washington, Seattle).

Van den Veyver, I. B., Chandler, N., Wilkins-Haug, L. E., Wapner, R. J., and Chitty, L. S.ISPD Board of Directors (2022). International society for prenatal diagnosis updated position statement on the use of genome-wide sequencing for prenatal diagnosis. *Prenat. Diagn.* 42 (6), 796–803. Epub 2022/05/19 PubMed PMID: 35583085. doi:10.1002/pd.6157

Wagner, T., Wirth, J., Meyer, J., Zabel, B., Held, M., Zimmer, J., et al. (1994). Autosomal sex reversal and campomelic dysplasia are caused by mutations in and around the SRY-related gene SOX9. *Cell* 79 (6), 1111–1120. Epub 1994/12/16 PubMed PMID: 8001137. doi:10.1016/0092-8674(94)90041-8

Zhen, L., Pan, M., Han, J., Yang, X., Liao, C., and Li, D. Z. (2015). Increased first-trimester nuchal translucency associated with thanatophoric dysplasia type 1. *J. Obstet. Gynaecol.* 35 (7), 685–687. Epub 2015/02/12 PubMed PMID: 25671245. doi:10.3109/01443615.2015.1006593

frontiers | Frontiers in Genetics

TYPE Brief Research Report
PUBLISHED 26 September 2022
DOI 10.3389/fgene.2022.994455

OPEN ACCESS

EDITED BY
Aleksandra Jezela-Stanek,
National Institute of Tuberculosis and Lung Diseases, Poland

REVIEWED BY
Brigitte Strizek,
University Hospital Bonn, Germany
Izabela Laczmanska,
Wroclaw Medical University, Poland

*CORRESPONDENCE
Hanna Moczulska,
hanna.moczulska@umed.lodz.pl

SPECIALTY SECTION
This article was submitted to Genetics of Common and Rare Diseases, a section of the journal Frontiers in Genetics

RECEIVED 14 July 2022
ACCEPTED 01 September 2022
PUBLISHED 26 September 2022

CITATION
Moczulska H, Pietrusinski M, Zezawska K, Serafin M, Skoczylas B, Jachymski T, Wojda K, Sieroszewski P and Borowiec M (2022), Cases of tetrasomy 9p and trisomy 9p in prenatal diagnosis—Analysis of noninvasive and invasive test results.
Front. Genet. 13:994455.
doi: 10.3389/fgene.2022.994455

Cases of tetrasomy 9p and trisomy 9p in prenatal diagnosis—Analysis of noninvasive and invasive test results

Hanna Moczulska[1]*, Michal Pietrusinski[1], Karolina Zezawska[1], Marcin Serafin[1], Beata Skoczylas[1], Tomasz Jachymski[2], Katarzyna Wojda[2], Piotr Sieroszewski[2] and Maciej Borowiec[1]

[1]Department of Clinical Genetics, Medical University of Lodz, Lodz, Poland, [2]Department of Fetal Medicine and Gynecology, Medical University of Lodz, Lodz, Poland

Objective: Tetrasomy 9p and trisomy 9p are rare chromosomal aberrations. The phenotypes of tetrasomy 9p and trisomy 9p are variable. Most cases are diagnosed in the postnatal period. The study aims to analyze the prenatal phenotype of tetrasomy 9p and trisomy 9p in terms of ultrasound and screening tests.

Methods: A set of 1573 prenatal tests performed from 2016 to 2021 was reviewed to identify all cases with trisomy 9p and tetrasomy 9p. In four cases with 9p gain, non-invasive and invasive test results were analyzed.

Results: Four cases with the 9p gain were diagnosed in the prenatal period: two cases with tetrasomy 9p and two cases with trisomy 9p. Nasal bone hypoplasia and ventriculomegaly are common features of 9p gain. In two out of four cases with the 9p gain, an increased risk of trisomy 21 was found in the combined first-trimester screening test.

Conclusion: Trisomy 9p and tetrasomy 9p are characterized by a variable phenotype in the prenatal period, manifesting in genetically abnormal fetuses. The tetrasomy 9p and trisomy 9p may suggest trisomy 21 in the first trimester.

KEYWORDS

tetrasomy 9p, trisomy 9p, prenatal diagnosis, amniocentesis, microarrary

Introduction

Tetrasomy 9p is a rare chromosomal aberration caused by the presence of four copies of the short arm of chromosome 9. The extra two copies form an additional isochromosome. Most cases of tetrasomy 9p occur *de novo* during maternal meiosis II nondisjunction (Dutly et al., 1998). The short arm is duplicated and the long arm is lost.

About 60 cases of tetrasomy 9p have been published, including over 20 prenatal cases (Vinkšel et al., 2019). Individuals with tetrasomy 9p demonstrated brain, heart, and genitourinary system malformations. Additionally, facial dysmorphia and intellectual disability were observed in patients with tetrasomy 9p. Fewer and less severe abnormalities were observed in cases with mosaicism (Chen et al., 2014). Symptoms vary in affected individuals, depending on the type and percentage of cells containing tetrasomy 9p. A prenatal diagnosis of mosaic tetrasomy 9p is rare. A false negative result in pregnancies with fetal mosaic tetrasomy 9p may be obtained, because the mosaic level of tetrasomy 9p may decrease after long-term tissue culture (Chen et al., 2014).

The phenotype of trisomy 9p is milder. More than 150 cases of trisomy 9p have been described. Most cases with trisomy 9p demonstrate a parental reciprocal translocation between chromosome nine and another autosome. In 9p trisomy, duplication may involve part of the short arm, the whole short arm, or the short arm, and part of the long arm of chromosome 9. The symptoms of 9p trisomy may be similar in affected individuals, regardless of the size of the duplicate 9p part. Trisomy 9p is usually diagnosed in the postnatal period (Guilherme et al., 2014). Little information has been published about the fetal phenotype of trisomy 9p; however, it is likely that trisomy 9 has a milder phenotype that does not allow detection during pregnancy.

As gains in 9p can be diagnosed invasively with karyotyping or aCGH and not by routine screening tests, the aim of our study was to analyze the prenatal phenotype of cases with trisomy 9p and tetrasomy 9p in ultrasound and screening tests.

Materials and methods

A sample of 1573 prenatal tests (1409 amniocentesis and 164 chorionic villus sampling) performed in the Department of Clinical Genetics of the Medical University of Lodz from 2016 to 2021 were reviewed to identify cases with trisomy 9p and tetrasomy 9p. The search identified four cases with 9p gain; in these cases, non-invasive and invasive test results were analyzed. In addition, a review of the literature was performed.

All prenatal genetic tests were ordered in response to a diagnosis of high-risk pregnancy in the Department of Clinical Genetics and the Department of Fetal Medicine and Gynecology of the Medical University of Lodz. The study itself was conducted in a tertiary referral center. The study group comprised women at high risk of having a child with a genetic disease. All patients were Caucasian. The patients were tested in the National Health System's prenatal screening program. The criteria for inclusion in the prenatal testing program comprises any of the following: the age above 35 years, the occurrence of a chromosomal aberration in the previous fetus or child, structural chromosomal aberration in the mother or father of the fetus, a significantly increased risk of having a child with a monogenic or multifactorial disease, abnormal fetal ultrasound or biochemical tests results that indicate increased the risk of chromosomal abnormalities or fetal abnormalities. Detailed ultrasound examinations were performed in all cases. In most cases, fetal echocardiography was performed, especially in cases of suspected fetal heart defects, in fetuses with non-cardiac defects, fetal chromosomal abnormalities, and in cases with a family history of heart defects. All scans were carried out by certified sonographers (certificates of the Foetal Medicine Foundation and the Polish Society of Gynaecologists and Obstetricians). Non-invasive tests consisted of the combined test (reimbursed in the National Health System's prenatal screening program) and the non-invasive prenatal screening testing NIPT (not reimbursed in Poland). Invasive procedures were indicated by abnormal fetal ultrasound, high risk of aneuploidy in screening tests, or history indicating an increased risk of genetic disease in the fetus. Fetal material was collected by amniocentesis or chorionic villus sampling. In each case, the clinical geneticist selected the appropriate genetic test. In our department, the first-line test is aCGH (array-based comparative genomic hybridization). In selected cases, the diagnosis is completed by an assessment of karyotype or molecular tests. aCGH was performed using Agilent, GenetiSure Pre-Screen Kit 8x60K with a resolution of approximately 0.50 Mb. According to standard protocols, samples were cultured for classical cytogenetic analysis. The chromosomes obtained in the metaphase were subjected to Giemsa staining after trypsin treatment and analyzed on the Cytovision karyotyping platform (Cytovision DM2500) (Caspersson et al., 1968; Sumner, 1982). Karyotype and aCGH results are described according to the International System for Human Cytogenomic Nomenclature (ISCN 2020) (Liehr, 2021). Schematic drawings of the observed chromosomal aberrations for all 4 cases are demonstrated in Figure 1. The study was conducted according to the Declaration of Helsinki on human subject research. The participants gave their written informed consent authorizing us to perform genetic tests and use the data for research and education.

Results

Four cases of 9p gain were diagnosed in the prenatal period: two cases with tetrasomy 9p and two cases with trisomy 9p (one case had an additional 22q11 duplication). Table 1 contains the prenatal sonographic features for the four described cases and other cases from the literature.

Case 1

A 32-year-old gravida, G3P1A1 (gravida, para, abortus), underwent amniocentesis at 16 weeks of gestation because of a

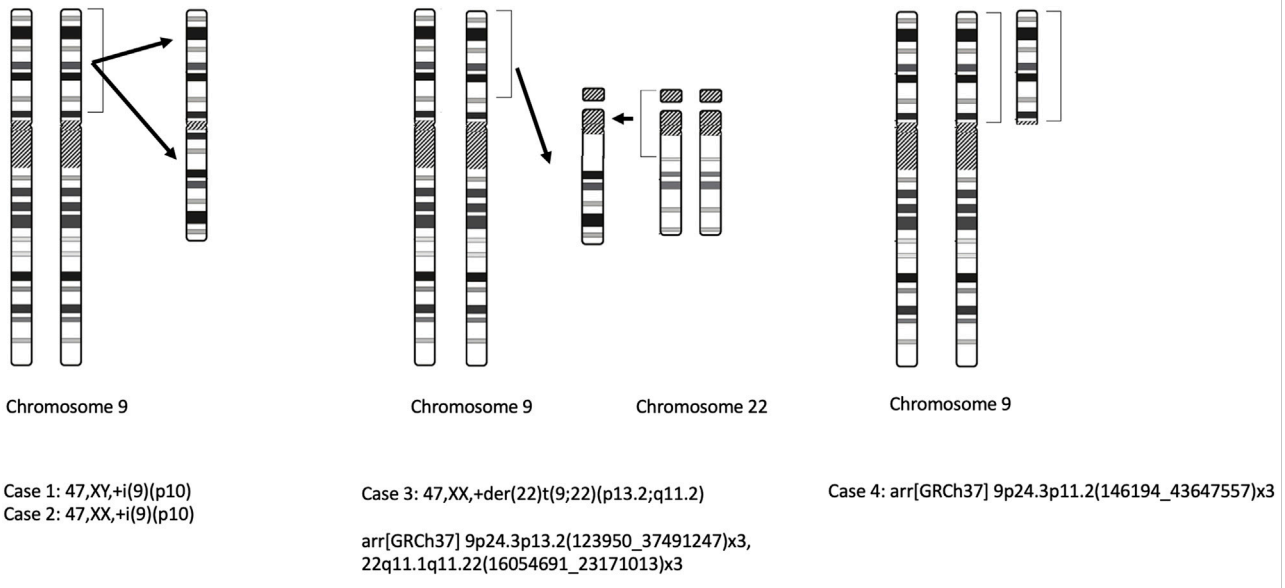

FIGURE 1
Schematic drawings of the observed chromosomal aberrations (case 1, 2, 3, 4).

high risk of fetal trisomy 21. There was no family history of congenital malformations. The nuchal translucency (NT) measured 3.0mm, and the nasal bone was absent. The combined first-trimester screening revealed a high risk for Down syndrome 1:35 [PAPP-A (pregnancy-associated plasma protein-A) 0.57 MoM (multiple of the median); BhCG (the β-subunit of human chorionic gonadotropin) 0.46 MoM]. NIPT (non-invasive prenatal testing) indicated a low risk of trisomy 21, 18, and 13. Amniocentesis was performed at 16 weeks of gestation. Fetal aCGH demonstrated 9p24.3p13.1 gain: arr [GRCh37] 9p24.3p11.2(146194_43647557)x3. Fetal karyotype identified a complete tetrasomy of the short arm of chromosome 9 47,XY,+i(9)(p10) (Liehr, 2021). Second-trimester sonography (19 weeks of gestation) showed nasal bone hypoplasia (4.4mm; <1st percentile), cleft lip and palate, abnormal posterior fossa (Dandy-Walker malformation), ventriculomegaly (posterior ventricle Vp 10.3 mm), ventricular septal defect, and humerus and femur shortening (humerus length HL 11th percentile; femur length FL 9th percentile). The pregnancy was terminated. No postmortem examination was performed.

Case 2

33-year-old gravida, G1P0A0, was consulted in the course of the first gestation. She was exposed to harmful medications for atopic dermatitis in early pregnancy—tetracycline and retinoid derivatives. The family and medical histories were unremarkable.

Medical data from the first trimester were unavailable, the patient reported that the ultrasound result was normal, and the combined test was not performed. Second-trimester sonography (18 weeks of gestation) demonstrated multiple abnormalities: agenesis of the corpus callosum, ventriculomegaly (Vp 11 mm), abnormal posterior fossa (Dandy-Walker malformation), bilateral cleft lip and palate, absent nasal bones, and retrognathia. In addition, pericardial effusion, increased renal echogenicity and pyelectasis, and clenched hands were found. Diagnostic amniocentesis was performed. Fetal karyotype showed following results—47,XX,+i(9)(p10). The pregnancy was terminated. No postmortem examination was performed.

Case 3

A 32-year-old gravida, G2P2A1, underwent amniocentesis at 19 weeks of gestation because of the high risk of fetal trisomy 21 and multiple malformations. There was no family history of congenital disabilities. At 13 weeks of pregnancy, an ultrasound examination revealed absent nasal bone, tricuspid regurgitation, and bradycardia (fetal heart rate 134/min.). The combined first-trimester screening revealed a high risk for Down syndrome 1:47 (PAPP-A 0.88 MoM; BhCG 4.36 MoM). NIPT indicated a low risk of trisomy 21, 18, and 13. The scope of NIPT included risk assessment for trisomy 21, trisomy 18, trisomy 13 and sex chromosomal abnormalities. At that time, the patient decided against an invasive procedure. Second-trimester sonography demonstrated ventriculomegaly (Vp 10 mm), nasal bone

TABLE 1 Prenatal sonographic features of four described cases and cases from the literature.

		First trimester	Second and third trimester									
			Ventriculo megaly	DWM	CCA	CLP	NB hypoplasia	Micro gnathia	Cardiac anomaly	Limb Deformation	GU anomaly	FGR
1	Case 1—tetrasomy 9p	↑ NT, NB(-)	x	x		x	x		x	x	x	x
2	Case 2—tetrasomy 9p	NA	x	x	x	x	x	x				
3	Case 3—trisomy 9p + dup 22q11	NB(-)	x	x			x		x	x	x	
4	Case 4—trisomy 9p	normal NT, NB	x							x		
5	Cazorla Calleja et al. Cazorla Calleja et al., (2003)—tetrasomy 9p	NA	x									x
6	Deurloo et al. Deurloo et al., 2004—tetrasomy 9p	NA	x	x							x	
7	Dhandha et al. Dhandha et al., 2002 case 1—tetrasomy 9p	NA	x	x		x						x
8	Dhandha et al. (Dhandha et al., 2002) case 2—tetrasomy 9p	NA				x			x	x	x	x
9	Dhandha et al. Dhandha et al., 2002 case 3—tetrasomy 9p	NA		x							x	x
10	Di Vera et al. di Vera et al., 2008—tetrasomy 9p	↑ NT	x	x		x			x		x	x
11	Dutly et al. Dutly et al., 1998 case 1– tetrasomy 9p	NA				x						x
12	Dutly et al. Dutly et al., 1998 case 2– tetrasomy 9p	NA								x		x
13	Hengstschlager et al. Hengstschläger et al., 2004—tetrasomy 9p	NA		x					x	x		
14	Jalal et al. Jalal et al., 1991—tetrasomy 9p	NA	x			x				x	x	
15	Khattabi et al. Zaghi et al., 2022 case 1—tetrasomy 9p	↑ NT, NB(-), CLP										
16	Khattabi et al. Khattabi et al., 2015 case 2—tetrasomy 9p	NA	x	x	x						x	x
17	Khattabi et al. Khattabi et al., 2015 case 3—tetrasomy 9p	↑ NT										
18	Kok Kilic et al. Kok Kilic et al., 2022—tetrasomy 9p	↑ NT	x			x		x	x			
19	Lazebnik et al. Lazebnik et al., 2015—tetrasomy 9p	normal NT, NB		x	x			x		x		x
20	McDowall et al. McDowall et al., 1989—tetrasomy 9p	NA	x	x	x	x						
21	Nakamura-Pereira et al. Nakamura-Pereira et al., 2009—tetrasomy 9p	↑ NT	x	x		x		x		x	x	
22	Podolsky et al. Podolsky et al., 2011—tetrasomy 9p	↑ NT, NB(-)							x			
23	Schaefer et al. Schaefer et al., (1991)—tetrasomy 9p	NA	x								x	
24	Tan et al. Tan et al., 2007—tetrasomy 9p	NA				x				x		x
25	Tang et al. Tang et al., (2004)—tetrasomy 9p	NA	x			x				x	x	
26	Vinksel et al. Vinkšel et al., 2019—tetrasomy 9p	↑ NT				x					x	
27	Wang et al. Wang et al., 2015—tetrasomy 9p	NA							x			

NT, nuchal translucency; NB, nasal bone; TR, tricuspid regurgitation; DWM, Dandy-Walker malformation; CCA, corpus callosum agenesis; GU, genitourinary; FGR, foetal growth restriction; CLP, cleft lip and palate; NA, not available

10.3389/fgene.2022.994455

hypoplasia, and ARSA (aberrant right subclavian artery). There was also suspicion of corpus callosum partial agenesis and Dandy-Walker malformation. At 19 weeks the patient underwent amniocentesis. After sampling the amniotic fluid, aCGH was performed. The following aberrations were revealed: arr[GRCh37] 9p24.3p13.2(123950_37491247) x3,22q11.1q11.22(16054691_23171013)x3. Fetal karyotype was not assessed due to cell culture failure. Sonography at 22 weeks showed Dandy-Walker malformation, mild ventriculomegaly (Vp 10 mm), hypoplasia of corpus callosum, nasal bones hypoplasia (3.9mm; <1st percentile), and shortening of the humerus and femur (FL 35mm; 3rd percentile, HL 31mm; 2nd percentile). Moreover, tricuspid regurgitation and pulmonary stenosis (Vmax = 95 cm/s) were detected.

At 28 and 32 weeks, subsequent examination showed mild pulmonary stenosis (Vmax = 105 cm/s), previously reported abnormalities in the brain, mild renal pelvis dilatation (5.5 mm), nasal bone hypoplasia (5.3mm; <1st percentile), long bones shortening (FL 35mm; 3rd percentile, HL 44mm; 1st percentile) and polyhydramnios (amniotic fluid index - AFI 30 cm). The baby was born in the 39th week of pregnancy, Apgar 9/9, weight 3000g and length 51 cm. The newborn karyotype revealed an additional derivative chromosome: 47,XX,+der (22)t (9;22) (p13.2;q11.2)dmat. The mother of the child was a carrier of a balanced translocation: 46,XX,t(9;22)(p13.2;q11.2). The father's karyotype was normal: 46,XY.

Case 4

A 28-year-old, G3P1A1, was referred to the clinic for suspected congenital fetal defects in second-trimester sonography. First-trimester sonography was normal. The combined first-trimester screening revealed a low risk for trisomy 21, 18, and 13 (PAPP-A 0.43 MoM; BhCG 1.19 MoM); risk for trisomy 21 1:1519, risk for trisomy 18 < 1:20000 and risk for trisomy 13 1:2275. At 21 weeks of gestation, bilateral ventriculomegaly (Vp 11.8 mm), club foot, and fetal growth restriction (10th percentile) were detected. Amniocentesis was performed at 24 weeks of gestation. aCGH study demonstrated trisomy: arr[GRCh37] 9p24.3p11.2 (146194_43647557)x3 (43.5 Mbp). Negative test results for cytomegalovirus (CMV) and *Toxoplasma gondii* were obtained. Parents reported that the delivery was at 39 weeks, and genetic testing in the newborn confirmed prenatal diagnosis.

Discussion

Our paper presents two prenatal cases of tetrasomy 9p and two cases of trisomy 9p. Tetrasomy 9p is characterized by a variable phenotype in the prenatal period (Dhandha et al., 2002; Vinkšel et al., 2019). The fetal phenotype of trisomy 9p is poorly described in the literature. Leichtman et al. described phenotypic overlap between tetrasomy 9p and trisomy 9p, and noted that tetrasomy 9p presents a more severe phenotype. The spectrum of symptoms may be continuous between tetrasomy 9p, mosaic tetrasomy 9p, and trisomy 9p. The phenotype may depend on the gene dosage effect (Leichtman et al., 1996). Our study indicates a similar relationship, with cases with tetrasomy 9p having a more severe phenotype (cases 1 and 2).

The clinical data of all the prenatal cases with tetrasomy 9p, plus our two cases with tetrasomy 9p and our two cases with 9p trisomy, are given in Table 1. Comparing cases from the literature is challenging, as they have been published in the last 10–20 years, and the quality of ultrasound examinations has increased significantly during this time. Nevertheless, the table shows that the most common defects in fetuses with tetrasomy 9p are ventriculomegaly, Dandy-Walker malformation, and cleft lip/palate (Table 1). These defects are quite unspecific and can be found in many genetically abnormal fetuses.

Brain defects are often reported in fetuses with tetrasomy 9p, with the most common abnormalities being ventriculomegaly and Dandy-Walker malformation. Deurloo et al. suggested that Dandy-Walker malformation may be a marker of tetrasomy 9p (Deurloo et al., 2004). In our study, all cases had ventriculomegaly, and three out of four had Dandy-Walker malformation. Agenesis of the corpus callosum is also observed in fetuses with tetrasomy 9p (McDowall et al., 1989; Lazebnik and Cohen, 2015). Two cases in our study demonstrated corpus callosum hypoplasia/agenesis (cases 2 and 3).

In cases of tetrasomy 9p, fetal facial dysmorphia consists of cleft lip and palate, micrognathia, and abnormal facial profile. Hypertelorism is often found in postnatal diagnosis (Jalal et al., 1991). Until now, binocular distance (BOD) has not been studied in prenatal cases with tetrasomy 9p, nor were the nasal bones. Podolsky et al. presented one case with the absence of nasal bone as a marker of tetrasomy 9p (Podolsky et al., 2011). Zaghi et al. described one case with tetrasomy 9p and absent nasal bone (Zaghi et al., 2022). Khattabi et al. presented a case with tetrasomy 9p and absent nasal bone diagnosed in the first trimester (Khattabi et al., 2015). In our study, three of the four fetuses had nasal bone hypoplasia. In two cases, nasal bone hypoplasia was diagnosed in the first trimester (cases 1 and 3).

Congenital heart defects are observed in 30% of fetuses with tetrasomy 9p, with the most common being defects in the ventricular septal and common atrioventricular canal, and complex heart defects (Dhandha et al., 2002; Kok Kilic et al., 2022). Interestingly, a persistent left superior vena cava is often seen, which may be the only symptom of tetrasomy 9p. Wang et al. presented a prenatal diagnosis of mosaic tetrasomy 9p in a fetus with isolated persistent left superior vena cava (Wang et al., 2015).

Defects of the genitourinary system are observed in 43% of cases with tetrasomy 9p. The severity of the lesions varies significantly from mild pyelectasia to bilateral multicystic dysplastic kidney. The amount of amniotic fluid is often abnormal and polyhydramnios is mainly observed (Tan et al., 2007). Oligohydramnios is found in fetuses with tetrasomy 9p and severe urinary tract defects (Schaefer et al., 1991).

The abnormalities caused by tetrasomy 9p were usually found in the second or third trimester. Single reports of tetrasomy 9p have been reported after first-trimester diagnosis (Nakamura-Pereira et al., 2009; Kok Kilic et al., 2022). Fortunately, modern ultrasound technology allows faster and more accurate early diagnosis of developmental abnormalities. In our group, nuchal translucency was increased in one case with 9p gain, and nasal bone hypoplasia was observed in three cases: two cases were diagnosed in the first trimester. A combined first-trimester screening test indicated a high risk of trisomy 21 in two fetuses (case 1, case 3). Our findings suggest that the clinical picture of the 9p gain in the first trimester may suggest the most common trisomies. Therefore invasive testing should be recommended in cases with a high risk for trisomy 21 (>1: 100) and normal NIPT, including aCGH. Common features include increased NT, absence of nasal bones, tricuspid regurgitation, and abnormal first-trimester maternal serum screening test. Our cases demonstrated decreased levels of PAPP-A (0.57 MoM, 0,88 MoM and 0.43 MoM) and variable free B-hCG levels (0.46 MoM, 4.3 MoM and 1.19 MoM). Khattabi et al. described a case with tetrasomy 9p in which maternal serum screening indicated a high risk of trisomy 21 (Khattabi et al., 2015); however, Lazebnik et al. presented a prenatal case with tetrasomy 9p with a low risk for trisomy 21, 18, and 13 (serum analytes: 1.11 MoM PAPP-A and 1.75 MoM BhCG) (Lazebnik and Cohen, 2015). The relationship between first-trimester maternal screening and the fetal 9p gain has not been investigated; as such, more cases are needed to thoroughly analyze the relationship between PAPP-A and BhCG levels and the fetal 9p gain.

Non-invasive prenatal testing (NIPT) is not routinely used in the prenatal screening of trisomy 9p and tetrasomy 9p, and hence few publications discuss this possibility. Wang et al. presented a case with mosaic tetrasomy 9p in the fetus, in which NIPT revealed "extra" genetic material derived from chromosome 9 (Wang et al., 2015). The first case of maternal mosaic tetrasomy 9p being incidentally detected on NIPT was reported by Shu et al.; in this case, NIPT was performed twice and both results revealed multiple chromosomal aberrations including elevation in DNA from chromosome 9p. The scope of NIPT included risk assessment for trisomy 21, trisomy 18, trisomy 13, sex chromosomal abnormalities, and genome-wide chromosomal aberrations at a resolution of 3 Mb or above. Amniocentesis was performed and a normal fetal aCGH result was obtained. Maternal blood karyotype revealed mos 47,XX,+dic(9;9)(q21.1;q21.1)[24]/46,XX[9], maternal fibroblasts were not examined. Subtelomeric multiplex ligation-dependent probe amplification (MLPA) was performed on uncultured maternal blood and on the maternal buccal swab. The blood test confirms mosaic 9p duplication, and the buccal swab result was normal. As the amniocentesis was normal, no clinical description or genetic testing was performed on the child after delivery (Shu et al., 2021). This case confirms that some cases with mosaic tetrasomy 9p may go undiagnosed in the general population.

In our study, the karyotype of case 3 shows the presence of derivative chromosome 22: 47,XX,+der(22)t(9;22)(p13.2;q11.2) dmat. 22q11.2 duplication syndrome is a condition characterized by variable clinical phenotype that includes heart defects, urogenital abnormalities, velopharyngeal insufficiency with or without cleft palate, mild learning difficulties with some individuals being essentially normal. The duplicated region contains 30 to 40 genes, however for many of these genes, little is known about their function. Genes that may influence the phenotype may be similar to genes involved in the same deleted region in DiGeorge syndrome (DGS; OMIM 188400) and velocardiofacial syndrome (VCFS; OMIM 192430) (mainly *TBX1*, *HIRA*, *CRKL*).

Trisomy 9p and tetrasomy 9p can be diagnosed using classical cytogenetic analysis and aCGH. The karyotype identifies the structure of a chromosomal aberration. aCGH offers higher test resolution than traditional G-band karyotyping and allows for more precise localization of the chromosomal breakpoints. Nowadays whole exome sequencing (WES) is sometimes performed as a first-line genetic test. WES can also diagnose chromosomal aberrations; however, it is not a good tool to diagnose them. The biggest advantage of microarrays over WES methods is the quality of the data post-processing in detecting specific copy number variations (CNVs). This is because WES methods mimic a traditional microarray method when so-called "pseudo probes" are created from the next-generation sequencing (NGS) reads to establish a log2 ratio value, which can then be used to estimate the actual copy number. In contrast, microarrays have "real probes" and during experiments, the signal intensity of these probes is compared directly to reference probes. Thus microarrays offer better overall genomic coverage and can detect intronic and intergenic alterations.

Conclusion

Trisomy 9p and tetrasomy 9p are characterized by a variable phenotype in the prenatal period which can be found in many genetically abnormal fetuses. The clinical picture of the 9p gain in the first trimester may suggest trisomy 21.

Data availability statement

The raw data supporting the conclusion of this article will be made available by the authors, without undue reservation.

Ethics statement

Ethical review and approval was not required for the study on human participants in accordance with the local legislation and institutional requirements. The patients/participants provided their written informed consent to participate in this study.

Author contributions

HM, MP, KZ, PS and MB contributed to conception and design of the study. HM, MS, TJ, KW, BS, PS, MB organized the database. HM wrote the first draft of the manuscript. MP, AZ wrote sections of the manuscript. All authors contributed to manuscript revision, read, and approved the submitted version.

Conflict of interest

The authors declare that the research was conducted in the absence of any commercial or financial relationships that could be construed as a potential conflict of interest.

Publisher's note

All claims expressed in this article are solely those of the authors and do not necessarily represent those of their affiliated organizations, or those of the publisher, the editors and the reviewers. Any product that may be evaluated in this article, or claim that may be made by its manufacturer, is not guaranteed or endorsed by the publisher.

References

Caspersson, T., Farber, S., Foley, G. E., Kudynowski, J., Modest, E. J., Simonsson, E., et al. (1968). Chemical differentiation along metaphase chromosomes. *Exp. Cell Res.* 49, 219–222. doi:10.1016/0014-4827(68)90538-7

Cazorla Calleja, M. R., Verdú, A., and Félix, W. (2003). Dandy-Walker malformation in an infant with tetrasomy 9p. *Brain Dev.* 25, 220–223. doi:10.1016/s0387-7604(02)00211-5

Chen, C. P., Wang, L. K., Chern, S. R., Wu, P. S., Chen, Y. T., Kuo, Y. L., et al. (2014). Mosaic tetrasomy 9p at amniocentesis: Prenatal diagnosis, molecular cytogenetic characterization, and literature review. *Taiwan. J. Obstet. Gynecol.* 53, 79–85. doi:10.1016/j.tjog.2013.12.002

Deurloo, K. L., Cobben, J. M., Heins, Y. M., de Ru, M., Wijnaendts, L. C. D., and van Vugt, J. M. G. (2004). Prenatal diagnosis of tetrasomy 9p in a 19-week-old fetus with dandy-walker malformation: A case report. *Prenat. Diagn.* 24, 796–798. doi:10.1002/pd.850

Dhandha, S., Hogge, W. A., Surti, U., and McPherson, E. (2002). Three cases of tetrasomy 9p. *Am. J. Med. Genet.* 113, 375–380. doi:10.1002/ajmg.b.10826

di Vera, E., Liberati, M., Celentano, C., Calabrese, G., Guanciali-Franchi, P. E., Morizio, E., et al. (2008). Rhombencephalosynapsis in a severely polymalformed fetus with non-mosaic tetrasomy 9p, in intracytoplasmic-sperm-injection pregnancy. *J. Assist. Reprod. Genet.* 25, 577–580. doi:10.1007/s10815-008-9257-7

Dutly, F., Balmer, D., Baumer, A., Binkert, F., and Schinzel, A. (1998). Isochromosomes 12p and 9p: Parental origin and possible mechanisms of formation. *Eur. J. Hum. Genet.* 6, 140–144. doi:10.1038/sj.ejhg.5200168

Guilherme, R. S., Meloni, V. A., Perez, A. B. A., Pilla, A. L., de Ramos, M. A. P., Dantas, A. G., et al. (2014). Duplication 9p and their implication to phenotype. *BMC Med. Genet.* 15, 142. doi:10.1186/s12881-014-0142-1

Hengstschläger, M., Bettelheim, D., Drahonsky, R., Repa, C., Deutinger, J., and Bernaschek, G. (2004). Prenatal diagnosis of tetrasomy 9p with Dandy-Walker malformation. *Prenat. Diagn.* 24, 623–626. doi:10.1002/pd.933

Jalal, S. M., Kukolich, M. K., Garcia, M., Benjamin, T. R., and Day, D. W. (1991). Tetrasomy 9p: An emerging syndrome. *Clin. Genet.* 39, 60–64. doi:10.1111/j.1399-0004.1991.tb02986.x

Khattabi, E. L., Jaillard, L., Andrieux, S., Pasquier, J., Perrin, L., Capri, L., et al. (2015). Clinical and molecular delineation of Tetrasomy 9p syndrome: Report of 12 new cases and literature review. *Am. J. Med. Genet. A* 167, 1252–1261. doi:10.1002/ajmg.a.36932

Kok Kilic, G., Pariltay, E., Karaca, E., Durmaz, B., Ekici, H., Imamoglu, M., et al. (2022). Prenatal diagnosis of a case with tetrasomy 9p confirmed by cytogenetics, FISH, microarray analysis and review. *Taiwan. J. Obstet. Gynecol.* 61, 122–126. doi:10.1016/j.tjog.2021.10.003

Lazebnik, N., and Cohen, L. (2015). Prenatal diagnosis and findings of tetrasomy 9p. *J. Obstet. Gynaecol. Res.* 41, 997–1002. doi:10.1111/jog.12706

Leichtman, L. G., Zackowski, J. L., Storto, P. D., and Newlin, A. (1996). Non-mosaic tetrasomy 9p in a liveborn infant with multiple congenital anomalies: Case report and comparison with trisomy 9p. *Am. J. Med. Genet.* 63, 434–437. doi:10.1002/(SICI)1096-8628(19960614)63:3<434::AID-AJMG4>3.0.CO;2-R

Liehr, T. (2021). International system for human cytogenetic or cytogenomic nomenclature (ISCN): Some thoughts. *Cytogenet. Genome Res.* 161, 223–224. doi:10.1159/000516654

McDowall, A. A., Blunt, S., Berry, A. C., and Fensom, A. H. (1989). Prenatal diagnosis of a case of tetrasomy 9p. *Prenat. Diagn.* 9, 809–811. doi:10.1002/pd.1970091110

Nakamura-Pereira, M., do Cima, L. C., Llerena, J. C., Guerra, F. A., and Peixoto-Filho, F. M. (2009). Sonographic findings in a case of tetrasomy 9p associated with increased nuchal translucency and Dandy-Walker malformation. *J. Clin. Ultrasound* 37, 471–474. doi:10.1002/jcu.20612

Podolsky, R., Saltzman, D., Auerbach, M., and Roman, A. S. (2011). Absent nasal bone as a marker of tetrasomy 9p. *Prenat. Diagn.* 31, 1313. doi:10.1002/pd.2877

Schaefer, G. B., Domek, D. B., Morgan, M. A., Muneer, R. S., and Johnson, S. F. (1991). Tetrasomy of the short arm of chromosome 9: Prenatal diagnosis and further delineation of the phenotype. *Am. J. Med. Genet.* 38, 612–615. doi:10.1002/ajmg.1320380422

Shu, W., Cheng, S. S. W., Xue, S., Chan, L. W., Soong, S. I., Kan, A. S. Y., et al. (2021). First case report of maternal mosaic tetrasomy 9p incidentally detected on non-invasive prenatal testing. *Genes* 12, 370. doi:10.3390/genes12030370

Sumner, A. T. (1982). The nature and mechanisms of chromosome banding. *Cancer Genet. Cytogenet.* 6, 59–87. doi:10.1016/0165-4608(82)90022-X

Tan, Y. Q., Chen, X. M., Hu, L., Guan, X. Y., and Lu, G. X. (2007). Prenatal diagnosis of nonmosaic tetrasomy 9p by microdissection and FISH: Case report. *Chin. Med. J.* 120, 1281–1283. doi:10.1097/00029330-200707020-00016

Tang, W., Boyd, B. K., Hummel, M., and Wenger, S. L. (2004). Prenatal diagnosis of tetrasomy 9p. *Am. J. Med. Genet. A* 126A, 328. doi:10.1002/ajmg.a.20511

Vinkšel, M., Volk, M., Peterlin, B., and Lovrecic, L. (2019). A systematic clinical review of prenatally diagnosed tetrasomy 9p. *Balk. J. Med. Genet.* 22, 11–20. doi:10.2478/bjmg-2019-0012

Wang, H., Xie, L. S., Wang, Y., and Mei, J. (2015). Prenatal diagnosis of mosaic tetrasomy 9p in a fetus with isolated persistent left superior vena cava. *Taiwan. J. Obstet. Gynecol.* 54, 204–205. doi:10.1016/j.tjog.2014.12.005

Zaghi, M., Janssens, K., Hectors, W., Loquet, P., and Blaumeiser, B. (2022). Tetrasomy 9p, a prenatal challenge: Two novel cases. *Reprod. Med.* 3, 42–49. doi:10.3390/reprodmed3010005

frontiers | Frontiers in Genetics

TYPE Original Research
PUBLISHED 28 September 2022
DOI 10.3389/fgene.2022.992073

OPEN ACCESS

EDITED BY
Aleksandra Jezela-Stanek,
National Institute of Tuberculosis and Lung Diseases, Poland

REVIEWED BY
Efthymia Vlachaki,
Aristotle University of Thessaloniki, Greece
Ling Qiu,
Peking Union Medical College Hospital (CAMS), China

*CORRESPONDENCE
Yongyi Zou,
zouyongyi@gmail.com
Yanqiu Liu,
lyq0914@126.com

†These authors have contributed equally to this work

SPECIALTY SECTION
This article was submitted to Genetics of Common and Rare Diseases, a section of the journal Frontiers in Genetics

RECEIVED 12 July 2022
ACCEPTED 08 September 2022
PUBLISHED 28 September 2022

CITATION
Luo H, Huang T, Lu Q, Zhang L, Xu Y, Yang Y, Guo Z, Yuan H, Shen Y, Huang S, Yang B, Zou Y and Liu Y (2022), Molecular prevalence of HBB-associated hemoglobinopathy among reproductive-age adults and the prenatal diagnosis in Jiangxi Province, southern central China.
Front. Genet. 13:992073.
doi: 10.3389/fgene.2022.992073

Molecular prevalence of *HBB*-associated hemoglobinopathy among reproductive-age adults and the prenatal diagnosis in Jiangxi Province, southern central China

Haiyan Luo[1,2†], Ting Huang[1,2†], Qing Lu[1,2], Liuyang Zhang[1,2], Yonghua Xu[1,2], Yan Yang[1,2], Zhen Guo[2,3], Huizhen Yuan[1,2], Yinqin Shen[1,2], Shuhui Huang[1,2], Bicheng Yang[1,2], Yongyi Zou[1,2]* and Yanqiu Liu[1,2]*

[1]Department of Medical Genetics, Jiangxi Maternal and Child Health Hospital, Nanchang, Jiangxi, China, [2]Jiangxi Key Laboratory of Birth Defect Prevention and Control, Jiangxi Maternal and Child Health Hospital, Nanchang, Jiangxi, China, [3]Department of Ultrasound, Jiangxi Maternal and Child Health Hospital, Nanchang, Jiangxi, China

Background and aims: Hemoglobinopathy associated with the *HBB* gene, with its two general subtypes as thalassemia and abnormal hemoglobin (Hb) variants, is one of the most prevalent hereditary Hb disorders worldwide. Herein we aimed to elucidate the prevalence of ß-thalassemia and abnormal hemoglobin variants and the prenatal diagnosis of the *HBB* gene in Jiangxi Province, southern central China.

Methods: Hematological indices and capillary Hb electrophoresis were conducted for 136,149 subjects who were admitted to Jiangxi Maternal and Child Health Hospital and requested for hemoglobinopathy investigation. Routine α- and ß-globin genotyping were performed by gap-polymerase chain reaction (Gap-PCR) and reverse dot-blot (RDB) hybridization for the 11,549 individuals suspected to be thalassemia carriers. For participants whose genotypes could not explain their hematological indices, further Sanger sequencing and Gap-PCR were conducted for the detection of rare or novel variants in related globin genes. Prenatal diagnosis was performed for 77 pregnant couples both carrying ß-thalassemia trait at appropriate gestational ages.

Results: Among the 11,549 subjects, 2,548 individuals were identified with *HBB*-associated hemoglobinopathy based on molecular analysis. A total of 2,358 subjects were identified as ß-thalassemia heterozygous carriers and nine cases were diagnosed as compound heterozygous ß-thalassemia. Additionally, 125 cases were detected with composite α- and ß-thalassemia and the remaining 56 individuals with abnormal Hb variants in the *HBB*. A total of 35 types of variants were identified in the *HBB* gene, including 26 types of ß-thalassemia and nine types of abnormal Hb variants. Four novel variants were

firstly reported, including one variant in *HBA2* and three variants in *HBB*. Overall, 77 prenatal samples underwent ß-thalassemia molecular diagnosis; 20 fetuses were identified with normal ß-thalassemia genotypes, 30 fetuses as ß-thalassemia heterozygotes, 11 as homozygotes, and 16 as compound heterozygotes in *HBB*.

Conclusion: We have demonstrated a relatively high prevalence rate at 1.872% of ß-hemoglobinopathies including common and rare ß-thalassemia as well as abnormal Hb variants among large child-bearing population in the Jiangxi area of southern central China for the first time. Our data presents that prenatal diagnosis is an effective way to prevent and control birth defects of ß-thalassemia.

KEYWORDS

HBB, hemoglobinopathy, mutation spectrum, prenatal diagnosis, central China-southern central China

Introduction

Hemoglobinopathies are one of the most common monogenic diseases worldwide (Ghosh et al., 2020). In the human body, hemoglobin (Hb) is a tetramer composed of two α-like and two *ß*-like globin chains, with the main function to deliver oxygen to the tissues (Ahmed et al., 2020). *ß*-Associated hemoglobinopathy is a group of hematological diseases caused by mutations in *ß*-globin genes, including *ß*-thalassemia and structural Hb variants (Kohne, 2011). *ß*-thalassemia (β-thal) is caused by reduced output of *ß*-globin chains, known as β^{+}, or absent production of *ß*-globin chains, known as β^{0} (Origa, 2017). The altered production of normal *ß*-globin chain results in an imbalance of alpha/nonalpha chain synthesis, which is the major determinant of the clinical and hematological severity of *ß*-thal (Muncie and Campbell, 2009). The most common mutation of *ß*-thalassemia is small nucleotide variation (SNV), while a few others appear to be large deletions (Schwartz et al., 1988). The structural hemoglobin (Hb) variant, which leads to variable symptoms from almost asymptomatic to severe hemolytic anemia, is characterized by structural abnormalities caused by alteration of the globin peptide chain conformation in the *ß*-globin chains, which is typically based on single amino acid substitution resulting from a point mutation (Clarke and Higgins, 2000; Taher et al., 2018). Most individuals with heterozygous Hb variants exhibit normal hematological parameters but may display distinct Hb fractions by capillary electrophoresis (Keren et al., 2008; Altinier et al., 2013).

Despite a high prevalence in tropical and subtropical regions, *ß*-thal and structural Hb variants in *HBB* are now widely distributed worldwide because of population migration, and show abundant genetic diversity (Weatherall and Clegg, 2001). So far, there have been over 947 variants in *HBB* reported worldwide according to the online hemoglobin database (http://globin.bx.psu.edu/cgi-bin/hbvar/query_vars3). Furthermore, increasing reports on the prevalence and mutation spectrum of *ß*-hemoglobinopathy among different ethnic groups and different regions have improved the prevention of this major health problem in recent decades. China, as a country located in southeastern Asia, has high incidence of *ß*-hemoglobinopathy, especially for *ß*-thal in the southern provinces (Long et al., 2014). Many large-scale studies among the Chinese southern population, such as those from Hainan, Guangdong, Guangxi, and Fujian Province, have revealed the frequency and distribution of *ß*-thalassemia mutations in these specific geographic areas (Zhuang et al., 2020; Huang H. et al., 2021; Zhou et al., 2021; Wang et al., 2022). Several other studies have revealed the prevalence and mutation spectrum of abnormal Hb variants in some provinces of China (Lou et al., 2014; Huang et al., 2019; Xu A. et al., 2020). However, no previous study has focused on *ß*-hemoglobinopathy among large child-bearing age population in the Jiangxi area, a province located in southern central China next to Fujian and Guangdong Province.

Here, we explored the prevalence and mutation spectrum of *ß*-associated common and rare thalassemia and structural Hb variants among large-scale population of reproductive ages in Jiangxi Province, and provided prenatal diagnosis for those at risk of giving birth to a child with severe *ß*-thal intermediate or *ß*-thal major. Our work may provide a basis for genetic counseling, public education, and as a starting point to improve the prevention of *ß*-thal.

Materials and methods

Subjects

A total of 136,149 subjects of child-bearing age admitted to Jiangxi Maternal and Child Hospital for routine examination from January 2015 to December 2021 were enrolled in our study. The investigated individuals were mainly acquired from the Outpatient Department of the Assisted Reproductive Centre,

Medical Genetics Centre, Obstetrics & Gynecology Department of our hospital. All of the included individuals came from rural or urban areas in Jiangxi Province and were aged from 18 to 50 years. This study was approved by the Ethics Committees of Jiangxi Maternal and Child Health Hospital, Jiangxi Province, China. All of the medical tests were performed after obtaining informed consent from the participants.

Hematological studies and hemoglobin electrophoresis analysis

Conventional peripheral complete blood count (CBC) and capillary Hb electrophoresis were primarily screened for all the participants. Two EDTA-Na tubes with 2 ml of peripheral venous blood were obtained from each subject for routine blood examination and hemoglobin electrophoresis screening. Erythrocyte correlative indices were detected using a Sysmex XE-2100 blood analyzer (Sysmex Corporation) according to the standard operating procedure. The composition and content of hemoglobin was analyzed by a Sebia capillary electrophoresis system (Sebia, Inc.) according to the manufacturer's instructions. Participants with erythrocyte indices with mean corpuscular volume (MCV) < 82 fL and (or) corpuscular hemoglobin (MCH) values <27 pg were taken as suspected thalassemia carriers. Subjects with hemoglobin A2 (HbA2) < 2.5% and HbA2 > 3.5% were suspected as probable α-thalassemia and *ß*-thalassemia carriers, respectively. Individuals screened with abnormal hemoglobin fraction or HbF values >5% were suspected as abnormal Hb variant or rare *ß*-thalassemia carriers.

Routine thalassemia genetic analysis

A total of 11,549 subjects (female: 7,911, male: 3,638), including suspected thalassemia carriers and a few individuals who demanded genetic testing, underwent routine molecular detection for thalassemia. Firstly, 2 ml of peripheral venous blood was collected in an EDTA tube, and the genomic DNA of the peripheral venous blood was extracted using the GeneRotex Nucleic Acid Extraction System (GeneRotex, Xian, China). A NanoDrop spectrophotometer (Thermo Scientific, Wilmington, DE, United States) was used to qualify and quantify DNA. Gap-PCR and PCR-RDB (Yaneng BioSciences, Shenzhen) were used to detect three common α-thalassemia deletions (-SEA, -α3.7, and -α4.2) and three α-thalassemia point mutations (Hb Constant spring (Hb CS) (CD142, TAA > CAA), Hb Quong Sze (Hb QS) (CD125, CTG > CCG), and Hb Westmead (CD122, CAC > CAG), as well as 16 types of SNVs in *HBB*, including CD41-42 (-TCTT), CD43 (G > T), IVS-II-654 (C > T), CD17 (A > T), CD14-15 (+G), −28 (A > G), −29 (A > G), CD71-72 (+A), CD26 (G > A), IVS-I-1 (G > T), IVS-I-1 (G > A), CD27-28 (+C), IVS-I-5 (G > C), Cap+40–43 (-AAAC), initiation codon (ATG > AGG), and CD31 (-C).

Rare and novel thalassemia genetic analyses

Gap-PCR was performed to detect six rare structural variations, including -THAI/, $-\alpha^{21.9}/$, $-\alpha^{27.6}/$, HK αα, anti4.2, *α* fusion gene for α-thal, and three rare *ß*-thal deletions, including Taiwanese, $G\gamma^{+}(A\gamma\delta\beta)^{0}$, and SEA-HPFH according to the manufacturer's protocols (Yaneng BioSciences, Shenzhen, China). Sanger sequencing was used to detect the rare or novel SNVs in *HBA1*, *HBA2,* and *HBB*. The primers used in our study were listed in Table 1.

Prenatal diagnosis

Chorionic villi sampling (CVS) in the first trimester, amniocentesis in the second trimester, and umbilical cord blood sampling in the third trimester were chosen based on the gestational age and willingness of the pregnant females. All of the fetal samples were collected from the pregnant mother under B-mode ultrasound-guidance at the appropriate gestational ages, with CVS from 12 to 14 weeks, amniocentesis from 18 to 26 weeks, and fetal blood sampling from 27 to 32 weeks. About 100 mg of villi tissue, 8 ml of amniotic fluid, or 2 ml of umbilical cord blood were collected. Extraction of fetal DNA was conducted using a QIAamp DNA Mini Kit (Qiagen, Germany) according to the manufacturer's protocols. A NanoDrop spectrophotometer (Thermo Scientific, Wilmington, DE, United States) was used to qualify and quantify the DNA.

Follow-up of pregnancy outcomes

The 77 couples were followed up by phone interview 1-year after prenatal diagnosis to record the outcomes of fetuses with severe thalassemia. Additionally, the phenotypes and development of fetuses with non-severe thalassemia were followed up 1 year after birth to validate the accuracy of the prenatal diagnosis. In our study, the mutant homozygote and double heterozygote were defined as severe forms of *ß*-thal.

Statistical analysis

Statistical analysis was performed using SPSS statistical software version 20.0 (International Business Machines Corporation). Descriptive analysis was used to show the genotype and allele frequencies in different populations. The

TABLE 1 Primers used for direct Sanger sequencing.

Primers	Sequence (5′→3′)	Length (bp)
HBA1-F	TGG AGG GTG GAG ACG TCC TG	20
HBA1-R	TCC ATC CCC TCC TCC CGC CCC TGC CTT TTC	30
HBA2-F	TGG AGG GTG GAG ACG TCC TG	20
HBA2-R	CCA TTG TTG GCA CAT TCC GG	20
HBB-F	AAC TCC TAA GCC AGT GCC AGA AGA GC	26
HBB-R	ATG CAC TGA CCT CCC ACA TTC CC	23

ratio of ß-thalassemia alleles, αβ-thalassemia, and abnormal Hb variants was calculated.

Results

Routine thalassemia genetic analysis and rare or novel thalassemia genetic analysis

Among the 11,549 subjects, 2,457 cases were detected with mutations by routine thalassemia testing, whereas the remaining 91 cases showed continuous hypochromic microcytic anemia, an increased HbA2 or HbF value, or an abnormal hemoglobin fraction by hematological screening and underwent further rare or novel thalassemia genetic analysis. Thirty individuals displaying an increased HbA2 value were identified with rare mutations in *HBB*, including CD54-58 (-TATGGGCAACCCT), -72 (T > A), codon 30 (AGG > AGC), -28(A > C), -31(A > G), SEA-HPFH, Taiwanese, IVS-I-6 (T > G), IVS-I-110 (G > A), and initiation codon ATG > GTG, with ten genotypes in all. Fifty-six individuals demonstrating abnormal hemoglobin fractions were identified as abnormal Hb variant carriers, including those with Hb J-Bangkok, Hb New York, Hb G-Taipei, Hb G-Coushatta, Hb D-Los Angeles, Hb Yaizu, Hb Deer Lodge, Hb E-Saskatoon, and Hb G-Siriraj, with a total of nine types. In addition, three individuals, all of whom showed normal HbA2 values and hematological parameters, were identified with three novel variants IVS-II-47 (G > C), IVS-II-300–308 (-A), IVS-II-806 (G > C) in *HBB*, separately. One individual were identified with the polymorphism IVS-II-81 C>T. Furthermore, one participant was identified with novel variant c.301-41_301-39delGGC in *HBA2* combined with the common ß-thal mutation IVS-II-654 (C > T).

Overall population prevalence of ß-hemoglobinopathies in the jiangxi region

In our study, 11,549 individuals were suspected cases of ß-hemoglobinopathies by hematological indices or capillary analysis, and all of them underwent further genetic analysis. A total of 2,548 cases were diagnosed with ß-hemoglobinopathy, including 2,367 cases with ß-thal, 125 cases with composite α-and ß-thal, and 56 cases with abnormal Hb variants. The overall prevalence rate of ß-hemoglobinopathies in Jiangxi Province was 1.872% (2,548/13,6149), and the prevalence rates of ß-thal, coinheritance of αβ-thal and Hb variants were 1.739% (2,367/13,6149), 0.092% (125/13,6149), and 0.041% (56/13,6149), respectively. Carriers of composite α- and ß-thal and Hb variants were detected for the first time in a large population of child-bearing adults in Jiangxi and the detailed information was listed as in Table 2.

Genotypes and mutation spectrum of ß-thal and structural Hb variants

We identified 83 genotypes in our cohort, with 34 of ß-thal, 39 of composite αβ-thal, and ten of abnormal Hb variants. Among the 2,367 subjects detected with ß-thal, we identified 26 kinds of ß-thal variants in all (Table.3). The most frequent genotype was $\beta^{IVS-II-654\ (C>T)}/\beta^{N}$, and $\beta^{CD41/42(-TTCT)}/\beta^{N}$, with a remarkable proportion of 45.42% and 22.64%, respectively. The other common genotypes were $\beta^{CD17(A>T)}/\beta^{N}$, $\beta^{-28(A>G)}/\beta^{N}$, and $\beta^{CD27/28(+C)}/\beta^{N}$, with the corresponding proportions of 10.69%, 7.52%, and 4.86%. As for the allele frequency, the four most frequent mutations were IVS-II-654 (C>T), CD41/42 (-TTCT), CD17 (A>T), and −28 (A>G), with corresponding proportions of 41.9%, 27.5%, 12.6%, and 9.1%, which accounted for 91.1% of all ß-thal mutant alleles. A total of 125 subjects

TABLE 2 Detailed constitution of ß-hemoglobinopathy among 13,6149 participants in the Jiangxi region.

Categories	Cases (n)	Ratio (%)
Heterozygous ß-thal carriers	2,358	1.732
Compound heterozygous ß-thal	9	0.007
Composite αβ-thal carriers	125	0.092
Abnormal Hb variants	56	0.041
Total	2,548	1.872

TABLE 3 Genotype constitution of *ß*-thalassemia in Jiangxi Province.

Genotypes	HGVS nomenclature	Cases (n)	Ratio (%)
IVS-II-654 (C>T)	c.316–197C>T	1,075	45.42
Codons 41/42 (-TTCT)	c.126_129delCTTT	536	22.64
Codon 17 (A>T)	c.52A>T	253	10.69
-28 (A>G)	c.-78A>G	178	7.52
Codons 27/28 (+C)	c.84_85insC	115	4.86
Codons 71/72 (+A)	c.216_217insA	45	1.90
Hb E	c.79G>A	49	2.07
-29 (A>G)	c.-79A>G	30	1.27
Codon 43 (G>T)	c.130G>T	26	1.10
CD54-58 (-TATGGGCAACCCT)	c.165_177 del TATGGGCAACCCT	13	0.55
Codons 14/15 (+G)	c.45_46insG	11	0.46
-28 (A>C)	c.-78A>C	5	0.21
Cap+40–43 (-AAAC)	c.-11_-8delAAAC	4	0.17
-31 (A>G)	c.-81A>C	3	0.13
IVS-I-1 (G>T)	c.92 + 1G>T	2	0.08
IVS-II-81 (C>T)	c.315 + 81C>T	1	0.04
IVS-II-47 (G>C)	c.315 + 47 G > C	1	0.04
IVS-II-300–308 (-A)	c.315 + 300-308delA	1	0.04
IVS-II-806 (G- > C)	c.315-45G > C	1	0.04
-72 (T>A)	c.-122T>A	1	0.04
Codon 30 (AGG>AGC)	c.93G>C	1	0.04
IVS-I-6 (T>G)	c.92 + 6T>G	1	0.04
IVS-I-110 (G>A)	c.93-21G>A	1	0.04
Initiation codon ATG>GTG	c.1A>G	1	0.04
SEA-HPFH	g.5201647_5229059del	2	0.08
Taiwanese	g.69997_71353del1357	2	0.08
-28 (A>G)/IVS-II-81 (C>T)	—	1	0.04
Hb E/Hb E	—	2	0.08
-28 (A>G)/-28 (A>G)	—	1	0.04
IVS-II-654 (C>T)/CD27/28 (+C)	—	1	0.04
IVS-II-654 (C>T)/CD 41/42 (-TTCT)	—	1	0.04
CD 41/42 (-TTCT)/CD 27/28 (+C)	—	1	0.04
IVS-II-654 (C>T)/-28 (A>G)	—	1	0.04
Hb E/IVS-I-1 (G>T)	—	1	0.04
Total	—	2,367	100

were detected as carriers of both α- and *ß*-globin variants (Table.4). Among them, 89.6% of genotypes consisted of common SNVs of the *ß*-globin gene combined with large deletions of the α-globin gene (–SEA/αα, -α3.7/αα, -α4.2/αα). Composite–SEA/αα and $\beta^{IVS-II-654\ (C>T)}/\beta^{N}$ was the most common genotype. In our study, 56 subjects were identified with silent structural Hb variants in *HBB*, with ten genotypes in total. All of these individuals displayed normal hematological indices but abnormal hemoglobin fraction by capillary electrophoresis (Table.5). Hb J-Bangkok was the most prevalent Hb variant, accounting for 42.86%, followed by Hb New York and Hb Taipei. We also identified four rare Hb variants, including Hb Yaizu, Hb Deer Lodge, Hb E-Saskatoon, and Hb G-Siriraj. Furthermore, four novel variants were identified, including one variant c.301-41_301-39delGGC in *HBA2* and three variants (c.315 + 47G>C, c.315 + 300-308delA, and c.315-45G>C) in *HBB*. The hematological characteristics of the three subjects with novel variants were shown in Table 6.

Prenatal diagnosis and postnatal follow-up outcomes

The screening strategy for pregnant or pre-pregnant couple in our study was recommended as follows: The

10.3389/fgene.2022.992073

TABLE 4 Genotypes of composite α- and ß-thalassemia in Jiangxi Region.

α-	β-	Cases (n)	Ratio (%)
$-\alpha^{3.7}/\alpha\alpha$	$\beta^{IVS-II-654\ (C>T)}/\beta^{N}$	20	16.00
--SEA/αα		18	14.40
$-\alpha^{4.2}/\alpha\alpha$		3	2.40
$\alpha^{CS}\alpha/\alpha\alpha$		3	2.40
$\alpha^{WS}\alpha/\alpha\alpha$		2	1.60
$\alpha^{QS}\alpha/\alpha\alpha$		2	1.60
$\alpha^{c.301-41\_301-39delGGC}\alpha/\alpha\alpha$		1	0.80
$-\alpha^{3.7}$/--SEA		1	0.80
--SEA/αα	$\beta^{Codons41/42\ (-TTCT)}/\beta^{N}$	14	11.20
$-\alpha^{3.7}/\alpha\alpha$		13	10.40
$-\alpha^{4.2}/\alpha\alpha$		6	4.80
$\alpha^{WS}\alpha/\alpha\alpha$		1	0.80
$\alpha^{CS}\alpha/\alpha\alpha$		1	0.80
$-\alpha^{4.2}/-\alpha^{4.2}$		1	0.80
$-\alpha^{3.7}$/--SEA		1	0.80
$\alpha^{QS}\alpha$/--SEA		1	0.80
--SEA/αα	$\beta^{Codon17(A>T)}/\beta^{N}$	3	2.40
$-\alpha^{3.7}/\alpha\alpha$		2	1.60
$-\alpha^{4.2}/\alpha\alpha$		2	1.60
$\alpha^{WS}\alpha/\alpha\alpha$		1	0.80
$\alpha^{CS}\alpha/\alpha\alpha$		1	0.80
--SEA/αα	$\beta^{-28\ (A>G)})/\beta^{N}$	4	3.20
$-\alpha^{3.7}/\alpha\alpha$		3	2.40
$-\alpha^{4.2}/\alpha\alpha$		1	0.80
$-\alpha^{3.7}$/--SEA		1	0.80
$-\alpha^{3.7}/\alpha\alpha$	β^{HbE}/β^{N}	4	3.20
$\alpha^{CS}\alpha/\alpha\alpha$		1	0.80
$-\alpha^{3.7}/-\alpha^{3.7}$		1	0.80
--SEA/αα	$\beta^{Codons27/28(+C)}/\beta^{N}$	2	1.60
$-\alpha^{3.7}/\alpha\alpha$		2	1.60
$-\alpha^{3.7}/\alpha\alpha$	$\beta^{HbE}/\beta^{\ HbE}$	1	0.80
$\alpha^{WS}\alpha/-\alpha^{3.7}$		1	0.80
--SEA/αα		1	0.80
$-\alpha^{3.7}/\alpha\alpha$	$\beta^{Codons71/72(+A)}/\beta^{N}$	1	0.80
--SEA/αα		1	0.80
--SEA/αα	$\beta^{-29\ (A>G)}/\beta^{N}$	1	0.80
--SEA/αα	$\beta^{CAP+40-43\ (-AAAC)}/\beta^{N}$	1	0.80
$-\alpha^{3.7}/\alpha\alpha$	$\beta^{IVS-I-1\ (G>T)}/\beta^{N}$	1	0.80
--SEA/αα	$\beta^{Codons41/42(-TTCT)}/\beta^{-28\ (A>G)}$	1	0.80
Total	—	125	100

female was genetically tested first, and if the female was determined to be a ß-thal carrier, her husband underwent further thalassemia genetic analysis. Prenatal diagnosis was recommended if both individuals in the couple were confirmed to be ß-thal trait carriers. In our study, 77 couples were identified as both being ß-thal carriers, and were considered to be at risk of having clinically affected offsprings. Prenatal diagnosis revealed 20 fetuses with normal genotypes in *HBB*, 26 fetuses as simple ß-thal carriers, four fetuses as composite α- and ß-thal carriers, 16 cases as

TABLE 5 Abnormal hemoglobin variants in *HBB* and the hematological characteristics in this cohort in Jiangxi Province.

Hb variant	HGVS nomenclature	Hb (g/L)	MCV (fL)	MCH (pg)	Abnormal Hb concentration	Cases (n)	Ratio (%)
Hb J-Bangkok	c.170G>A (p.Gly57Asp)	128.6 ± 8.3	92.1 ± 1.8	29.9 ± 1.0	51.5 ± 0.6	24	42.86
Hb New York	c.341T>A (p.Val114Glu)	120.7 ± 10.1	89.5 ± 2.7	29.1 ± 0.5	43.9 ± 0.4	11	19.64
Hb G-Taipei	c.68A>G (p.Glu23Gly)	134.5 ± 7.5	86.4 ± 0.7	28.2 ± 0.6	39.5 ± 0.7	10	17.86
Hb G-Coushatta	c.68A>C (p.Glu23Ala)	140.7 ± 16.4	83.0 ± 0.9	30.0 ± 1.5	41.5 ± 0.7	3	5.36
Hb D-Los Angeles	c.364G>C (p.Glu122Gln)	137.0 ± 12.7	86.5 ± 2.3	28.9 ± 1.1	39.1 ± 1.5	3	5.36
Hb Yaizu	c.238G>A (p.Asp80Asn)	130	85.4	26.4	39.8	1	1.79
Hb Deer Lodge	c.8A>G (p His3Arg)	130	80.8	26.9	44.4	1	1.79
Hb E-Saskatoon	c.67G>A (p.Glu23Lys)	127	84.5	29.8	40.5	1	1.79
Hb G-Siriraj	c.22G>A (p.Glu8Lys)	123	85.2	30.3	30.6	1	1.79
Hb J-Bangkok and IVS-II-81 C>T	—	135	87.6	29.8	50.8	1	1.79
Total	—	—	—	—	—	56	100

TABLE 6 Hematological characteristics of the four subjects with novel variants.

Subject	Sex	Age (years)	Genotype	Hb (g/L)	MCV (fL)	MCH (pg)	HbA2 (%)	Ferritin (ng/ml)
No.1	Female	25	$\alpha^{c.301\text{-}41\_301\text{-}39delGGC}\alpha/\alpha\alpha$ $\beta^{IVS\text{-}II\text{-}654\ (C>T)}/\beta^{N}$	107	60.4	19.1	5.5	60.0
No.2	Female	23	$\alpha\alpha/\alpha\alpha$ $\beta^{IVS\text{-}II\text{-}47(G>C)}/\beta^{N}$	94	68.6	20.8	2.3	15.67
No.3	Male	25	$\alpha\alpha/\alpha\alpha$ $\beta^{IVS\text{-}II\text{-}300\text{-}308(-A)}/\beta^{N}$	105	60.4	19.1	2.6	12.54
No.4	Female	23	$\alpha\alpha/\alpha\alpha$ $\beta^{IVS\text{-}II\text{-}806(G>C)}/\beta^{N}$	98	72.1	26.8	3.2	—

"/" indicates "unknown"; The reference ranges of ferritin are from 30 ng/ml ~ 204 ng/ml.

compound heterozygous ß-thal patients, and 11 fetuses as homozygous ß-thal patients. The information on prenatal diagnosis was listed in detail in Supplementary Table S1.

No post-operative complications were found in 77 pregnant women with thalassemia, and 24 of the 77 pregnancies were terminated due to predicted severe ß-thal intermediate or major, including 10 with ß-thal homozygote and 14 with ß-thal double heterozygote. Following induced abortion, the fetal umbilical cord blood was sampled for genetic confirmation of ß-thal, which showed consistent results with prenatal diagnosis. All normal fetuses and those with ß-thal minor continued with the pregnancy. All of the pregnancy outcomes of the 77 families were listed in Supplementary Table S1. Telephone follow-up after the prenatal diagnosis revealed no thalassemia phenotypes in normal babies 6 months after birth, the babies with ß-thal minor had no or mild anemia symptoms and normal development milestones, while three babies with ß-thal double heterozygote demonstrated moderate anemia symptoms.

Discussion

Here, we presented a large-scale genetic analysis of *HBB*-associated hemoglobinopathy among adults of child-bearing age in Jiangxi Province. The results showed a high prevalence of 1.872% for hemoglobinopathy of ß-globin in China, with the respective carrier rate at 1.739% for ß-thal, 0.092% for the composite αß-thal, and 0.041% for the abnormal Hb variant. Based on previous studies, prevalence rate of ß-hemoglobinopathies among child-bearing population in typical geographic areas such as Guangxi (Xiong et al., 2010), Guangdong (Xu et al., 2004), Hubei, (Cheng et al., 2022), and

TABLE 7 Comparison of ß-thal frequency among reproductive-age adults in different geographic areas in China.

References PMID	Geographic areas	Subjects (n)	Methods	Frequency of ß-thal	Frequency of αβ-thal
Zheng, 2021 34893129	Guilin, Guangxi Zhuang Autonomous Region	19,482	Gap-PCR + PCR-RDB	4.56% (889/19482)	0.63% (123/19,482)
Xu, 2020 15113860	Five regional centres in Guangdong Province	7,792	Gap-PCR + PCR-RDB	2.54% (198/7,792)	0.26% (20/7,792)
Wang, 2022 35119136	Hainan Province	166,936	Gap-PCR + PCR-RDB	1.38% (2,305/166,936)	1.18% (1,976/166,936)
Wang, 2021 34893128	Guiyang in Guizhou Province	4,572	PCR-RDB	1.99% (91/4,572)	0.15% (7/4,572)
He, 2017 28674233	Changsha in Hunan Province	7,500	PCR-RDB	1.9% (143/7,500)	0.08% (6/7,500)
Cheng, 2022 35244037	Eastern, Central, Western regions of Hubei Province	11,875	PCR-Flow cytometry	1.92% (228/11875)	0.03% (3/11,875)
Lin, 2014 25000193	Three geographical areas of Jiangxi Province	9,489	PCR-RDB	1.70% (161/9,489)	0.12% (11/9,489)
Li, 2020 32719015	Sichuan Province	42,155	Gap-PCR + PCR-RDB	0.75% (317/42,155)	0.045% (19/42,155)

Hunan Province (He et al., 2017) were listed in Table.7. Frequencies of ß-hemoglobinopathies in Jiangxi Province showed difference from other reports in China probably mainly due to geographic and ethnic background. The carrier rate of ß-thal and αβ-thalassemia in our study showed a slightly higher prevalence rate than the previously reported 1.82% in Jiangxi Province (Lin et al., 2014) mainly because of the wider geographic areas contained and more comprehensive of rare ß-thal in our study. Furthermore, the prevalence of abnormal Hb variants in *HBB* (0.041%) was determined among child-bearing adults in Jiangxi Province for the first time in our study, which was significantly lower than the reported 0.222% in Southeastern China (Huang et al., 2019; Xu L. et al., 2020) and the reported 0.185% for Hb variants in *HBB* in Dongguan Region of Guangdong Province (Lou et al., 2014). Notably, since Hb E is a special Hb variant with ß-thal hematological trait, we classified Hb E as ß-thal instead of abnormal Hb variant in our study, otherwise the carrier rate of abnormal Hb variant would have increased to 0.086% (116/136,149). We also observed some differences in the ß-thal mutation spectrum in Jiangxi Province compared to those of other provinces in China. For example, in contrast to Guangxi, Guangdong, and Hainan (Xu et al., 2004; Xiong et al., 2010; Wang et al., 2022), CD41/42 (-TCTT) is not the most prevalent mutation in Jiangxi Province, while compared with its surrounding provinces, such as Hunan and Hubei (Liu et al., 2019; Cheng et al., 2022), Jiangxi Province shares a more similar mutation spectrum, with IVS-II-654 (C>T), CD41/42 (-TCTT), and CD17 (A>T) as the three most frequent genotypes in these areas, accounting for almost 80% of all genotypes. Likewise, the spectrum of structural Hb variants in *HBB* in Jiangxi Province is similar to those reported in previous studies, with the most three common variants as Hb New York, Hb J-Bangkok, and Hb G-Taipei, while Hb YaiZu, Hb Deer Lodge, and Hb E-Saskatoon had been seldom reported previously in China.

β-thalassemia is clinically classified into four types, including ß-thal silent, ß-thal trait, ß-thal intermediate, and ß-thal major. ß-thalassemia intermediate, with the genotype of β^+/β^+ or β^+/β^0, has a more complex molecular basis than the other three types (Thein, 2013). Patients affected with ß-thal intermediate usually present with diverse phenotypes from mild-to-moderate anemia that does not require lifelong dependence on blood transfusion. In contrast, individuals with ß-thal major, with the genotype of β^+/β^0 or β^0/β^0 and severe anemia (Hb persistently <70 g/L), require regular blood transfusions and standardized iron-free therapy to survive (Writing Group For Practice Guidelines For Diagnosis And Treatment Of Genetic Diseases Medical Genetics Branch Of Chinese Medical Association et al., 2020). Cure of this disease depends on successful bone-marrow transplantation, which is expensive and has treatment-associated complications (Ali et al., 2021). Therefore, severe ß-thal intermediate or ß-thal major presents a major public health problem and a social burden in highly prevalent areas. For the prevention of this disease, prenatal diagnosis is the most useful method for a continuous decline in birth rates of babies with ß-thal major (Huang L. F. et al., 2021). Genotyping is strongly recommended for inclusion in the prenatal diagnosis of ß-thal, since precise prenatal diagnosis is crucial to prevent the development of thalassemia and for genetic counseling. Apart from prenatal diagnosis, pre-implantation genetic testing (PGT) for thalassemia has emerged as a new choice for

some families, which, although expensive, causes less harm to the pregnant females.

Accurate genetic testing is the basis of effective birth defect prevention of thalassemia in pre-pregnancy or prenatal genetic counseling. Although traditional genetic testing is a low-cost and time-saving strategy, it only focuses on the most common regional mutations, which may lead to missed diagnosis of rare or novel variants. Therefore, further supplementary molecular testing is required for individuals whose genotypes cannot explain the hematological indices in clinical practice. In our study, 30 participants with increased HbA2 values and microcytic hypochromic hematological profiles were identified with rare ß-thal mutations. Overall, 10 types of rare ß-thal mutations that had not been previously reported in Jiangxi Province were identified, representing 1.18% (30/2,548) of all the mutations, with IVS-I-6 (T>G) identified for the first time worldwide. Among the 30 cases with rare ß-thal mutations, the most common genotype was CD54-58 (-TATGGGCAACCCT), followed by -28 (A>C), suggesting that these two mutations show a more frequent carrier rate than some of the 17 point mutations tested by traditional PCR-RDB method. In addition, we also identified four novel variants, including *HBA2*:c.301-41_301-39delGGC, *HBB*:IVS-II-47 (G>C), IVS-II-300–308 (-A), and IVS-II-806 (G>C), even though their pathogenesis still requires further study. Notably, we found that participants with the variant β^+ Cap+40–43 (-AAAC) identified by traditional thalassemia genetic testing, did not demonstrate the hematological characteristics of increased HbA2 values or microcytic hypochromic when iron-deficiency is excluded. As reported by Li, the pathogenicity of this variant remains uncertain and may be regarded as a silent ß-thal allele (Zhao et al., 2020). Moreover, based on our findings, we propose that the two frequent mutations CD54-58 (-TATGGGCAACCCT) and -28 (A>C) should be included into traditional genetic testing based on specific geographic background in Jiangxi Province. Secondly, hematological indices of CBC test and hemoglobin electrophoresis are both indispensable for the correct recognition of ß-hemoglobinopathies. Finally, more comprehensive and efficient molecular testing approaches may be considered for identification of both common and rare variants of thalassemia simultaneously.

Despite these strengths, certain limitations of our study should also be acknowledged. As mutations in *HBD* can cover the typical increased HbA2 value for individuals with ß-thal (Chen et al., 2020), missed diagnosis may occur based on the current hematological screening strategy as the hematological parameters might be normal or borderline indices for some rare thalassemia mutation types or Hb variants. Thus, it is possible that silent mutations in α-globin genes, α triplications, or Hb variants without abnormal Hb composition were missed in this study. In recent years, the combined Gap-PCR and next-generation sequencing (NGS) has emerged and used as an alternative more complete and versatile molecular approach for thalassemia genetic testing (Shang et al., 2017), even though it is considered scalable, cost-effective, and comprehensive. Besides, another alternative efficient, accurate, and cost-effective single platform technology generating longer PCR fragments including intergenic and intragenic regions to identify other rare variants undetectable by the typical panel test have been studied and validated (Xu L. et al., 2020). Studies revealed that this new emerging methods with universal approach to comprehensive analysis of variants in homologous genes *HBA1*/*HBA2*, cis or trans configuration, and complex structural rearrangements are hardly associated with false-negative and false-positive results (Liang et al., 2021).

Conclusion

In summary, we have provided the most comprehensive mutation spectrum of thalassemia and abnormal Hb variants mutation spectrum in the *HBB* gene among adults of reproductive-age in Jiangxi Province to date. We also provided intensive genetic counseling and prenatal diagnosis for couples with indications to avoid the birth of fetuses with ß-thal intermediate or major. Our work may provide as a baseline for genetic counseling, public education, and as a reference to improve the prevention of ß-thal.

Data availability statement

The original contributions presented in the study are included in the article/Supplementary Material, further inquiries can be directed to the corresponding author.

Ethics statement

The studies involving human participants were reviewed and approved by The studies involving human participants were reviewed and approved by Ethics Committee of Jiangxi Maternal and Child Health Hospital (No. EC-KT-202216). The patients/participants provided their written informed consent to participate in this study.

Author contributions

HL and TH conceived and designed the study. QL and YX performed the hematological screening tests, LZ, YY, and YS conducted some of the genetic detection and ZG conducted the B-mode ultrasound-guidance during the fetal sampling. HY performed the CVS, amniocentesis or umbilical cord blood sampling. SH and BY contributed to track the objects

of research. YZ and YL provided writing guidance and correction. HL and TH wrote the manuscript together. All the authors have read and approved the manuscript.

Funding

This study was supported by Jiangxi Provincial Key Laboratory of Birth Defect for Prevention and Control (No. 20202BCD42017 to YL). National Natural Science Foundation of China (Grant No. 82160318 to YZ), Key Research and Development Program of Jiangxi Province (Grant No. 20192BBGL70006 to ZG), Provincial Health Commission Program of Jiangxi (Grant No.SKJP220211066 to TH, No. SKJP220211247 to HL and 202130792 to YZ).

Acknowledgments

We are grateful to all subjects participating in this study and thanks are also expressed to Dr. Chen for his kind assistance with the manuscript preparation.

Conflict of interest

The authors declare that the research was conducted in the absence of any commercial or financial relationships that could be construed as a potential conflict of interest.

Publisher's note

Supplementary material

The Supplementary Material for this article can be found online at: https://www.frontiersin.org/articles/10.3389/fgene.2022.992073/full#supplementary-material

References

Ahmed, M. H., Ghatge, M. S., and Safo, M. K. (2020). Hemoglobin: Structure, function and Allostery. *Subcell. Biochem.* 94, 94345–94382. doi:10.1007/978-3-030-41769-7_14

Ali, S., Mumtaz, S., Shakir, H. A., Khan, M., Tahir, H. M., Mumtaz, S., et al. (2021). Current status of beta-thalassemia and its treatment strategies. *Mol. Genet. Genomic Med.* 9 (12), e1788. doi:10.1002/mgg3.1788

Altinier, S., Varagnolo, M., Zaninotto, M., and Plebani, M. (2013). Identification and quantification of hemoglobins in whole blood: The analytical and organizational aspects of capillarys 2 Flex Piercing compared with agarose electrophoresis and HPLC methods. *Clin. Chem. Lab. Med.* 51 (4), 791–797. doi:10.1515/cclm-2012-0061

Chen, M., Huang, H., Chen, L., Lin, N., Zhang, M., Lin, Y., et al. (2020). First report of the spectrum of δ-globin gene mutations among women of reproductive age in Fujian area-Discrimination of δ-thalassemia, α-thalassemia, and Iron Deficiency Anemia. *J. Clin. Lab. Anal.* 34 (11), e23479. doi:10.1002/jcla.23479

Cheng, Y., Chen, M., Ye, J., Yang, Q., Wang, R., Liu, S., et al. (2022). The prevalence and outcomes of α- and β-thalassemia among pregnant women in Hubei Province, Central China: An observational study. *Med. (Abingdon)* 101 (9), e28790. doi:10.1097/MD.0000000000028790

Clarke, G. M., and Higgins, T. N. (2000). Laboratory investigation of hemoglobinopathies and thalassemias: Review and update. *Clin. Chem.* 46 (8), 1284–1290. doi:10.1093/clinchem/46.8.1284

Ghosh, K., Ghosh, K., Agrawal, R., and Nadkarni, A. H. (2020). Recent advances in screening and diagnosis of hemoglobinopathy. *Expert Rev. Hematol.* 13 (1), 13–21. doi:10.1080/17474086.2019.1656525

He, J., Zeng, H., Zhu, L., Li, H., Shi, L., and Hu, L. (2017). Prevalence and spectrum of thalassaemia in Changsha, Hunan province, China: Discussion of an innovative screening strategy. *J. Genet.* 96 (2), 327–332. doi:10.1007/s12041-017-0779-6

Huang, H., Chen, M., Chen, L., Zhang, M., Wang, Y., Lin, N., et al. (2021). Prenatal diagnosis of thalassemia in 695 pedigrees from southeastern China: A 10-year follow-up study. *J. Clin. Lab. Anal.* 35 (10), e23982. doi:10.1002/jcla.23982

Huang, H., Xu, L., Chen, M., Lin, N., Xue, H., Chen, L., et al. (2019). Molecular characterization of thalassemia and hemoglobinopathy in Southeastern China. *Sci. Rep.* 9 (1), 3493. doi:10.1038/s41598-019-40089-5

Huang, L. F., Yu, L. L., Nikuze, L., Singh, S., Jiang, J. X., Jiang, J. L., et al. (2021). Spectrum of β-thalassemia mutations in some areas of Guangxi Zhuang Autonomous region of southern China: A study on a Pediatric population aged 0-15 Years. *Hemoglobin* 45 (5), 318–321. doi:10.1080/03630269.2022.2041435

Keren, D. F., Hedstrom, D., Gulbranson, R., Ou, C. N., and Bak, R. (2008). Comparison of Sebia Capillarys capillary electrophoresis with the Primus high-pressure liquid chromatography in the evaluation of hemoglobinopathies. *Am. J. Clin. Pathol.* 130 (5), 824–831. doi:10.1309/AJCPQY80HZWHHGZF

Kohne, E. (2011). Hemoglobinopathies: Clinical manifestations, diagnosis, and treatment. *Dtsch. Arztebl. Int.* 108 (31-32), 532–540. doi:10.3238/arztebl.2011.0532

Liang, Q., Gu, W., Chen, P., Li, Y., Liu, Y., Tian, M., et al. (2021). A more universal approach to comprehensive analysis of thalassemia alleles (CATSA). *J. Mol. Diagn.* 23 (9), 1195–1204. doi:10.1016/j.jmoldx.2021.06.008

Lin, M., Zhong, T. Y., Chen, Y. G., Wang, J. Z., Wu, J. R., Lin, F., et al. (2014). Molecular epidemiological characterization and health burden of thalassemia in Jiangxi Province, P. R. China. *PLoS ONE* 9 (7), e101505. doi:10.1371/journal.pone.0101505

Liu, Q., Jia, Z. J., Xi, H., Liu, J., Peng, Y., and Wang, H. (2019). Analysis on the genotype of 5018 cases of thalassemia in Hunan area. *Zhongguo Shi Yan Xue Ye Xue Za Zhi* 27 (6), 1938–1942. doi:10.19746/j.cnki.issn.1009-2137.2019.06.037

Long, J., Huang, G., Liang, W., Liang, B., Chen, Q., Xie, J., et al. (2014). The prevalence of schizophrenia in mainland China: Evidence from epidemiological surveys. *Acta Psychiatr. Scand.* 130 (4), 244–256. doi:10.1111/acps.12296

Lou, J. W., Wang, T., Liu, Y. H., He, Y., Zhong, B. M., Liu, J. X., et al. (2014). Prevalence and molecular characterization of structural hemoglobin variants in the Dongguan region of Guangdong province, southern China. *Hemoglobin* 38 (4), 282–286. doi:10.3109/03630269.2014.928779

Muncie, H. L., Jr, and Campbell, J. (2009). Alpha and beta thalassemia. *Am. Fam. Physician* 80 (4), 339–344.

Origa, R. (2017). β-Thalassemia. *Genet. Med.* 19 (6), 609–619. doi:10.1038/gim.2016.173

Schwartz, E., Cohen, A., and Surrey, S. (1988). Overview of the beta thalassemias: Genetic and clinical aspects. *Hemoglobin* 12 (5-6), 551–564. doi:10.3109/03630268808991644

Shang, X., Peng, Z., Ye, Y., AsanZhang, X., Chen, Y., et al. (2017). Rapid Targeted next-generation sequencing platform for molecular screening and clinical genotyping in subjects with hemoglobinopathies. *EBioMedicine* 23, 23150–23159. doi:10.1016/j.ebiom.2017.08.015

Taher, A. T., Weatherall, D. J., and Cappellini, M. D. (2018). Thalassaemia. *Lancet* 391 (10116), 155–167. doi:10.1016/S0140-6736(17)31822-6

Thein, S. L. (2013). The molecular basis of β-thalassemia. *Cold Spring Harb. Perspect. Med.* 3 (5), a011700. doi:10.1101/cshperspect.a011700

Wang, M., Zhang, X., Zhao, Y., Lu, Z., and Xiao, M. (2022). Prevalence and genetic analysis of thalassemia in childbearing age population of Hainan, the Free Trade Island in Southern China. *J. Clin. Lab. Anal.* 36 (3), e24260. doi:10.1002/jcla.24260

Weatherall, D. J., and Clegg, J. B. (2001). Inherited haemoglobin disorders: An increasing global health problem. *Bull. World Health Organ.* 79 (8), 704–712.

Writing Group For Practice Guidelines For Diagnosis And Treatment Of Genetic Diseases Medical Genetics Branch Of Chinese Medical AssociationShang, X., Wu, X., Zhang, X., Feng, X., and Xu, X. (2020). Clinical practice guidelines for beta-thalassemia. *Zhonghua Yi Xue Yi Chuan Xue Za Zhi* 37 (3), 243–251. doi:10.3760/cma.j.issn.1003-9406.2020.03.004

Xiong, F., Sun, M., Zhang, X., Cai, R., Zhou, Y., Lou, J., et al. (2010). Molecular epidemiological survey of haemoglobinopathies in the Guangxi Zhuang Autonomous Region of southern China. *Clin. Genet.* 78 (2), 139–148. doi:10.1111/j.1399-0004.2010.01430.x

Xu, A., Chen, W., Xie, W., Wang, Y., and Ji, L. (2020). Hemoglobin variants in southern China: Results obtained during the measurement of glycated hemoglobin in a large population. *Clin. Chem. Lab. Med.* 59 (1), 227–232. doi:10.1515/cclm-2020-0767

Xu, L., Mao, A., Liu, H., Gui, B., Choy, K. W., Huang, H., et al. (2020). Long-molecule sequencing: A new approach for identification of clinically significant DNA variants in α-thalassemia and β-thalassemia carriers. *J. Mol. Diagn.* 22 (8), 1087–1095. doi:10.1016/j.jmoldx.2020.05.004

Xu, X. M., Zhou, Y. Q., Luo, G. X., Liao, C., Zhou, M., Chen, P. Y., et al. (2004). The prevalence and spectrum of alpha and beta thalassaemia in Guangdong province: Implications for the future health burden and population screening. *J. Clin. Pathol.* 57 (5), 517–522. doi:10.1136/jcp.2003.014456

Zhao, Y., Jiang, F., and Li, D. Z. (2020). Hematological characteristics of β-globin gene mutation -50 (G>A) (HBB: c.-100G>A) carriers in mainland China. *Hemoglobin* 44 (4), 240–243. doi:10.1080/03630269.2020.1793774

Zhou, B. Y., Wang, Y. X., Xu, S. S., Gu, H., and Li, M. Z. (2021). Molecular spectrum of α- and β-thalassemia among Young individuals of Marriageable age in Guangdong province, China. *Biomed. Environ. Sci.* 34 (10), 824–829. doi:10.3967/bes2021.112

Zhuang, J., Jiang, Y., Wang, Y., Zheng, Y., Zhuang, Q., Wang, J., et al. (2020). Molecular analysis of α-thalassemia and β-thalassemia in Quanzhou region Southeast China. *J. Clin. Pathol.* 73 (5), 278–282. doi:10.1136/jclinpath-2019-206179

frontiers | Frontiers in Genetics

TYPE Case Report
PUBLISHED 31 October 2022
DOI 10.3389/fgene.2022.1002089

OPEN ACCESS

EDITED BY
Przemysław Kosinski,
Medical University of Warsaw, Poland

REVIEWED BY
Jader de Jesus Cruz,
Centro Hospitalar Universitário Lisboa Central, Portugal
Nicola Volpe,
University Hospital of Parma, Italy

*CORRESPONDENCE
Cheng Weiwei,
wwcheng29@shsmu.edu.cn
Wu Yi,
thomasguo1122@163.com

†These authors have contributed equally to this work

SPECIALTY SECTION
This article was submitted to Genetics of Common and Rare Diseases, a section of the journal Frontiers in Genetics

RECEIVED 24 July 2022
ACCEPTED 28 September 2022
PUBLISHED 31 October 2022

CITATION
Biwei H, Min S, Yanlin W, Xinrong Z, Li G, Renyi H, Jinling S, Shan W, Yi W and Weiwei C (2022), Case report: Prenatal diagnosis of Ectrodactyly–Ectodermal dysplasia–Cleft syndrome (EEC) in a fetus with cleft lip and polycystic kidney. *Front. Genet.* 13:1002089. doi: 10.3389/fgene.2022.1002089

Case report: Prenatal diagnosis of Ectrodactyly–Ectodermal dysplasia–Cleft syndrome (EEC) in a fetus with cleft lip and polycystic kidney

He Biwei[1,2†], Su Min[3†], Wang Yanlin[1], Zhao Xinrong[1], Gao Li[1], Hua Renyi[1], Sun Jinling[1], Wang Shan[1], Wu Yi[1*] and Cheng Weiwei[1*]

[1]Prenatal Diagnostic Center, International Peace Maternity and Child Health Hospital, School of Medicine, Shanghai JiaoTong University, Shanghai, China, [2]Shanghai Key Laboratory of Embryo Original Disease, Shanghai, China, [3]Department of Reproductive Genetics, International Peace Maternity and Child Health Hospital, School of Medicine, Shanghai Jiao Tong University, Shanghai, China

Ectrodactyly–ectodermal dysplasia–cleft (EEC) syndrome is an autosomal dominant disorder characterized by ectrodactyly, ectodermal dysplasia, and orofacial clefting. Reduced penetrance is manifested in these core features and additional under-recognized features, especially in prenatal cases. Here, we present a fetus with EEC syndrome at 22 weeks gestation, in which the cleft lip and palate and the right polycystic kidney are shown by prenatal ultrasound. A *de novo* missense mutation of R304W in the *TP63* gene is confirmed by whole-exome sequencing associated with EEC syndrome. We further investigate the reported *TP63*-related prenatal cases and provide a more complete picture of the prenatal phenotypic spectrum about EEC. It illustrates the potential severity of genitourinary anomalies in *TP63*-related disorders and highlights the need to counsel for the possibility of EEC syndrome, given the occurrence of genitourinary anomalies with orofacial cleft or limb deformities.

KEYWORDS

EEC, p63, prenatal phenotypic spectrum, genitourinary anomalies, whole-exome sequencing

Introduction

Ectrodactyly–ectodermal dysplasia–cleft (EEC, OMIM 604292) syndrome is a rare, autosomal dominant syndrome characterized by 1) ectrodactyly or lobster-claw deformity, 2) ectodermal dysplasia (anomalies in hair, teeth, nail, skin, sweat gland, lacrimal duct, breast, and nipple development), and 3) cleft lip and/or cleft palate. Additional clinical features have also been described: genitourinary and external ear malformations, hearing loss, chronic respiratory infections, ventricular cardiomyopathy, and developmental delay (Yin et al., 2010; Goldsmith et al., 2014; Zheng et al., 2019).

There is a wide range of variability in clinical manifestations with occasional non-penetrance.

The tumor protein p63 gene (*TP63*) mutations account for most and possibly all cases of classical EEC syndrome, which is located on chromosome 3q27 and encodes a transcription factor homologous to the tumor suppressors p53 and p73 (Ianakiev et al., 2000; Barrow et al., 2002; Bertola et al., 2004; Mikkola, 2007; Yin et al., 2010). Genomic organization of TP63 is complexed with at least six different isoforms (Yin et al., 2010). TP63 mutations result in amino acid substitutions in the DNA-binding domain common to all known p63 isoforms (Brunner et al., 2002). The five arginine codons Arg204, Arg227, Arg279, Arg280, and Arg304 are the most frequently mutated residues, which commonly affect CpG sites, accounting for about 80% of EEC syndrome cases (Barrow et al., 2002; Yin et al., 2010).

Up to now, over 200 cases of EEC syndrome have been reported in the literature, whereas almost all of them were postnatal cases. Prenatal data concerning the EEC syndrome are still very limited. The prenatal detection of EEC syndrome depends on which features can be detectable by ultrasound. There are few literature reports available on antenatal ultrasound findings in patients with EEC; furthermore, only a few studies have focused on prenatal findings in patients with genitourinary anomalies. Consequently, genitourinary anomalies remain a common but under-recognized feature of EEC syndrome (Hyder et al., 2017).

Recently, whole-exome sequencing (WES) has provided the opportunity for molecular genetic screening of rare human diseases. Here, we report a fetus with cleft lip and palate and right polycystic kidney and identify a pathogenic variation of the *TP63* gene by WES associated with EEC syndrome. We also summarize the prenatal ultrasound phenotypes caused by TP63 mutations. Prenatal characteristics of the TP63 mutations are determined to extend the prenatal phenotypes of EEC and improve the accuracy of prenatal diagnosis.

Materials and methods

Patient samples

A woman was referred to our prenatal diagnosis center due to suspicious fetal structural anomalies. Ultrasound showed an enlarged bladder during the first trimester screening scan for chromosomal anomalies. Chorionic sampling could not be performed due to the posterior placenta. The woman accepted amniocentesis and chromosome microarray analysis (CMA) as the first-line genetic testing at 17 weeks. After 3 weeks, the CMA and karyotyping results were both normal. However, the routine fetal anatomy scan showed cleft lip and right kidney dysplasia. Parents decided to terminate the pregnancy by the intra-amniotic injection of rivanol solution after signing the informed consent, and they accepted trio whole-exome sequencing (trio-WES) to identify the underlying etiology. Autopsy was recommended to obtain more detailed phenotypic information. The study was approved by the Medical Ethics Committee of the International Peace Maternity and Child Health Hospital (GKLW 2019-24).

Chromosomal microarray analysis

CMA was performed using the Affymetrix CytoScan 750K Array (Affymetrix, Inc., Santa Clara, CA, United States), and CNVs were determined by Affymetrix Chromosome Analysis Suite software 3.2 (Affymetrix, Inc., Santa Clara, CA, United States). The pathogenicity of CNVs was evaluated under the technical standards of the American College of Medical Genetics and Genomics and the Clinical Genome Resource in 2019.

Whole-exome sequencing

Peripheral blood of the trio was collected; then, the DNA was extracted and purified. The targeted TP63 exons and flanking regions were captured by the customized clinical exome chip (BGI V4). The library was built under the manufacturer's recommendations and sequenced on BGI MiSeq 2000. Over 150 M of raw sequences were generated, resulting in an average depth of 150X in the target region and 95% regions with coverage >30X. Low-quality and adapter reads were removed using Trimmomatic (Trimmomatic.0.39) (Bolger et al., 2014). The remained high-quality reads were aligned to the human genome GRCh37/hg19 with the Burrows–Wheeler Aligner (Li and Durbin, 2010). Genome Analysis Toolkit 4 (Van der Auwera et al., 2013) was used to identify short variants. The duplicates were marked by the MarkDuplicates function, base quality scores were recalibrated by the BQSR function, and finally, the variants were called by the HaplotypeCaller algorithm. Candidate events were displayed using the Integrative Genomics Viewer (IGV); the position and quality of variants, as well as strand orientation, were checked carefully.

Sanger sequencing

PCR primers were designed to amplify exon 8 of TP63. The mutation of the proband was sequenced from a 640-bp DNA fragment amplified using the primer pair 5′-CTGGTAGTACGT TGGCGATG-3′ and 5′-ATAAGGAGGTGGAAGGATGG-3'. Sanger sequencing was performed using the ABI 3730xl DNA automated sequencer (Applied Biosystems, Foster City, CA, United States).

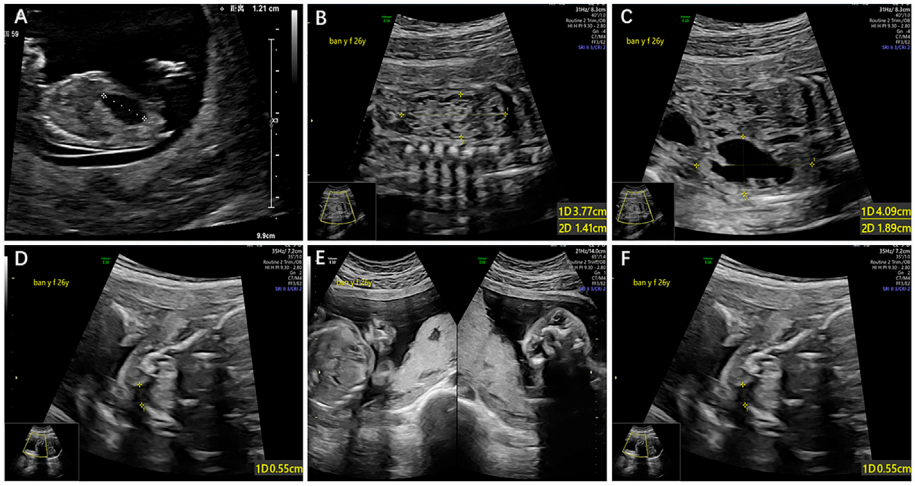

FIGURE 1
(A): Enlarged bladder with the diameter of 12 mm, **(B)** right multicystic kidney, **(C)** left hydronephrosis with the width of 4 cm, **(D)** cleft palate, **(E)** and **(F)**cleft lip.

Case presentation

A 35-year-old G2P0 woman at the gestational age of 11 + 6 was referred to the prenatal diagnosis center of the International Peace Maternity and Child Health Hospital, due to an enlarged fetal bladder. The ultrasound showed a normal nuchal translucency (NT = 1.3 mm) and an enlarged bladder with the diameter of 12 mm (Figure 1A). It was her secondary pregnancy after one ectopic in 2019. The couple was not consanguineous, and the family history was unremarkable for any other known congenital anomalies or otherwise. After 1 week, a repeated ultrasound showed a slightly reduced bladder with a diameter of 10 mm. Considering the advanced maternal age and contingency of ultrasound findings, chorionic villus sampling (CVS) was then suggested. However, CVS could not be performed due to the posterior placenta. Non-invasive prenatal testing (NIPT) was conducted at 15 weeks of gestation, and the NIPT result was negative. At 17 weeks, the woman accepted amniocentesis and chromosome microarray analysis (CMA) as the first-line genetic testing. After 3 weeks, the CMA and karyotyping results were both normal. At 22 weeks, the routine fetal anomaly scan showed multiple structural abnormalities including the right multicystic kidney, left hydronephrosis, and cleft lip and palate (Figures 1B–F).

The parents opted to terminate the pregnancy *via* induction. Amniocentesis was performed to obtain the amniotic fluid prior to the intra-amniotic injection of rivanol solution after signing the informed consent, and they accepted the trio whole-exome sequencing (trio-WES) to identify the underlying etiology. No ectrodactyly or lobster-claw deformity was observed (Figure 2A). External examination showed no positive signs of ectodermal dysplasia (sparse hair, nail dysplasia, abnormal teeth, lacrimal duct obstruction, sweat gland dysplasia, etc.,) and was consistent with the gestational age of the fetus (Figure 2A). The autopsy confirmed bilateral cleft lip and palate (bilateral cleft lip, alveolar cleft, and complete cleft palate), right renal dysplasia, and hydronephrosis of the left kidney (Figures 2B–D).

Different diseases were considered based on the aforementioned findings, including triploidy, microdeletion and microduplication syndromes, and single-gene disorders. To further search the underlying genetic causes, karyotyping and chromosomal microarray analysis (CMA) were performed, and both the results were normal (data not shown), suggesting no pathogenic copy number variations. The trio whole-exome sequencing (WES) was then performed, and a *de novo* missense mutation (c.1027C > T R304W) was detected in exon 8 of the *TP63* gene (Figure 3A). Nevertheless, none of the mutation at this site was found in the parents. Sanger sequencing confirmed this conclusion (Figure 3B). This mutation is pathogenic to EEC and had been demonstrated to disrupt the DNA-binding affinity of p63 and resulted in reduced transactivation activity (Browne et al., 2011).

Discussion

EEC syndrome is a rare genetic disorder characterized by the following triad: 1) ectrodactyly, more precisely, limb malformations. The classic limb malformation is ectrodactyly, also called lobster claw, or split hands and/or feet, which is caused due to the lack of one or more central digits. Other limb deformities such as syndactyly, polydactyly, and abnormal size

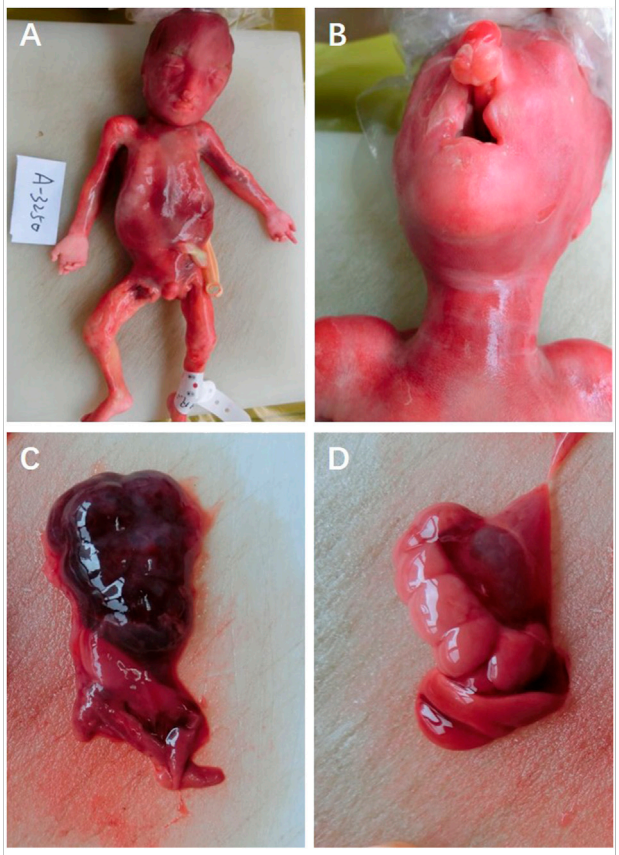

FIGURE 2
(A) Fetal appearance, **(B)** cleft lip and palate, **(C)** right renal dysplasia, and **(D)** hydronephrosis of the left kidney.

or shape of digital phalange of one or more fingers are also observed with an increasing number of literature studies being reported (Kumar et al., 2007; Koul et al., 2014). 2) Ectodermal dysplasia, which means the abnormal development of structures derived from the embryonic ectodermal layer. The common manifestations include sparse hair, nail dysplasia, abnormal teeth, lacrimal duct obstruction, and sweat gland dysplasia (Kumar et al., 2007; Goldsmith et al., 2014; Koul et al., 2014). 3) Cleft lip with or without palate (Iqbal Ali et al., 2013), which is often observed in patients with EEC syndrome.

Tumor protein p63 (TP63) encodes a high sequence homology of the p53 family of transcription factors, which is the master regulator during ectodermal and epidermal development. Disruption of TP63 in humans results in several overlapping disorders, such as ankyloblepharon-ectodermal defects cleft lip/palate (AEC) syndrome, acro–dermo–ungual–lacrimal–tooth (ADULT) syndrome, cleft lip/palate syndrome 3 (EEC3), limb-mammary syndrome, split-hand/foot malformation type 4 (SHFM4), isolated cleft lip/cleft palate (orofacial cleft 8), and Rapp–Hodgkin syndrome (RHS) (Rinne et al., 2007). The functional domain of TP63 contains an N-terminal transactivation domain, a central DNA-binding domain (DBD), an oligomerization domain, a sterile-alpha motif domain, and a C-terminal transactivation inhibitory domain. Several isoforms with different N-terminal ends are found with distinct biological properties (Bourdon, 2007). TAp63α, which represents the full gene product, is expressed in oocytes (Suh et al., 2006), while ΔNp63α, which lacks the N-terminal transactivation domain, is the major isoform expressed in the epidermis (Yang et al., 1999). The ratio of ΔNp63 and TAp63 isoforms may govern the maintenance of epithelial stem cell compartments and regulate the initiation of epithelial stratification from the undifferentiated embryonal ectoderm (Straub et al., 2010). EEC is mainly caused by point mutations in the DBD, which may impair the p63 protein binding to DNA. Five frequently mutated amino acids (R204, R227, R279, R280, and R304), which are all located in the CpG

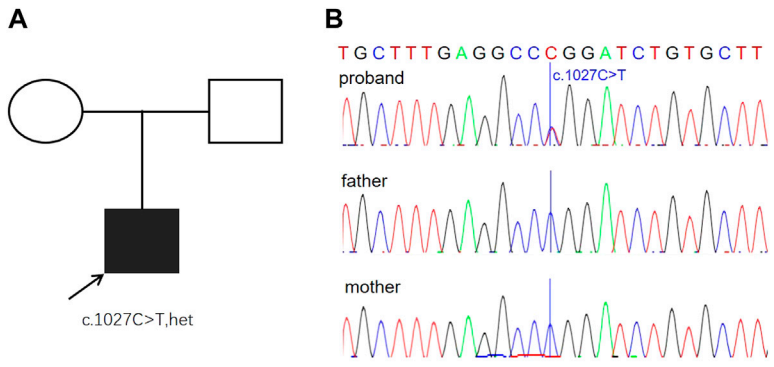

FIGURE 3
Genetic findings from the family. **(A)** Pedigree of the family with segregation of the identified TP63 mutation. The square represents male, and circles represent female. The filled symbol indicates the affected individual. **(B)** Variation of c.1027C > T is a *de novo* missense mutation (R304W) identified in the proband. The parents were tested and did not carry the mutation. Blue lines indicate the point mutation.

TABLE 1 Phenotypic characteristics of EEC syndrome associated with R304 mutations.

	Family	Patient	Confirmed *de novo*	Mutation		Limb deformity[a]	Facial clefting[b]	Ectodermal dysplasia[c]	Others[d]
				Nucleotide	Amino acid				
Wessagowit et al. (2000)	1	1	1	C1027T	R304W	E (1) and S (1)	L (1) and P (1)	H (1), N (1), T (1), and ND (1)	G (1)
van Bokhoven et al. (2001)	2	3	1	C1027T	R304W	E (1) and S (2)	L (3) and P (3)	H (3), S (2), N (3),T (2), and L (3)	K (2) and HL (2)
	5	5	4	G1028A	R304Q	E (5) and S (1)	L (4) and P (4)	H (5), S (2), N (3), T (4), and L (5)	K (2) and G (1)
Hamada et al. (2002)	1	1	1	C1027T	R304W	E (1) and S (1)	—	N (1) and ND (1)	—
	5	6	5	G1028A	R304Q	E (5), S (3), O (2), and P (1)	L (3) and P (4)	H (2), S (2), N (2), T (1), ND (3), and L (2)	HL (4), U (3), ID (2), AF (1), and K (1)
de Mollerat et al. (2003)	1	1	0	C1027T	R304W	E (1) and S (1)	L (1) and P (1)	H (1) and N (1)	—
	2	2	0	G1028A	R304Q	E (2) and S (1)	L (2) and P (2)	H (2), N (2), T (2), and L (2)	—
	1	1	0	G1028C	R304P	E (1), S (1), and O (1)	L (1)	H (1) and T (1)	ID (1) and BL (1)
Dianzani et al. (2003)	1	5	0	G1028A	R304Q	E (1), S (4), O (1), and P (3)	L (5) and P (5)	H (1), N (5), and L (5)	—
Paranaíba et al. (2010)	1	1	1	C1027T	R304W	E (1)	L (1) and P (1)	H (1), S (1), N (1), T (1), and L (1)	ID (1) and HL (1)
Okamura et al. (2013)	1	1	0	G1028A	R304Q	E (1) and S (1)	P (1)	H (1), N (1), T (1), and L (1)	—
Gawrych et al. (2013)	1	1	0	C1027T	R304W	S (1) and O (1)	L (1) and P (1)	H (1), S (1), and ND (1)	SD (1)
Brueggemann and Bartsch (2016)	1	2	0	G1028A	R304Q	E (1) and S (1)	L (2) and P (2)	H (1), S (1), and N (1)	—
Wenger et al. (2018)	1	1	1	C1027T	R304W	—	L (1) and P (1)	N (1) and ND (1)	K (1) and U (1)
	1	2	0	G1028A	R304Q	E (1) and S (2)	L (2) and P (2)	N (2), T (2), ND (2), and L (2)	K (2), U (2), and SD (1)
Total	25	33	14	—	—	E (22), S (20), O (5), and P (4)	P (28) and L (27)	N (25), L (21), H (20), T (15), ND (9), and S (9)	K (8), HL (7), U (6), ID (4), SD (2), and G (2)

[a]E, ectrodactyly; O, oligodactyly; P, polydactyly; S, syndactyly.
[b]L, cleft lip; P, cleft palate.
[c]H, hair; L, lacrimal ducts; N, nail; ND, nasolacrimal duct; S, skin; T, teeth.
[d]BL, blindness; G, genital deformities; HL, hearing loss; K, kidney malformations; ID, intellectual disability; SD, speech delay; U, urinary tract anomalies.

islands, explain almost 90% of the EEC patients (Brunner et al., 2002).

Remarkably, p63 mutations in a mouse model result in an EEC syndrome-like phenotype [20.22]. P63-deficient mice lack all squamous epithelia and their derivatives, including hair, whiskers, teeth, and the mammary, lacrimal, and salivary glands (Mills et al., 1999; Yang et al., 1999). Particularly striking are severe limb truncations with forelimbs showing a complete absence of the phalanges and carpals and variable defects of ulnae and radiae and hindlimbs that are lacking altogether. Similarly, ECC syndrome patients manifest as a generalized ectodermal dysplasia (which presents as sparse hair, dry skin, pilosebaceous gland dysplasia, lacrimal duct obstruction, and oligodontia) and classic limb malformation (which presents as the lack of one or more central digits). Additionally, the truncated secondary palate and hypoplastic maxilla and mandibula in p63-deficient mice correspond to cleft lip with or without the cleft palate in EEC syndrome patients. Thus, the heterozygous mutation of TP63 plays an important role in EEC syndrome, whereas the genetic basis underlying the variable expressivity and incomplete penetrance of EEC remains unclear. VernerssonLindahl et al. (2013) discovered that clefting and skin defects are caused by loss of Trp63 function, while limb anomalies are due to gain- and/or

dominant-negative effects of Trp63 by utilizing two mouse models with alleles encoding Trp63R279H (Trp63Aam1-R279HN and Trp63Aam2-R279H). Furthermore, their studies identified TAp63 as a strong modifier of EEC-associated phenotypes, with regard to both penetrance and expressivity. At present, no specific molecular pathway has been reported to be associated with genitourinary anomalies caused by the p63 mutation. Nardi et al. (1992) speculated that the altered gene in EEC syndrome affected the ectoderm and its derivatives, leading to the two fundamental types of GU defects: abnormal glandular urethral development causing hypospadias and anomalous genesis of the ureteric bud.

Remarkable clinical variability has been observed for different TP63 mutations. Regarding the special amino acid mutation of R304 observed in the present case, we summarized the clinical presentations of the reported 33 cases with EEC syndrome and the R304 mutation (Table 1) (Wessagowit et al., 2000; van Bokhoven et al., 2001; Hamada et al., 2002; de Mollerat et al., 2003; Dianzani et al., 2003; Paranaíba et al., 2010; Gawrych et al., 2013; Okamura et al., 2013; Brueggemann and Bartsch, 2016; Wenger et al., 2018). Orofacial cleft, the most significant feature of EEC syndrome, is presented in approximately 80% of patients. Most of the patients presented with cleft lip and palate (26/33), while only three cases are observed with isolated cleft lip or isolated cleft palate (Hamada et al., 2002; de Mollerat et al., 2003; Okamura et al., 2013). Among limb malformations, the penetrance of ectrodactyly, syndactyly, oligodactyly, and polydactyly are 63%, 57%, 14%, and 11% respectively. The ectodermal dysplasia of nail, lacrimal, hair, and teeth quite commonly occurs in over 40% of EEC cases. Genitourinary anomalies, including the kidney and urinary problems, were reported in 28% (10/33). Conductive hearing loss is not scarce and was detected in about 20% (7/33). Strikingly, neurodevelopment disorders, such as intellectual disability and speech delay, were reported in a relatively high percentage of 20% (7/33), which is higher than other under-recognized features.

The prenatal spectrum of EEC fetuses is quite different from that of postnatal cases. This is mainly because ectodermal dysplasia, the notable characteristic in most postnatal EEC cases, could not be detected by antenatal ultrasound. In addition, the incomplete penetrance makes it even harder for prenatal diagnosis. To further delineate the prenatal spectrum of EEC syndrome, we summarized the prenatal EEC cases from the literature. Up to now, only 14 fetal cases have been reported, including our fetus (not limited to the R304W mutation) (Supplementary Table S1) (Witters et al., 2001; Hamada et al., 2002; Janssens et al., 2008; Simonazzi et al., 2012; Gawrych et al., 2013; Enriquez et al., 2016; Hyder et al., 2017; Yang et al., 2017; Wenger et al., 2018; Liu et al., 2019; Friedmann et al., 2020). Cleft lip and palate is the most common prenatal ultrasound finding with the highest incidence of 64.3% (9/14). It would be higher if the autopsy results are accounted. To our surprise, the kidney malformations, including hydronephrosis and cystic dysplasia, rank the second with a percentage of 57.1% (8/14). The prevalence of genitourinary abnormalities in postnatal cases is much lower than that in prenatal cases, which might be due to the lack of renal ultrasound scans in postnatal patients.

Genitourinary abnormalities are an under-recognized feature of EEC in prenatal cases. There are very few recorded cases available on the prenatal ultrasound outcomes in patients with EEC, while most studies report fetuses with classic findings of cleft lip and palate or clefting of the hands and feet. Several studies have focused on the prenatal outcomes in patients with genitourinary abnormalities. Here, we report a fetus with cleft lip and palate, right polycystic kidney, and fetal megacystis (first trimester) and identify a pathogenic variation of the *TP63* gene by WES associated with EEC syndrome. To the best of our knowledge, this is the first report in China that described a fetus who went on to receive a diagnosis of prenatal EEC with genitourinary anomalies (right polycystic kidney and fetal megacystis). In our case, the earliest finding was an enlarged bladder with the diameter of 12 mm in the first trimester. Although the diameter of the bladder decreased gradually into a normal size, the fetus was finally diagnosed as the right multicystic kidney and left hydronephrosis. In other world countries, similarly, there are a less number of reports. Enriquez et al. (2016) reported a similar EEC fetus with unusual bladder distension at 14 weeks of gestation, who was finally confirmed to have multiple abnormalities of the lower genitourinary tract after autopsy. Janssens et al. (2008) also reported a fetus of EEC syndrome with bladder distension, mild bilateral hydronephrosis, and a prune belly. Our case presented with cleft lip and palate, right polycystic kidney, and fetal megacystis. Considering the solitary cleft lip and palate, negative family history, and lack of clefting of the hands and feet, the diagnosis of EEC would have been quite difficult without WES. In our case, an abnormal enlarged bladder in the first trimester would imply the possibility of genitourinary abnormalities. We suggest that physicians should alert the occurrence of EEC syndrome when genitourinary anomalies are observed with orofacial cleft or other findings. Prenatal WES is very useful to find the true etiology when negative results are presented in karyotyping and CMA.

Conclusion

Prenatal diagnosis of some certain monogenetic disorders has long been proved difficult due to very few cases and limited ultrasound phenotypes. We reported a fetus of EEC syndrome with genitourinary anomalies, cleft lip and palate, and no symptoms of ectrodactyly or syndactyly. To the best of our knowledge, this is the first report in China that described a

fetus who went on to receive a diagnosis of prenatal EEC with genitourinary anomalies (right polycystic kidney and fetal megacystis). Furthermore, a compilation of the prenatal manifestations of EEC is provided through a literature review, which can provide convenience for clinical applications. High penetrance is observed both in orofacial cleft and genitourinary malformations, while genitourinary anomalies are usually an under-recognized feature of EEC. Our case emphasizes the phenotypic spectrum of *TP63*-related disorders to include polycystic kidneys and fetal megacystis in the first trimester as a prenatal feature of EEC. Therefore, EEC syndrome should be suspected when patients have genitourinary anomalies with orofacial cleft or limb deformities. Finally, our report also reinforces the recommendation that the application of WES could help clarify unexpected prenatal findings, significantly improve the accuracy of prenatal diagnosis of genitourinary anomalies, and add prenatal phenotypic characteristics to known single-gene disorders.

Data availability statement

The datasets for this article are not publicly available due to concerns regarding participant/patient anonymity. Requests to access the datasets should be directed to the corresponding authors.

Ethics statement

The studies involving human participants were reviewed and approved by the Medical Ethics Committee of the International Peace Maternity and Child Health Hospital (GKLW 2019-24). The patients/participants provided their written informed consent to participate in this study. Written informed consent was obtained from the individual(s) for the publication of any potentially identifiable images or data included in this article.

Author contributions

HB and SM interpreted the data and wrote the manuscript. WYa, ZX, and GL collected clinical information and provided genetics counseling. HR, SJ, and WS provided patient samples and determined the phenotype based on the clinical criteria. WYi and CW designed the study and revised the manuscript.

Funding

The research was supported by the Shanghai Sailing Program (20YF1453800), and the Shanghai Municipal Commission of Science and Technology Program (19411960900 and 18411963500), and the Interdisciplinary Program of Shanghai Jiao Tong University (ZH2018QNB14).

Acknowledgments

The authors thank Dr. Yao Shifa for assistance with the ultrasound images.

Conflict of interest

The authors declare that the research was conducted in the absence of any commercial or financial relationships that could be construed as a potential conflict of interest.

Publisher's note

Supplementary material

The Supplementary Material for this article can be found online at: https://www.frontiersin.org/articles/10.3389/fgene.2022.1002089/full#supplementary-material

References

Barrow, L. L., van Bokhoven, H., Daack-Hirsch, S., Andersen, T., van Beersum, S. E., Gorlin, R., et al. (2002). Analysis of the p63 gene in classical EEC syndrome, related syndromes, and non-syndromic orofacial clefts. *J. Med. Genet.* 39 (8), 559–566. doi:10.1136/jmg.39.8.559

Bertola, D. R., Kim, C. A., Albano, L. M., Scheffer, H., Meijer, R., and van Bokhoven, H. (2004). Molecular evidence that AEC syndrome and Rapp-Hodgkin syndrome are variable expression of a single genetic disorder. *Clin. Genet.* 66 (1), 79–80. doi:10.1111/j.0009-9163.2004.00278.x

Bolger, A. M., Lohse, M., and Usadel, B. (2014). Trimmomatic: A flexible trimmer for illumina sequence data. *Bioinforma. Oxf. Engl.* 30 (15), 2114–2120. doi:10.1093/bioinformatics/btu170

Bourdon, J. C. (2007). p53 Family isoforms. *Curr. Pharm. Biotechnol.* 8 (6), 332–336. doi:10.2174/138920107783018444

Browne, G., Cipollone, R., Lena, A. M., Serra, V., Zhou, H., van Bokhoven, H., et al. (2011). Differential altered stability and transcriptional activity of

ΔNp63 mutants in distinct ectodermal dysplasias. *J. Cell Sci.* 124 (13), 2200–2207. doi:10.1242/jcs.079327

Brueggemann, F. B., and Bartsch, O. (2016). A recurrent TP63 mutation causing EEC3 and Rapp-Hodgkin syndromes. *Clin. Dysmorphol.* 25 (2), 50–53. doi:10.1097/MCD.0000000000000117

Brunner, H. G., Hamel, B. C., and Van Bokhoven, H. (2002). The p63 gene in EEC and other syndromes. *J. Med. Genet.* 39 (6), 377–381. doi:10.1136/jmg.39.6.377

de Mollerat, X. J., Everman, D. B., Morgan, C. T., Clarkson, K. B., Rogers, R. C., Colby, R. S., et al. (2003). P63 mutations are not a major cause of non-syndromic split hand/foot malformation. *J. Med. Genet.* 40 (1), 55–61. doi:10.1136/jmg.40.1.55

Dianzani, I., Garelli, E., Gustavsson, P., Carando, A., Gustafsson, B., Dahl, N., et al. (2003). Rapp-Hodgkin and AEC syndromes due to a new frameshift mutation in the TP63 gene. *J. Med. Genet.* 40 (12), e133. doi:10.1136/jmg.40.12.e133

Enriquez, A., Krivanek, M., Flöttmann, R., Peters, H., and Wilson, M. (2016). Recurrence of split hand/foot malformation, cleft lip/palate, and severe urogenital abnormalities due to germline mosaicism for TP63 mutation. *Am. J. Med. Genet. A* 170 (9), 2372–2376. doi:10.1002/ajmg.a.37816

Friedmann, I., Campagnolo, C., Chan, N., Hardy, G., and Saleh, M. (2020). TP63-mutation as a cause of prenatal lethal multicystic dysplastic kidneys. *Mol. Genet. Genomic Med.* 8 (11), e1486. doi:10.1002/mgg3.1486

Gawrych, E., Bińczak-Kuleta, A., Janiszewska-Olszowska, J., and Ciechanowicz, A. (2013). Ectrodactyly-ectodermal dysplasia-cleft syndrome (EEC syndrome) with a developmental delay caused by R304W mutation in the tp63 gene. *Ann. Acad. Med. Stetin.* 59 (1), 11–14.

Goldsmith, T., Eytan, O., Magal, L., Solomon, M., Israeli, S., Warshauer, E., et al. (2014). A mutation in TP63 causing a mild ectodermal dysplasia phenotype. *J. Invest. Dermatol.* 134 (8), 2277–2280. doi:10.1038/jid.2014.159

Hamada, T., Chan, I., Willoughby, C. E., Goudie, D. R., and McGrath, J. A. (2002). Common mutations in Arg304 of the p63 gene in ectrodactyly, ectodermal dysplasia, clefting syndrome: Lack of genotype-phenotype correlation and implications for mutation detection strategies. *J. Invest. Dermatol.* 119 (5), 1202–1203. doi:10.1046/j.1523-1747.2002.19526.x

Hyder, Z., Beale, V., O'Connor, R., and Clayton-Smith, J. (2017). Genitourinary malformations: An under-recognized feature of ectrodactyly, ectodermal dysplasia and cleft lip/palate syndrome. *Clin. Dysmorphol.* 26 (2), 78–82. doi:10.1097/MCD.0000000000000172

Ianakiev, P., Kilpatrick, M. W., Toudjarska, I., Basel, D., Beighton, P., and Tsipouras, P. (2000). Split-hand/split-foot malformation is caused by mutations in the p63 gene on 3q27. *Am. J. Hum. Genet.* 67 (1), 59–66. doi:10.1086/302972

Iqbal Ali, M., Aravinda, K., Nigam, N. K., and Ali, I. (2013). Two interesting cases of EEC syndrome. *J. Oral Biol. Craniofac. Res.* 3 (1), 45–48. doi:10.1016/j.jobcr.2013.02.001

Janssens, S., Defoort, P., Vandenbroecke, C., Scheffer, H., and Mortier, G. (2008). Prune belly anomaly on prenatal ultrasound as a presenting feature of ectrodactyly-ectodermal dysplasia-clefting syndrome (EEC). *Genet. Couns.* 19 (4), 433–437.

Koul, M., Dwivedi, R., and Upadhyay, V. (2014). Ectrodactyly-ectodermal dysplasia clefting syndrome (EEC syndrome). *J. Oral Biol. Craniofac. Res.* 4 (2), 135–139. doi:10.1016/j.jobcr.2014.08.002

Kumar, H. N., Kugar, T. S., Rao, R. J., and Kodkany, S. (2007). EEC syndrome. *Indian J. Ophthalmol.* 55 (2), 162–163. doi:10.4103/0301-4738.30725

Li, H., and Durbin, R. (2010). Fast and accurate long-read alignment with Burrows-Wheeler transform. *Bioinforma. Oxf. Engl.* 26 (5), 589–595. doi:10.1093/bioinformatics/btp698

Liu, Y., Wang, L., Yang, Y. K., Liang, Y., Zhang, T. J., Liang, N., et al. (2019). Prenatal diagnosis of fetal skeletal dysplasia using targeted next-generation sequencing: An analysis of 30 cases. *Diagn. Pathol.* 14 (1), 76. doi:10.1186/s13000-019-0853-x

Mikkola, M. L. (2007). p63 in skin appendage development. *Cell cycleGeorget. Tex.)* 6 (3), 285–290. doi:10.4161/cc.6.3.3798

Mills, A. A., Zheng, B., Wang, X. J., Vogel, H., Roop, D. R., and Bradley, A. (1999). p63 is a p53 homologue required for limb and epidermal morphogenesis. *Nature* 398 (6729), 708–713. doi:10.1038/19531

Nardi, A. C., Ferreira, U., Netto, N. R., Jr, Magna, L. A., Rodini, E. S. O., and Richieri-Costa, A. (1992). Urinary tract involvement in EEC syndrome: A clinical study in 25 Brazilian patients. *Am. J. Med. Genet.* 44, 803–806. doi:10.1002/ajmg.1320440617

Okamura, E., Suda, N., Baba, Y., Fukuoka, H., Ogawa, T., Ohkuma, M., et al. (2013). Dental and maxillofacial characteristics of six Japanese individuals with ectrodactyly-ectodermal dysplasia-clefting syndrome. *Cleft Palate. Craniofac. J.* 50 (2), 192–200. official publication of the American Cleft Palate-Craniofacial Association. doi:10.1597/11-123

Paranaíba, L. M., Martelli-Júnior, H., de Miranda, R. T., Bufalino, A., Abdo Filho, R. C., and Coletta, R. D. (2010). Ectrodactyly-ectodermal dysplasia-clefting syndrome associated with p63 mutation and an uncommon phenotype. *Cleft Palate. Craniofac. J.* 47 (5), 544–547. official publication of the American Cleft Palate-Craniofacial Association. doi:10.1597/09-063

Rinne, T., Brunner, H. G., and van Bokhoven, H. (2007). p63-associated disorders. *Cell cycleGeorget. Tex.)* 6 (3), 262–268. doi:10.4161/cc.6.3.3796

Simonazzi, G., Miccoli, S., Salfi, N., Bonasoni, M. P., Bocciardi, R., Ravazzolo, R., et al. (2012). A novel p63 mutation in a fetus with ultrasound detection of split hand/foot malformation. *Prenat. Diagn.* 32 (3), 296–298. doi:10.1002/pd.2932

Straub, W. E., Weber, T. A., Schäfer, B., Candi, E., Durst, F., Ou, H. D., et al. (2010). The C-terminus of p63 contains multiple regulatory elements with different functions. *Cell Death Dis.* 1 (1), e5. doi:10.1038/cddis.2009.1

Suh, E. K., Yang, A., Kettenbach, A., Bamberger, C., Michaelis, A. H., Zhu, Z., et al. (2006). p63 protects the female germ line during meiotic arrest. *Nature* 444 (7119), 624–628. doi:10.1038/nature05337

van Bokhoven, H., Hamel, B. C., Bamshad, M., Sangiorgi, E., Gurrieri, F., Duijf, P. H., et al. (2001). p63 Gene mutations in eec syndrome, limb-mammary syndrome, and isolated split hand-split foot malformation suggest a genotype-phenotype correlation. *Am. J. Hum. Genet.* 69 (3), 481–492. doi:10.1086/323123

Van der Auwera, G. A., Carneiro, M. O., Hartl, C., Poplin, R., Del Angel, G., Levy-Moonshine, A., et al. (2013). From FastQ data to high confidence variant calls: The genome analysis Toolkit best practices pipeline. *Curr. Protoc. Bioinforma.* 43 (1110), 11. doi:10.1–11.10.3310.1002/0471250953.bi1110s43

Vernersson Lindahl, E., Garcia, E. L., and Mills, A. A. (2013). An allelic series of Trp63 mutations defines TAp63 as a modifier of EEC syndrome. *Am. J. Med. Genet. A* 161A (8), 1961–1971. doi:10.1002/ajmg.a.36074

Wenger, T., Li, D., Harr, M. H., Tan, W. H., Pellegrino, R., Stark, Z., et al. (2018). Expanding the phenotypic spectrum of TP63-related disorders including the first set of monozygotic twins. *Am. J. Med. Genet. A* 176 (1), 75–81. doi:10.1002/ajmg.a.38516

Wessagowit, V., Mellerio, J. E., Pembroke, A. C., and McGrath, J. A. (2000). Heterozygous germline missense mutation in the p63 gene underlying EEC syndrome. *Clin. Exp. Dermatol.* 25 (5), 441–443. doi:10.1046/j.1365-2230.2000.00683.x

Witters, I., Van Bokhoven, H., Goossens, A., Van Assche, F. A., and Fryns, J. P. (2001). Split-hand/split-foot malformation with paternal mutation in the p63 gene. *Prenat. Diagn.* 21 (13), 1119–1122. doi:10.1002/pd.181

Yang, A., Schweitzer, R., Sun, D., Kaghad, M., Walker, N., Bronson, R. T., et al. (1999). p63 is essential for regenerative proliferation in limb, craniofacial and epithelial development. *Nature* 398 (6729), 714–718. doi:10.1038/19539

Yang, Y., Huang, L. Y., Han, J., and Li, D. Z. (2017). Prenatal diagnosis of Ectrodactyly-Ectodermal dysplasia-Cleft (EEC) syndrome in a Chinese woman with a TP63 mutation. *Eur. J. Obstet. Gynecol. Reprod. Biol.* 213, 146–147. doi:10.1016/j.ejogrb.2017.04.012

Yin, W., Ye, X., Shi, L., Wang, Q. K., Jin, H., Wang, P., et al. (2010). TP63 gene mutations in Chinese P63 syndrome patients. *J. Dent. Res.* 89 (8), 813–817. doi:10.1177/0022034510366804

Zheng, J., Liu, H., Zhan, Y., Liu, Y., Wong, S. W., Cai, T., et al. (2019). Tooth defects of EEC and AEC syndrome caused by heterozygous TP63 mutations in three Chinese families and genotype-phenotype correlation analyses of TP63-related disorders. *Mol. Genet. Genomic Med.* 7 (6), e704. doi:10.1002/mgg3.704

frontiers | Frontiers in Pediatrics

TYPE Case Report
PUBLISHED 09 November 2022
DOI 10.3389/fped.2022.1004485

OPEN ACCESS

EDITED BY
Aleksandra Jezela-Stanek,
National Institute of Tuberculosis and Lung Diseases, Poland

REVIEWED BY
Cristina Skrypnyk,
Arabian Gulf University, Bahrain
Frederic Tort,
Hospital Clinic of Barcelona, Spain

CORRESPONDENCE
Ruixia Tian
tianruixia_01@163.com

SPECIALTY SECTION
This article was submitted to Genetics of Common and Rare Diseases, a section of the journal Frontiers in Pediatrics

RECEIVED 27 July 2022
ACCEPTED 24 October 2022
PUBLISHED 09 November 2022

CITATION
Zhao X, Li X, Sun W, Jia J-a, Yu M and Tian R (2022) Prenatal case report of Barth syndrome caused by novel *TAFAZZIN* mutation: Clinical characteristics of fetal dilated cardiomyopathy with ascites.
Front. Pediatr. 10:1004485.
doi: 10.3389/fped.2022.1004485

Prenatal case report of Barth syndrome caused by novel *TAFAZZIN* mutation: Clinical characteristics of fetal dilated cardiomyopathy with ascites

Xuliang Zhao[1], Xu Li[2], Weiwei Sun[3], Jian-an Jia[1], Min Yu[4] and Ruixia Tian[4]

[1]Department of Laboratory, The 901th Hospital of the Joint Service of the People's Liberation Army, Hefei, China, [2]Department of Radiology, Anhui Children's Hospital, Hefei, China, [3]Department of Medical, Beijing Chigene Translational Medicine Research Center, Beijing, China, [4]Department of Obstetrics and Gynecology, The 901th Hospital of the Joint Service of the People's Liberation Army, Hefei, China

Barth syndrome (BTHS) is a rare X-linked recessive genetic disease, which appears in infancy with myocardial and skeletal muscle diseases, neutropenia, growth retardation, and other clinical features. *TAFAZZIN* is the pathogenic gene of BTHS, which encodes the tafazzin protein of the inner membrane of the mitochondria, a phosphatidyltransferase involved in cardiolipin remodeling and functional maturation. At present, BTHS has been widely reported, but prenatal cases are rare. We report a 24^{+4}-week fetus with clinical manifestations including left ventricular insufficiency and ascites. After induced labor, whole exome sequencing detection of fetal skin tissue showed that *TAFAZZIN* had the mutation c.311A > C/*p*.His104Pro and that his mother was the carrier. This His104Pro mutation has hitherto not been reported, and it is rated as likely to be pathogenic according to the American College of Medical Genetics and Genetics guidelines. Molecular dynamics and protein expression experiments on the His104Pro mutation showed that the stability of the local protein structure and protein expression were reduced. In conclusion, the case presented in this study enriches our knowledge of the *TAFAZZIN* mutation spectrum and suggests that His104Pro may lead to cardiac structural abnormalities in the early embryo. The possibility of BTHS should be considered when an abnormal cardiac structure or ascites appear in a prenatal ultrasound.

KEYWORDS

tafazzin, prenatal diagnosis, LVNC, WES, congenital heart disease

Introduction

Barth syndrome (BTHS, OMIM#302060) is a rare X-linked recessive disorder characterized by cardiomyopathy, skeletal myopathy, growth retardation, neutropenia, and increased urinary excretion of 3-methylglutaric acid (3-MGCA) (1). This syndrome was first reported in 1983 and described as a triad of mitochondrial myopathy, neutropenia, and dilated cardiomyopathy (DCM) with high mortality in

infants (2, 3). *TAFAZZIN* mutation is the main causative factor of BTHS. This gene encodes the tafazzin (TAFAZZIN) protein, a phosphatidyltransferase located in the inner membrane of the mitochondria, which plays a key role in cardiolipin (CL) remodeling. Decreased TAFAZZIN enzyme activity can affect the formation of respiratory chain supercomplexes and cause cardiomyopathy (4, 5). Children with BTHS mainly present with DCM, and more than half of the cases are accompanied by left ventricular non-compaction (LVNC) (1, 5). Although the cardiomyopathy phenotype of patients will gradually improve over time or remain stable after a certain point, their cardiac ejection function may continue to decrease. Thus, heart failure may be a major cause of death in patients with BTHS (3, 5).

To date, BTHS has been widely reported, but prenatal cases are relatively rare. Here, we identified a fetus with an abnormal cardiac structure, cardiac insufficiency, and ascites upon prenatal ultrasound examination at only 24^{+4} weeks. After induced labor, the skin tissue was tested for genetic diagnosis by trio-whole exome sequencing (trio-WES). Bioinformatic prediction and construction of a molecular dynamics (MD) model showed that a novel *TAFAZZIN* missense mutation was the key pathogenic factor for the fetal phenotype in this case. The results of this study enrich our knowledge of the mutation spectrum of *TAFAZZIN* and provide a reliable basis for predicting recurrence risk in future pregnancies for the genetic counseling of the family.

Case report

Case presentation

A 31-year-old pregnant woman presented to us, mentioning that her first fetus was induced following fetal heart abnormalities and ascites. Routine ultrasound examination at 24^{+4} weeks of this pregnancy showed that the biparietal diameter of the fetus was 57 mm, the head circumference was 218 mm, and the femoral length was 45 mm. In the fetal heart, the apex of the heart pointed to the left side of the chest, and the cardiothoracic proportion was high, at approximately 0.45. The left atrium and ventricle were obviously enlarged, and the oval valve of the atrial septum was visible. Myocardial thickening was observed. The left ventricular wall was approximately 4.2 mm thick, while the right was approximately 2.2 mm thick. Free fluid was visible in the pericardial cavity, with approximately 4.0 and 3.7 mm outside the left and right ventricles, respectively. We noted pulmonary artery stenosis, pulmonary valve echo enhancement and thickening, and no obvious opening and closing movement. Color Doppler flow imaging showed moderate regurgitation at the mitral valve orifice of the fetus, with a regurgitation velocity of 210 cm/s. Full systolic regurgitation was visible at the tricuspid valve orifice, and the regurgitation velocity was 180 cm/s. A wave reversal was visible in the venous catheter, and pulsation was visible in the umbilical vein. In addition, 16 mm free fluid and thickening of abdominal subcutaneous tissue were seen in the abdominal cavity of the fetus (**Figures 1A–C**).

Both parents are healthy people in a non-consanguineous marriage. After being fully informed of the relevant risks, the couple decided to terminate their pregnancy. After induction of labor, physical examination showed that the fetal abdomen was swollen. The autopsy revealed increased fetal ascites, a significantly enlarged heart, and hypertrophy of the myocardium. The fetal heart tissue was taken for pathological examination, which showed that the endocardium was thickened and fibrotic, the dense myocardium was relatively thin, and the ventricular wall muscle layer remained loose (**Figures 1D–F**).

Genetic analysis

The work described in this case report was conducted in accordance with the Code of Ethics of the World Medical Association (Declaration of Helsinki) for experiments involving humans (https://www.wma.net/policies-post/wma-declaration-of-helsinki-ethical-principles-for-medical-research-involving-human-subjects/). This study was reviewed by the ethics committee of the 901st Hospital of the Joint Service of the People's Liberation Army (ID: 202112001). The pregnant woman and her family members signed informed consent statements for this study and agreed to the publication of the clinical data and images of her fetus.

We collected the induced labor fetal tissue (approximately 2 g of skin tissue from the inner thigh) and extracted 3 ml of peripheral venous blood (treated with EDTA for anticoagulation) from both husband and wife for trio-WES. Leukocyte DNA was extracted according to the operation steps of the genome extraction kit (CoWin Biotech Co., Inc., Beijing, China). After the library was constructed, the designed sequence was captured by an Illumina NovaSeq 6,000 high-throughput sequencer (Illumina Co., Inc., San Diego, CA, USA). The screened mutations were checked against frequency databases of normal people, including dbSNP (www.ncbi.nlm.nih.gov/snp/), ExAC (www.exac.broadinstitute.org/), and 1,000 Genomes (www.1000genomes.org/), and the hazard was predicted and analyzed.

The genetic sequencing results showed that the mutation occurred in exon 3 of *TAFAZZIN* on the fetal hemizygote, NM_001303465: c.311A > C/*p*.His104Pro. The father had the wild-type form, and the mother carried the mutation. Sanger sequencing confirmed the existence of the mutation (**Figure 2A**). This mutation was not included in the frequency database of normal people, and biohazard prediction and

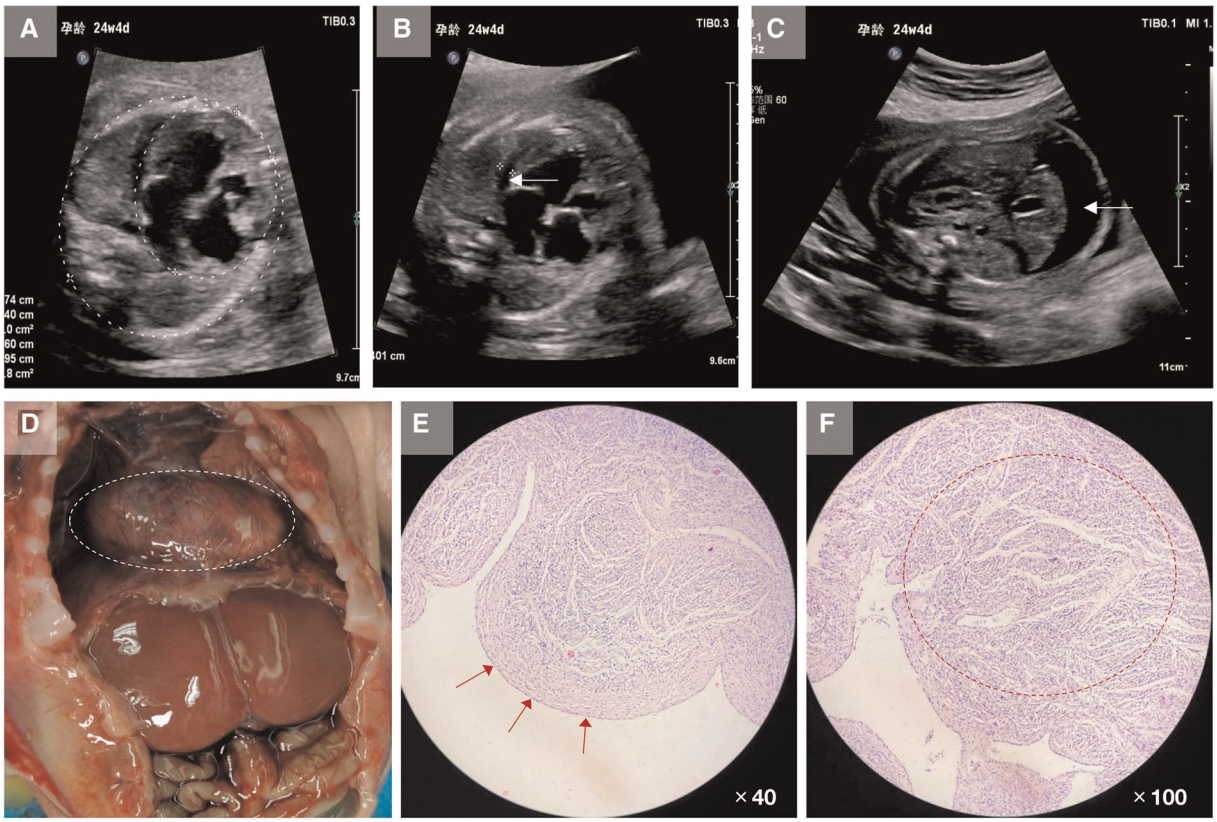

FIGURE 1
Clinical characteristics of the fetus in this study. (A) Ultrasound showed that the fetal cardiothoracic area ratio was increased, approximately 0.45, and the left atrium and left ventricle sizes were increased substantially. (B) Ultrasound showed hypertrophy of fetal myocardium and free fluid in the pericardial cavity (white arrow). (C) Ultrasound showed a large amount of free fluid in the fetal abdominal cavity and thickened abdominal skin tissue (white arrow). (D) After induced labor, autopsy revealed the heart was considerably enlarged. (E) Pathological sections showed thickening and fibrosis of the endocardial tissue (red arrows). (F) The muscular trabeculae were thick, the sinus recess of the myocardium persisted, the deep depression was staggered, the formation of dense myocardium in the corresponding area was reduced and thin, and the ventricular wall muscle layer remained loose (red circle).

analysis software suggested that this variation can lead to changes in protein structure (**Table 1**). According to the guidelines of the American College of Medical Genetics and Genomics, the His104Pro mutation is rated as likely to be pathogenic, and the rating evidence was PM1 + PM2 + PP3 + PP4 (6).

MD analysis

In brief, we queried the TAFAZZIN protein sequence in the National Center for Biotechnology Information database (https://www.ncbi.nlm.nih.gov/nuccore/NM_001303465.2/) and downloaded the crystal model file of TAFAZZIN from the UniProt database (https://www.uniprot.org/uniprotkb/Q16635/entry#structure). We used single template modeling in Modeller10.1 (https://salilab.org/modeller/). The His104Pro mutant structure was constructed using PyMOL 2.5 (https://pymol.org/2/), based on the crystal structure, and wild-type and mutant proteins were simulated by MD in the GROMACS 5.1.4 program package (http://www.gromacs.org/) under a constant pressure and temperature ensemble. Finally, Chimera 1.15 (http://www.cgl.ucsf.edu/chimera/) was used to analyze the interaction.

MD results showed that the wild-type and mutant structures reached equilibrium at approximately 4,000 ps, and the value after equilibrium was approximately 2.6 Å. Conservation analysis showed that His104 was highly conserved among various species. The results of structural analysis showed that the main chain of wild-type His104 formed a hydrogen bond with Lys101, and the side chain formed a hydrogen bond with Glu73. The His104Pro mutation breaks the hydrogen bond between Lys101 and Glu73. In addition, because Pro104 is a five-membered ring containing an N structure with strong structural rigidity, the spatial steric resistance formed may cause the structure of the α-helix to become a loop, affecting its ability to interact with surrounding structures and resulting in reduced local structural stability (**Figures 2B,C**).

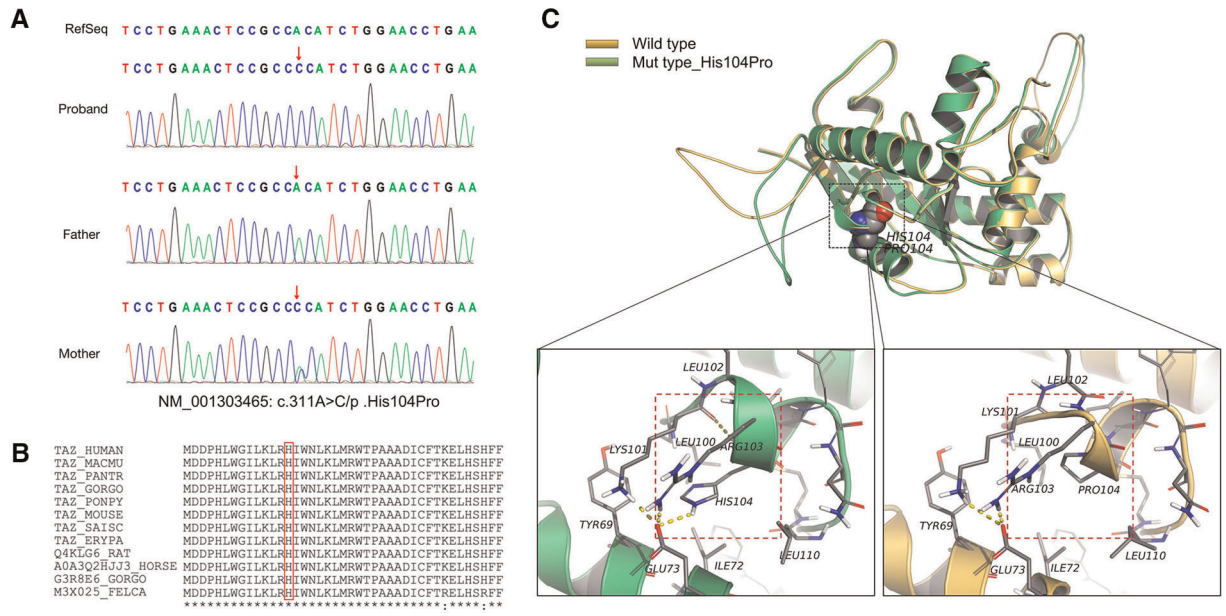

FIGURE 2
Information on the mutation found in this case. (**A**) The results of gene detection showed that *TAFAZZIN* had a missense mutation, c.311A > C/*p*.His104Pro. The father carried the wild-type form, while the mother carried the mutation. Sanger sequencing confirmed the existence of the mutation. (**B**) His104 is conserved between species (red box). (**C**) The crystal structure model analysis results show that the main chain N–H bond of His104 forms a hydrogen bond with Lys101, and the side chain forms a hydrogen bond with Glu73. When the mutation of His104Pro occurs, the hydrogen bond between Lys101 and Glu73 is broken because Pro104 has a five-membered ring structure with greater rigid strength than the straight-chain structure. Simultaneously, owing to the steric hindrance of Pro104, the secondary structure (part of the α-helix) may become a loop domain (red box). Therefore, the His104Pro mutation may reduce the stability of the local protein structure and affect its biological function.

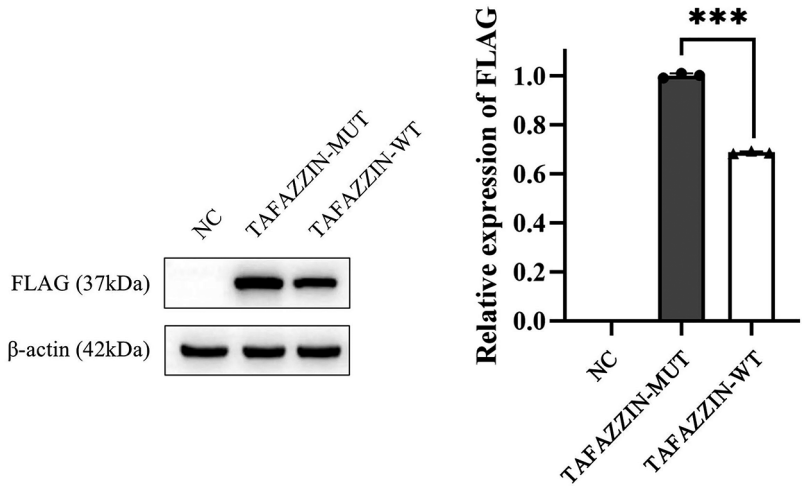

FIGURE 3
Western blotting results show that the protein expression in TAFAZZIN-MUT (the His104Pro mutant) is significantly lower than that in TAFAZZIN-WT (the wild type), indicating that His104Pro may reduce human TAFAZZIN protein expression and affect relevant biological functions. *, $p < 0.05$; NC, negative control.

Western blot (WB)

We first constructed wild-type (TAFAZZIN-WT) and mutant (TAFAZZIN-MUT) plasmids of TAFAZZIN: the target fragment of TAFAZZIN-WT was amplified with high fidelity polymerase Phanta® Max Super-Fidelity DNA Polymerase (#P505; Vazyme Inc., Nanjing, China) and transfected into the vector pECMV-3 × FLAG-N. Then the

TABLE 1 Hazard prediction and analysis of the novel *TAFAZZIN* mutation.

Gene	*TAFAZZIN* (OMIM#300394)
Transcript	NM_001303465
Variant	c.311A > C/*p*.His104Pro
Prediction software	
Provean	Deleterious (−5.1)
SIFT (www.sift.bii.a-star.edu.sg/)	Damaging (0.039)
Polyphen2_HDIV (www.sift.bii.a-star.edu.sg/)	Benign (0.0)
Polyphen2_HVAR (www.sift.bii.a-star.edu.sg/)	Benign (0.001)
MutationTaster (www.mutationtaster.org/)	Disease_causing (0.999954)
M-CAP (http://bejerano.stanford.edu/mcap/)	Damaging (0.763338)
REVEL	Deleterious (0.707)
Distributed frequency database	
dbSNP (www.ncbi.nlm.nih.gov/snp/)	Not included
ExAC (www.exac.broadinstitute.org/)	Not included
1,000 Genome (www.1000genomes.org/)	Not included

TAFAZZIN-WT plasmid was constructed using a ClonExpress® II One Step Cloning Kit (#C215; Vazyme Inc.) for recombination transformation. The constructed plasmid was transfected into human Hek293T cells with 5 μl Lip2000 reagent (Thermo Fisher Scientific Inc., Waltham, MA, USA). The protein (80 μg) was extracted with protein lysate (Beyotime Inc., Shanghai, China), and the protein expression was examined by WB analysis. The results were analyzed using ImageJ software, and it was found that the protein expression of the TAFAZZIN-MUT group was significantly lower than that of the TAFAZZIN-WT group; it was reduced by approximately 31.37% ($p < 0.001$). This indicates that the variation in His104Pro might lead to a decrease in protein expression, thereby affecting protein function (**Figure 3**). Antibody information: first antibody mouse anti-human FLAG (Cat. #8146; Cell Signaling Technology Inc., Danvers, MA, USA), mouse anti-human β-actin (Cat. #3700; Cell Signaling Technology Inc.), dilution ratio 1:1,000; anti-mouse IgG, HRP-linked antibody (Cat. #7076; Cell Signaling Technology Inc.), dilution ratio 1:5,000.

Discussion

To date, more than 200 patients with BTHS have been reported, most of whom were male, which is related to the X-linked inheritance of the disease (7, 8). Although BTHS has been widely reported, prenatal cases are rare (**Table 2**). In this study, prenatal ultrasound of a fetus revealed LVNC and ascites at 24^{+4} weeks gestation. After induced labor, fetal skin tissue and peripheral blood samples from the parents were extracted for genetic screening, and it was found that the fetus and its mother carried a novel missense mutation of *TAFAZZIN*, His104Pro. We predicted and analyzed that the mutation could affect protein function through a variety of bioinformatics software models. MD studies showed that the structural stability of the mutant His104Pro was reduced owing to the destruction of the surrounding hydrogen bonds. The WB analysis showed that the His104Pro mutation resulted in decreased protein expression. Through the results of this study, we expanded our knowledge of the mutation spectrum of *TAFAZZIN*; furthermore, we studied the harmful biological implications of the novel His104Pro mutation, demonstrating that it may lead to cardiac dysplasia in the early embryo.

Owing to the poor clinical specificity of BTHS, the diagnosis rate in the fetal period is particularly low. Cardonick et al. (9) first reported a 33-week-old fetus with congenital heart disease, asymmetric intrauterine growth retardation, oligohydramnios, and other phenotypes, with ventricular dysfunction continuing after birth. Finally, the infant was confirmed as having BTHS by 3-MGCA and neutrophil measurements. In a case from 2006, Brady et al. (10) reported a fetus with ascites and cardiac enlargement detected by ultrasound at 32 weeks of gestation. After induction of labor, the embryonic heart tissue was described as having endocardial elastic fiber hyperplasia, endocardial myocardial fiber cavitation, and other pathological features at autopsy. Steward et al. (11) reported several prenatal cases with BTHS family genetic histories in 2010, finding unexplained male fetal edema and serious cardiac structural abnormalities such as DCM and LVNC in ultrasonic diagnosis. According to previous prenatal case reports, BTHS can cause cardiac structural abnormalities of varying severity in the fetal period, and this may be accompanied by intrauterine growth retardation, ascites, and edema. Combined with the ultrasonic characteristics of LVNC and ascites observed in this study, we suggest that when unknown cardiac structural abnormalities such as DCM and LVNC accompanied by ascites or edema are found in prenatal diagnosis, the possibility of BTHS should be considered.

TAFAZZIN, also known as G4.5, causes BTHS. It was previously named *TAZ* and is located in the gene-rich region Xq28 (12). TAFAZZIN protein can participate in phospholipid biosynthesis and remodeling of the acyltransferase superfamily. It also plays a key role in CL remodeling. Defective CL has been demonstrated to considerably damage mitochondrial function and structure (13). Many types of *TAFAZZIN* mutations have been reported, including loss of function mutations, such as frameshift and nonsense mutations, and splice and missense mutations. These mutations are distributed throughout the 11 exons of *TAFAZZIN* and can lead to complete protein loss, reduced expression level, or reduced function, such as

TABLE 2 Characteristics of previously reported prenatal cases of Barth syndrome.

Family	Case	Gestation period	Ascites	Edema	DCM	LVNC	EFE	Pancreas atrophy	Neutropenia	Other	Outcome	Mutation	Ref.
F1	1	31 W	-	+	+	-	+	+	+	NA	Died of pleural effusion and ascites 3 days after birth.	Arg94Gly	(9)
F2	2	$32^{+}5$ W	+	-	-	-	-	-	-	Cardiac enlargement	Death 12 days after birth. Autopsy showed cardiac enlargement. Under the microscope, endocardial fibroelastosis and subendocardial muscle cell vacuolization were suggested. Electron microscopy showed that the mitochondria were enlarged, and the cristae were disordered.	Arg94Gly	(10)
F3	3	30 W	-	-	+	-	-	-	-	NA	Induced labor	Arg94Gly	(11)
F3	4	31 W	+	-	+	NA	NA	+	NA	NA	Drainage of pleural effusion and ascites after cesarean section at 34 weeks, and death on the third day after birth. Autopsy showed renal tubular/cortical and pontosubicular neuronal necrosis.		(11)
F3	5	31 W	-	-	+	-	+	+	-	NA	-		(11)
F4	6	37 W	-	-	+	+	+	NA	+	NA	Stillbirth in cesarean section	c.583 + 5G > A	(11)
F5	7	22 W	-	-	+	-	-	-	-	NA	Delivered at 32 weeks owing to fetal distress and died of ventricular arrhythmia 1 week after birth.	Gly197Arg	(11)
F6	8	NA	-	-	-	-	-	-	-	IUGR	DCM was detected 8 months after birth.	Ile209Asn	(11)
F6	9	33^{+4} W	-		+	-	-	-	+	IUGR	Unknown	His69Gln	(11)
F7	10	22 W	NA	NA	NA	NA	NA	NA	NA	Multiple malformations	-	Gln280GlyfsX30	(11)
Our study	11	24^{+4} W	+	+	+	+	+	-	NA	-	Induced labor	His104Pro	Our study

W, weeks; DCM, dilated cardiomyopathy; LVNC, left ventricular non-compaction; EFE, endocardial fibroelastosis; IUGR, intrauterine growth retardation; NA, Not applicable; Ref., reference.

10.3389/fped.2022.1004485

mitochondrial mistargeting, altered TAFAZZIN macroscopic assembly or folding, and assembly defects (12, 14). In prenatal BTHS cases, including this one, the main *TAFAZZIN* mutation type is a missense mutation, while splicing and frameshift mutations have also been reported sporadically. Noteworthily, most missense variations in prenatal cases are cause pathological changes that affect the binding of protein and substrate. For example, in three cases, the hot spot mutation Arg94Gly (located on the surface of TAFAZZIN) weakens the positive charge of arginine and prevents protein and substrate binding (9–11). Moreover, the His104Pro mutation, identified in this study, and His69Gln and Gly197Arg, previously reported, are located in the buried region. The His69Gln and Gly197Arg mutations have been confirmed to result in protein conformation changes due to altered residue charge, thus affecting substrate binding (11, 14). MD showed that the His104Pro mutation also affected the stability of the protein structure owing to altered charge. WB results revealed that the expression of the mutant protein decreased by approximately 31.37%, indicating that His104Pro decreased protein stability. However, at present, there is not enough evidence supporting that different types or locations of *TAFAZZIN* mutations are related to the severity of BTHS phenotype or prenatal pathological changes (15).

BTHS was once considered simple congenital heart disease; however, increasing numbers of clinical reports have shown that it is a syndrome involving multiple systems. Approximately 70% of children with BTHS show cardiomyopathy, but there are great variations among different individuals. For example, most patients' cardiomyopathy occurs in the form of DCM, LVNC, and endocardial fibroelastosis, while some children can further develop ventricular arrhythmia, heart failure, and even sudden cardiac death owing to myocardial cell damage (16, 17). Neutropenia is the main hematological abnormality index of BTHS patients, which may lead to serious infection. Although cardiomyopathy is the main symptom of this syndrome, some children only show infantile infections rather than heart problems at the first diagnosis (5). The molecular mechanism of BTHS neutrophil deficiency is unclear, but some studies have shown that the stability of respiratory chain complexes is reduced owing to a lack of CL, which increases the reactive oxygen species content and induces phosphatidylserine exposure, resulting in increased neutrophil clearance (18). In addition, skeletal myopathy is also a common BTHS phenotype, usually in the form of non-progressive proximal myasthenia and motor retardation. Children with BTHS generally have a higher rate of protein hydrolysis, which leads to a reduction of skeletal muscle content. The damage to CL remodeling and fatty acid composition caused by *TAFAZZIN* mutation may be one factor contributing to this skeletal myopathy (19). As BTHS may affect the heart and immune system and cause skeletal myopathy, we believe that clinical diagnosis should be combined with multi-system examination.

At present, there is no specific treatment plan for BTHS. Generally, symptomatic treatment is carried out according to the phenotype of the child. Most children with heart failure mainly rely on the use of conventional anti-heart failure drugs including β-receptor blockers or angiotensin-converting enzyme inhibitors, while some children may need surgical treatment such as mitral valve replacement or heart transplantation (20, 21). In recent years, research on gene replacement therapy using the adeno-associated virus as a vector has made some progress in a *TAFAZZIN* knockout mouse model. The mice in the experimental treatment group showed increased *TAFAZZIN* expression and restored myocardial and skeletal muscle function (22). Although this technology still requires extensive research using human studies, this animal model has provided strong evidence suggesting it as a potentially effective treatment option for BTHS in humans.

In summary, we report a prenatal case of LVNC with ascites observed during a routine ultrasound examination at 24^{+4} weeks of gestation. Genetic testing of the fetal hemizygotes suggests that a novel *TAFAZZIN* mutation leads to BTHS. This study emphasizes that if cardiac structural abnormalities such as DCM, LVNC, or endocardial fibroelastosis are found in prenatal diagnosis, clinicians should pay attention when a male fetus presents with edema and other phenotypes that may have suggestive value for the further identification of BTHS.

Data availability statement

The datasets presented in this study can be found in online repositories. The names of the repository/repositories and accession number(s) can be found in the article/ Supplementary Materials.

Ethics statement

The studies involving human participants were reviewed and approved by This study was reviewed by the ethics committee of the 901th Hospital of the Joint Service of the People's Liberation Army (ID: 202112001). The patients/ participants provided their written informed consent to participate in this study. Written informed consent was obtained from the individual(s) for the publication of any potentially identifiable images or data included in this article.

Author contributions

XZ wrote the main manuscript and conducted the molecular genetics experiments. XZ, XL, and JJ prepared the clinical data and image data. WS contributed to the revision of the manuscript, gene evaluation, and the inspection of the gene database analysis. MY and RT critically revised the manuscript. All authors contributed to the article and approved the submitted version.

Acknowledgments

The authors are grateful to the patient and their family for participation in this study, as well as the help of all the physicians during medical treatment.

Conflict of interest

The authors declare that the research was conducted in the absence of any commercial or financial relationships that could be construed as a potential conflict of interest.

Publisher's note

References

1. Clarke SLN, Bowron A, Gonzalez IL, Groves SJ, Newbury-Ecob R, Clayton N, et al. Barth syndrome. *Orphanet J Rare Dis*. (2013) 8:23. doi: 10.1186/1750-1172-8-23

2. Barth PG, Scholte HR, Berden JA, Van der Klei-Van Moorsel JM, Luyt-Houwen IE, Van 't Veer-Korthof ET, et al. An X-linked mitochondrial disease affecting cardiac muscle, skeletal muscle and neutrophil leucocytes. *J Neurol Sci*. (1983) 62(1-3):327–55. doi: 10.1016/0022-510x(83)90209-5

3. Jefferies JL. Barth syndrome. *Am J Med Genet C Semin Med Genet*. (2013) 163C(3):198–205. doi: 10.1002/ajmg.c.31372

4. Schlame M. Cardiolipin remodeling and the function of tafazzin. *Biochim Biophys Acta*. (2013) 1831(3):582–8. doi: 10.1016/j.bbalip.2012.11.007

5. Rigaud C, Lebre A-S, Touraine R, Beaupain B, Ottolenghi C, Chabli A, et al. Natural history of barth syndrome: a national cohort study of 22 patients. *Orphanet J Rare Dis*. (2013) 8:70. doi: 10.1186/1750-1172-8-70

6. Richards S, Aziz N, Bale S, Bick D, Das S, Gastier-Foster J, et al. Standards and guidelines for the interpretation of sequence variants: a joint consensus recommendation of the American college of medical genetics and genomics and the association for molecular pathology. *Genet Med*. (2015) 17(5):405–24. doi: 10.1038/gim.2015.30

7. Miller PC, Ren M, Schlame M, Toth MJ, Phoon CKL. A Bayesian analysis to determine the prevalence of Barth syndrome in the pediatric population. *J Pediatr*. (2020) 217:139–44. doi: 10.1016/j.jpeds.2019.09.074

8. Roberts AE, Nixon C, Steward CG, Gauvreau K, Maisenbacher M, Fletcher M, et al. The Barth syndrome registry: distinguishing disease characteristics and growth data from a longitudinal study. *Am J Med Genet A*. (2012) 158A(11): 2726–32. doi: 10.1002/ajmg.a.35609

9. Cardonick EH, Kuhlman K, Ganz E, Pagotto LT. Prenatal clinical expression of 3-methylglutaconic aciduria: Barth syndrome. *Prenat Diagn*. (1997) 17(10):983–8. doi: 10.1002/(sici)1097-0223(199710)17:10<983::aid-pd174>3.0.co;2-0

10. Brady AN, Shehata BM, Fernhoff PM. X-linked fetal cardiomyopathy caused by a novel mutation in the TAZ gene. *Prenat Diagn*. (2006) 26(5):462–5. doi: 10.1002/pd.1438

11. Steward CG, Newbury-Ecob RA, Hastings R, Smithson SF, Tsai-Goodman B, Quarrell OW, et al. Barth syndrome: an X-linked cause of fetal cardiomyopathy and stillbirth. *Prenat Diagn*. (2010) 30(10):970–6. doi: 10.1002/pd.2599

12. Pang J, Bao Y, Mitchell-Silbaugh K, Veevers J, Fang X. Barth syndrome cardiomyopathy: an update. *Genes (Basel)*. (2022) 13(4):656. doi: 10.3390/genes13040656

13. Houtkooper RH, Vaz FM. Cardiolipin, the heart of mitochondrial metabolism. *Cell Mol Life Sci*. (2008) 65(16):2493–506. doi: 10.1007/s00018-008-8030-5

14. Garlid AO, Schaffer CT, Kim J, Bhatt H, Guevara-Gonzalez V, Ping P. TAZ Encodes tafazzin, a transacylase essential for cardiolipin formation and central to the etiology of Barth syndrome. *Gene*. (2020) 726:144148. doi: 10.1016/j.gene.2019.144148

15. Ronvelia D, Greenwood J, Platt J, Hakim S, Zaragoza MV. Intrafamilial variability for novel TAZ gene mutation: Barth syndrome with dilated cardiomyopathy and heart failure in an infant and left ventricular noncompaction in his great-uncle. *Mol Genet Metab*. (2012) 107(3):428–32. doi: 10.1016/j.ymgme.2012.09.013

16. Claypool SM, Boontheung P, McCaffery JM, Loo JA, Koehler CM. The cardiolipin transacylase, tafazzin, associates with two distinct respiratory components providing insight into Barth syndrome. *Mol Biol Cell*. (2008) 19 (12):5143–55. doi: 10.1091/mbc.e08-09-0896

17. Ikon N, Ryan RO. Barth syndrome: connecting cardiolipin to cardiomyopathy. *Lipids*. (2017) 52(2):99–108. doi: 10.1007/s11745-016-4229-7

18. Finsterer J, Frank M. Haematological features in Barth syndrome. *Curr Opin Hematol*. (2013) 20(1):36–40. doi: 10.1097/MOH.0b013e32835a01d9

19. Vreken P, Valianpour F, Nijtmans LG, Grivell LA, Plecko B, Wanders RJ, et al. Defective remodeling of cardiolipin and phosphatidylglycerol in Barth syndrome. *Biochem Biophys Res Commun*. (2000) 279(2):378–82. doi: 10.1006/bbrc.2000.3952

20. Mangat J, Lunnon-Wood T, Rees P, Elliott M, Burch M. Successful cardiac transplantation in Barth syndrome – single-centre experience of four patients. *Pediatr Transplant*. (2007) 11(3):327–31. doi: 10.1111/j.1399-3046.2006.00629.x

21. Lei M, Wu L, Terrar DA, Huang CL-H. Modernized classification of cardiac antiarrhythmic drugs. *Circulation*. (2018) 138(17):1879–96. doi: 10.1161/CIRCULATIONAHA.118.035455

22. Suzuki-Hatano S, Saha M, Rizzo SA, Witko RL, Gosiker BJ, Ramanathan M, et al. AAV-mediated TAZ gene replacement restores mitochondrial and cardioskeletal function in Barth syndrome. *Hum Gene Ther*. (2019) 30(2): 139–54. doi: 10.1089/hum.2018.020

frontiers | Frontiers in Genetics

TYPE Case Report
PUBLISHED 29 November 2022
DOI 10.3389/fgene.2022.1010078

OPEN ACCESS

EDITED BY
Przemysław Kosinski,
Medical University of Warsaw, Poland

REVIEWED BY
Jiancheng Han,
Capital Medical University, China
Takeshi Aiba,
National Cerebral and Cardiovascular Center, Japan

*CORRESPONDENCE
Kaiyu Zhou,
kaiyuzhou313@163.com
Haiyan Yu,
fanjy422@163.com
Yifei Li,
liyfwcsh@scu.edu.cn

†These authors have contributed equally to this work

SPECIALTY SECTION
This article was submitted to Genetics of Common and Rare Diseases, a section of the journal Frontiers in Genetics

RECEIVED 02 August 2022
ACCEPTED 03 November 2022
PUBLISHED 29 November 2022

CITATION
Huang H, Jing S, Wu S, Wei L, Zhang Q, Hua Y, Li Y, Yu H and Zhou K (2022), Case Report: A novel *KNCH2* variant-induced fetal heart block and the advantages of fetal genomic sequencing in prenatal long-term dexamethasone exposure.
Front. Genet. 13:1010078.
doi: 10.3389/fgene.2022.1010078

Case Report: A novel *KNCH2* variant-induced fetal heart block and the advantages of fetal genomic sequencing in prenatal long-term dexamethasone exposure

Huiping Huang[1,2†], Siyuan Jing[1†], Shaoying Wu[3], Li Wei[1], Qian Zhang[1], Yimin Hua[1], Yifei Li[1*], Haiyan Yu[4*] and Kaiyu Zhou[1*]

[1]Key Laboratory of Birth Defects and Related Diseases of Women and Children of MOE, Department of Pediatrics, West China Second University Hospital, Sichuan University, Chengdu, China, [2]Department of Pediatrics, The First People's Hospital of Shuangliu District, West China Airport Hospital of Sichuan University, Chengdu, China, [3]Department of Pediatrics, The Second People's Hospital of Liangshan Yi Autonomous Prefecture, Xichang, China, [4]Key Laboratory of Birth Defects and Related Diseases of Women and Children of MOE, Department of Obstetrics and Gynecology, West China Second University Hospital, Sichuan University, Chengdu, China

Background: Fetal bradycardia is a common but severe condition. In addition to autoimmune-mediated fetal heart block, several types of channelopathies induce high-degree atrioventricular block (AVB). Long QT syndrome (LQTS) is a major cause of non-autoimmune-mediated fetal heart block. Due to the limitations of prenatal diagnostic technologies, LQTS is seldom identified unless fetal genetic screening is performed. Thus, long-term prenatal dexamethasone (DEX) exposure can become a challenge for these patients. We report on a rare case of a novel *KCNH2* variant related to LQTS and associated with high-degree fetal AVB with long-term DEX exposure. This case led us to review our prenatal administration strategy for such patients.

Case Presentation: A fetus was identified with high-degree AVB (2:1 transduction at 28 + 2 gestational weeks). Typical tests of immune function in the pregnant woman were conducted including tests for thyroid function, rheumatic screening, autoimmune antibodies (such as anti-Ro/SSA and anti-La/SSB), and anti-nuclear antibodies (anti-ANA). Following the recommended protocol, the pregnant patient received DEX (0.75 mg/day) during pregnancy. Subsequently, the fetal AVB changed from 2:1 to prolonged AV intervals with ventricular tachycardia, which suggested a therapeutic benefit of DEX in some respects. However, a high-degree AVB

Abbreviations: ANAs, anti-nuclear antibodies; AVB, atrioventricular block; CAVB, complete atrioventricular block; DEX, dexamethasone; ECG, electrocardiogram; LQTS, long QT syndrome; MAFs, minor allele frequencies; SCD, sudden cardiac death; SDM, site-directed mutator; TDP, torsades de pointes.

with a significantly prolonged QTc interval was identified in the neonate following birth. Genetic testing revealed that a *KCNH2* c.1868C>A variant induced LQTS. The body length remained approximately -3.2 SD from the reference value after prenatal long-term DEX exposure, which indicated a developmental restriction. Additionally, the functional validation experiments were performed to demonstrate the prolonged duration of calcium transit both in depolarization and repolarization with the *KCNH2* c.1868C>A variant.

Conclusion: Genetic screening should be recommended in fetuses with autoimmune antibody negative high-degree AVB, especially for 2: 1 transduction AVB and in fetuses with changes in fetal heart rhythm following initial DEX treatment. Genetic screening may help identify genetic variant–related channelopathies and avoid unexpected prenatal exposure of DEX and its possible long-term adverse postnatal complications.

KEYWORDS

fetal bradycardia, long QT syndrome, kcnh2, prenatal management, dexamethasone exposure, case report

Introduction

Fetal heart block is a rare and threatening disease and is the most commonly observed type of fetal bradycardia. Among all fetal heart block patients, > 50% of cases are associated with maternal autoimmune diseases, and the incidence of fetal heart block in pregnancies with positive anti–SSA(Ro) and anti–SSB(La) test results is 2%–5% (Manolis et al., 2020). Fetuses with positive antibody screens represent an estimated 25% of neonatal lupus patients. Studies suggest that transplacental anti-nuclear antibodies (ANAs) may attack the cardiac conduction system of the fetus. Suryawanshi et al. (2020) used single-cell RNA-sequencing to determine the immunological activity of immune cells in human heart samples that were positive for anti-SSA/Ro and associated with congenital heart block (CHB). Researchers found increased and heterogeneous interferon responses in various cell types of the CHB heart compared with healthy controls, which contributed to subsequent fibrosis in the heart. Thus, in autoimmune antibody–positive pregnancies, dexamethasone (DEX) is typically administered to prevent the progression of or to cause the reversal of fetal heart block. However, there are also a large number of patients with fetal heart block without positive antibodies. Thus, the administration strategy for DEX treatment has always been challenging when weighing the benefits of DEX treatment on antibody-negative fetuses (Liao et al., 2021; Tang et al., 2021). According to the current therapeutic protocol, DEX is most recommended for such patients; yet the risks of long-term DEX administration is an ongoing debate.

Attempts have been made to identify potential causes of fetal heart block. Studies have reported that long QT syndrome (LQTS) may present as severe fetal bradycardia or as fetal heart block with a 2:1 transduction (Adler et al., 2020). LQTS does not require DEX treatment, and it is difficult to distinguish between LQTS with heart block and autoimmune-associated fetal heart block that require DEX treatment during pregnancy unless fetal genetic testing is performed to identify genetic variant–related arrhythmias (Martínez-Barrios et al., 2022). Moreover, cases with negative antibody screens commonly present postnatally with adverse arrhythmias including LQTS and high-degree AVB. LQTS is considered a clinical disorder with a genetic origin and is characterized by delayed repolarization of cardiomyocytes, electrocardiographic (ECG) QT prolongation, an elevated risk of syncope, and sudden cardiac death caused by polymorphic ventricular tachycardia that is known as torsades des pointes (TdP) (Tang et al., 2021). The loss of function variants in *KCNH2* are the leading cause of LQTS (Liao et al., 2021). Three encoding ion channel genes have been identified as responsible for most of the LQTS cases: *KCNQ1* (Kv7.1 channel) causing LQT1 (Adler et al., 2020), *KCNH2* (Kv11.1 channel) causing LQT2 (Martínez-Barrios et al., 2022), and *SCN5A* (Nav1.5 channel) causing LQTS (Dai et al., 2021). Thus, the early and timely ability to distinguish congenital LQTS and autoimmune-associated fetal heart block is critical to avoid unnecessary long-term prenatal DEX exposure.

Herein, we report on a rare case of a novel *KCNH2* variant-related LQTS with an associated high-degree fetal AVB. After prenatal DEX administration, only a prolonged AV interval was identified *in utero*. Thus, the fetus received long-term DEX exposure. Postnatal ECG and genetic testing revealed that the neonate had LQTS and a *de novo KCNH2* variant, respectively. This case led us to review our prenatal DEX administration strategy for patients and suggests that genetic testing should be conducted in autoimmune antibody-negative fetuses to avoid long-term DEX exposure given that DEX treatment leads to improved outcomes.

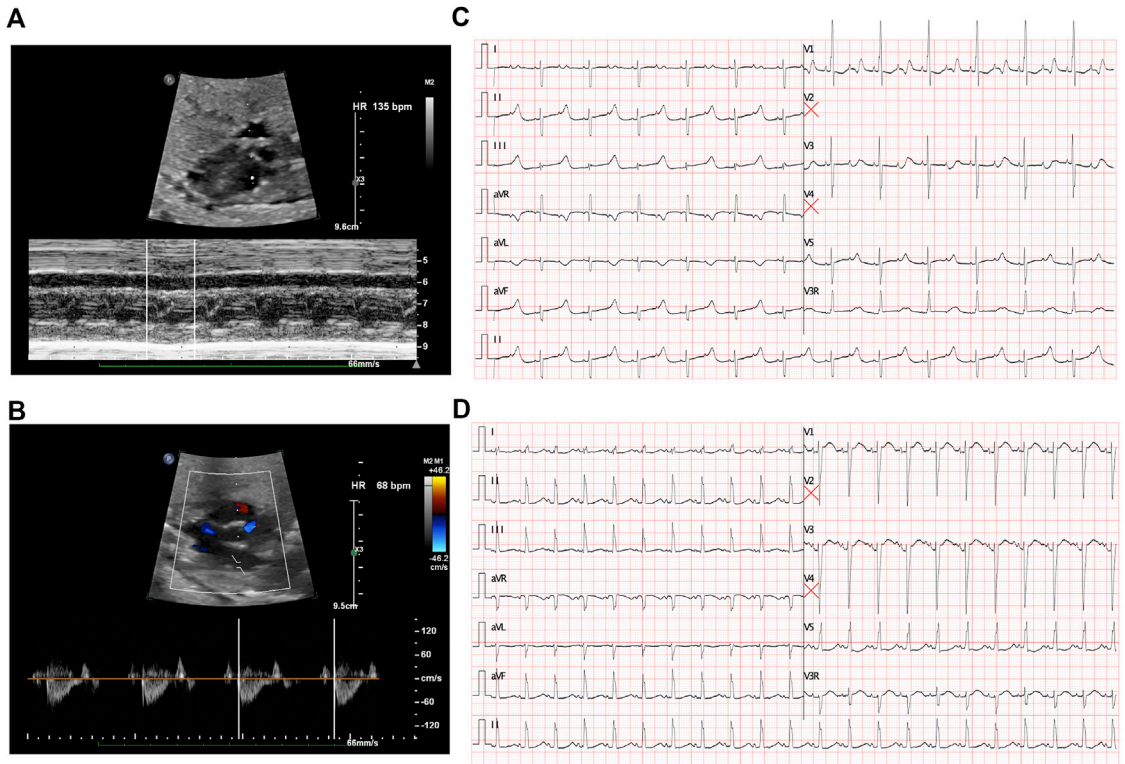

FIGURE 1
Fetal echocardiography to determine bradycardia. **(A)** M-mode echocardiography demonstrated an atrial rate of 135 beats per minute before treatment. **(B)** Doppler demonstrated a ventricular rate of 68 beats per minute before treatment and indicated a 2:1 AV block. **(C)** ECG presented a 2:1 transduction atrioventricular block postnatally. **(D)** ECG revealed a significant prolonged QTc interval after birth.

Case presentation

Ethical compliance

This report was approved by the ethics committee of the West China Second Hospital of Sichuan University (approval number 2014-034). Informed consent was obtained from the patient's parents prior to performing whole-exon sequencing and for the inclusion of the patient's clinical and imaging details in subsequent publications.

History of illness

A 30-year-old pregnant woman was admitted to our center at 28 + 0 gestational weeks for a general fetal screening, and a fetal ultrasound demonstrated fetal bradycardia. Fetal echocardiography was then performed at 28 + 2 gestational weeks to determine if the fetus suffered from a high-degree AVB (2:1 transduction). The fetal echocardiography demonstrated a normal intracardiac structure and normal cardiac function with a 10 out of 10 cardiovascular profile score. Tests for immune activity in pregnant women were performed including thyroid function, rheumatic screening, autoimmune antibodies (such as anti-Ro/SSA and anti-La/SSB), and ANA. All aforementioned tests were negative. In addition, a test was performed for potential viral infections, including tests for adenovirus, coxsackie virus, and B-19 virus, and all were negative. Following the recommended protocol, the pregnant patient received DEX (0.75 mg/day) during pregnancy. Subsequently, the fetal AVB changed from 2:1 to a prolonged AV interval with ventricular tachycardia, which suggests a therapeutic benefit of DEX in some aspects in the pregnant woman administrated DEX (beginning at 4.5 mg/day with a dose reduction at 34 + 3 gestational weeks when the 2:1 transduction AVB changed to prolonged AV with an interval of 147 ms) until delivery at 37 + 0 gestational weeks. Following birth, the neonate was confirmed to have a significantly prolonged QTc interval with high-degree AVB (2:1 transduction). Transient ventricular tachycardia was identified using a Holter monitor. The neonate's parents had no positive or related family history of arrhythmia, cardiomyopathy, congenital heart disease, or coronary artery disease. The ECGs assessments of the parents presented normal performance (Supplementary Figure S1).

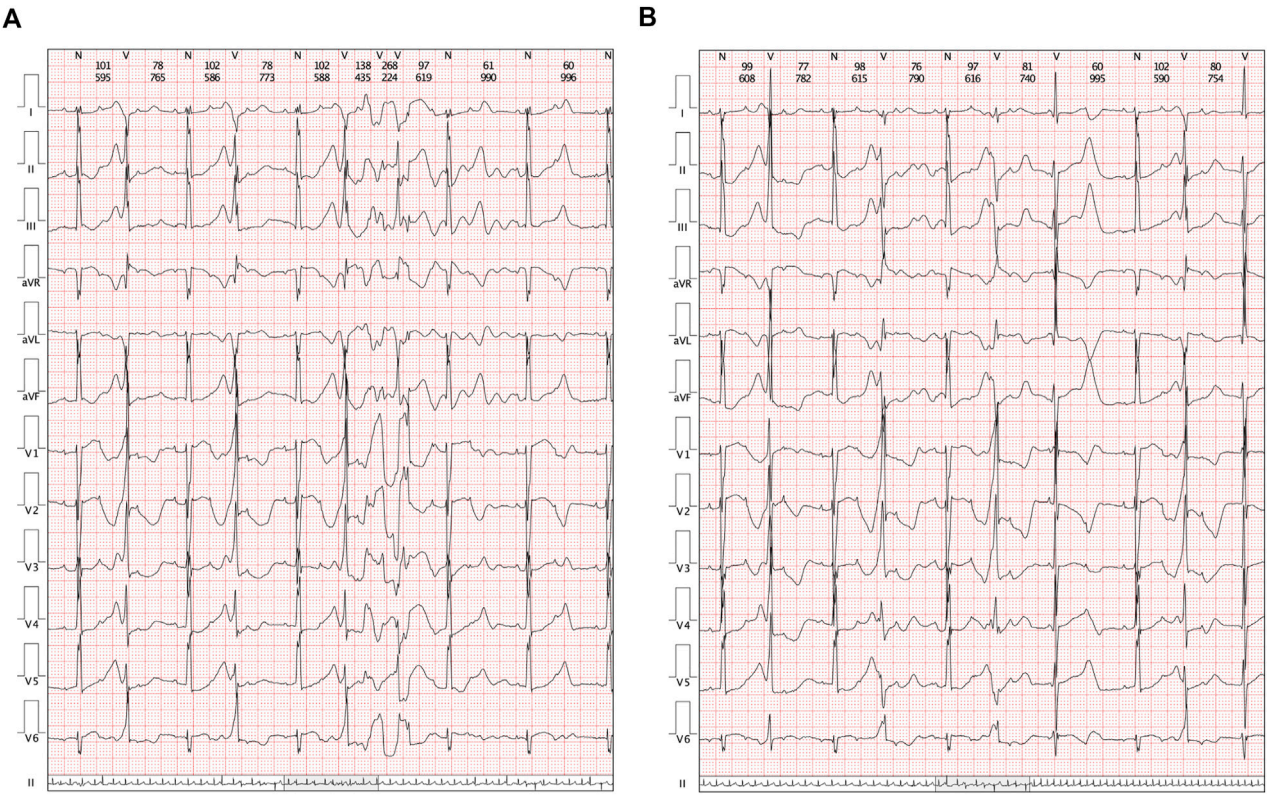

FIGURE 2
Clinical manifestations in Holters. **(A)** Transit ventricular tachycardia was identified. **(B)** Holter demonstrated a paired premature ventricular contraction.

The first intrapartum fetal echocardiography exam was performed at 28 + 2 gestational weeks, and the development of the four cardiac chambers and valvar movements were normal. The atrial rate was 135 beats/min, while the ventricular rate was 68 beats/min (Figures 1A and B), and the cardiovascular system profile was normal (10/10 points). Thus, a diagnosis of fetal AVB (second degree, type II) was identified. The maternal autoimmune antibody test results were negative for anti–Ro/SSA (0.8 RU/mL, n.v. < 20 RU/mL), anti–La/SSB (<0.5 RU/mL, n.v. < 20 RU/mL), and ANAs (negative, n.v. < 1:100). The IgM result for adenovirus, coxsackie virus, and B-19 were all negative. Next, DEX (4.5 mg/day) was provided to the mother. During fetal follow-up at 34 + 3 gestational weeks, a fetal AVB of 2:1 transduction changed into a first-degree AVB with a prolonged AV interval (147 ms) as the ventricular rate was 130–142 beats/min and the cardiovascular system profile remained normal. Thus, the DEX treatment seemed to confer some benefits in this case. At this point, the dosage of DEX was reduced to 1.5 mg/day until delivery.

A cesarean section was performed at 37 + 0 gestational weeks. After birth, bradycardia was also documented, and the ventricular rate was approximately 65 beats/min with an acceptable SpO_2 of approximately 98%. An ECG of the neonate demonstrated a 2:1 transduction AVB (Figure 1C). One week later, the ECG revealed a significantly prolonged QTc interval (498–534 ms, Figure 1D). Moreover, Holter monitoring demonstrated transit ventricular tachycardia (Figure 2A) and doublet premature ventricular contractions (Figure 2B). A slight elevation of cTnI was also observed (0.162 ug/L, n.v. < 0.06 ug/L). The autoimmune antibody test results of the neonate were negative. ECG confirmed the presence of a patent foramen ovale, tricuspid regurgitation (mild) with an ejection fraction of 71%, and fractional shortening of 38%. Thus, a diagnosis of LQTS was suspected for this patient, and whole-exon sequencing was performed to identify any potential genetic variants. This was the first child between the couple.

Molecular results

To evaluate any potential genetic causes of the neonate's condition, a peripheral blood sample was obtained from the patient in an ethylenediaminetetraacetic acid anticoagulant blood sample tube and stored at 4 °C for <6 h. DNA was

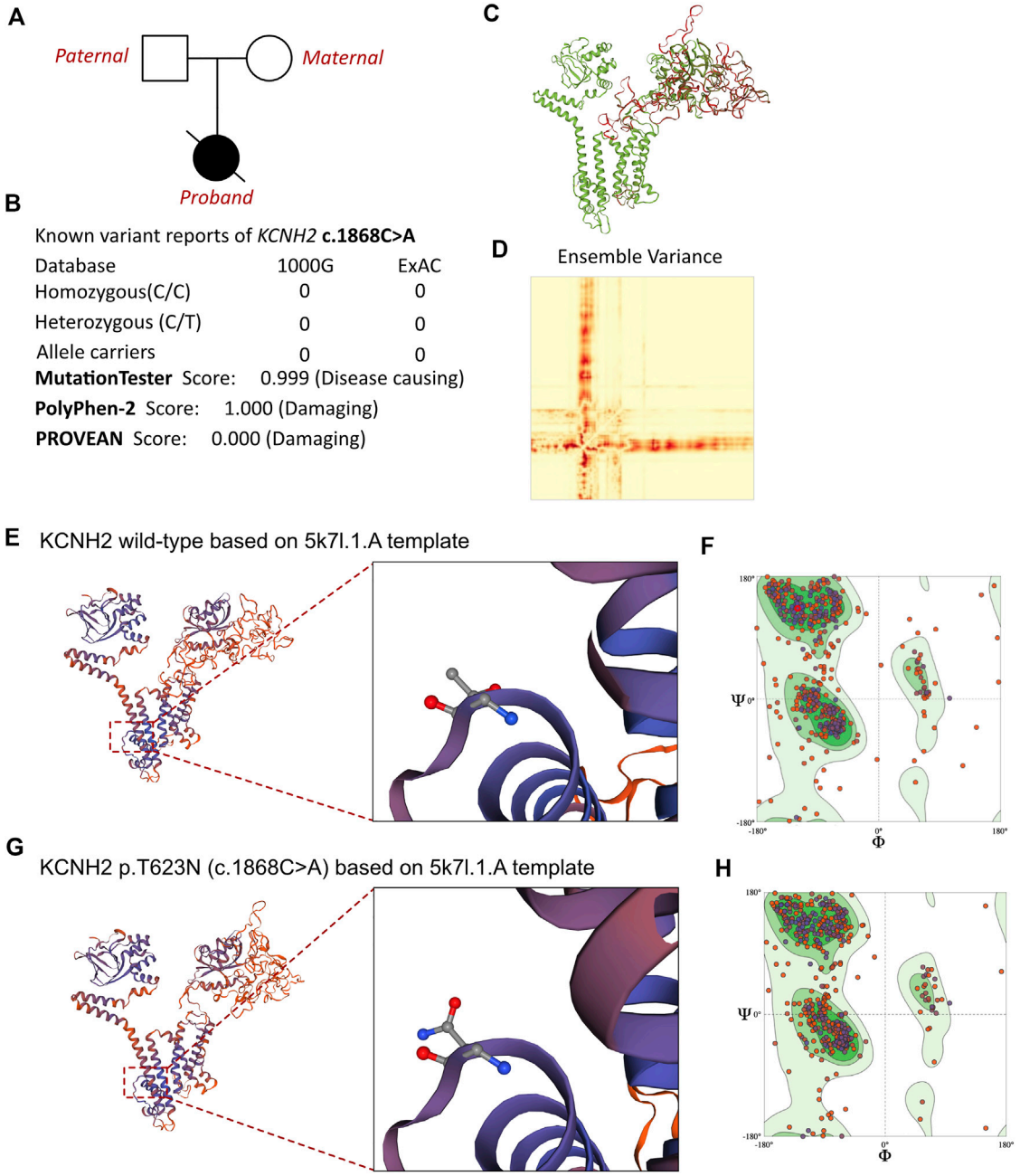

FIGURE 3
Effects of *KCNH2* c.1868C>A mutation on molecular protein structure. **(A)** Family pedigree tree of this proband. **(B)** Summary of current reports on the individuals of *KCNH2* and its predicted damages on the molecular function of the c.1868C>A variant. **(C)** SWISS-MODEL to predict the variant's wild type and mutated protein crystal structure, and the variant impaired a large proportion of molecular structure. **(D)** Ensemble variance between the wild type and mutant protein structure. **(E,G)** SWISS-MODEL to predict the variant's wild-type and mutated protein crystal structures using 5k7l.1.A template, and structural changes were identified. **(F)** Ramachandran plots of wild-type KCNH2. **(H)** Ramachandran plots of KCNH2 with the p.T623N variant.

extracted using the Blood Genome Column Medium Extraction Kit (Tiangen Biotech, Beijing, China) in accordance with the manufacturer's instructions. Protein-coding exome enrichment was performed using the xGen Exome Research Panel v.1.0, which is composed of 429,826 individually synthesized and quality-controlled probes targeting 49.11 Mb of protein-coding regions (>23,000 genes) of the human genome. Whole-exon sequencing was performed using the NovaSeq 6000 platform

(Illumina, San Diego, CA, USA), and the raw data were processed using FastP to remove adapters and filter out low-quality reads. Paired-end reads were aligned with the Ensembl GRCh38/hg38 reference genome using the Burrows–Wheeler Aligner tool. Variant annotation was performed in accordance with database-sourced minor allele frequencies (MAFs) and practical guidelines on pathogenicity that were issued by the American College of Medical Genetics. The annotation of MAFs was performed based on the 1000 Genomes, dbSNP, ESP, ExAC, Provean, Sift, Polypen2_hdiv, Polypen2_hvar, and Chigene in-house MAF databases using the R software program (R Foundation for Statistical Computing, Vienna, Austria). A novel mutation in *KCNH2* was finally identified. While the parents also received WES analysis, and both of them were absent of *KCNH2* c.1868C>A variant. The family pedigree tree of this proband had been presented in (Figure 3A). To our knowledge, *KCNH2* c.21868C>A has never before been reported in the 1000G and ExAC databases (Figure 3B). There was no other cardiomyopathy or arrhythmia-related genetic mutation identified by our whole-exon sequencing analysis. Besides, all the genetic variants related with sudden cardiac death (SCD) had been ruled out. As the parents of this neonate did not present with any symptoms of cardiovascular disease, the neonate was considered to be the proband.

MutationTaster and Polyphen-2 were used with the R software to predict the pathogenicity of *KCNH2* c.1868C>A and assess the effects of this mutation on the protein structure (Figure 3B). As there were *KCNH2* protein crystal structure data available, analysis was performed using SWISS-MODEL (https://swissmodel.expasy.org/) with the 5k7l.1.A template (Figures 3E,G). The capability of the protein structure was estimated using Ramachandran plots (Figures 3F,H). The differences between wild-type and *KCNH2* p.T623N mutant crystal structures were estimated by ensemble variance (Figures 3C,D). Changes in the free energy of the model were estimated using the mutation cutoff scanning matrix (mCSM) method (http://biosig.unimelb.edu.au/mcsm/). The signature vector that was ultimately generated was used to train the predictive classification and regression model for calculating the change in the Gibbs folding free energy induced by the mutations.

Based on laboratory analyses and the neonate's clinical manifestations, a genetic disorder was strongly suspected. Whole-exon sequencing was performed using the Illumina NovaSeq 6000 platform, and a *de novo* c.1868C>A (p.T623N) heterozygous mutation was identified in the *KCNH2* gene. Neither of the neonate's parents carried this variant. According to the American College of Medical Genetics, these variants have an uncertain pathogenicity (PM1+PM2_Supporting + PP3). The variant we identified, *KCNH2* c.1868C>A, had not been reported in any population. This is the first report of this variant. An analysis performed with MutationTester revealed that this mutation is considered pathogenic due to amino acid sequence changes, the protein features affected, and a loss of helix superstructure (probability = 0.999 for c.1868C>A). PolyPhen 2.0 predicted this mutation of p.T623N to be "probably damaging" (score = 1.0, sensitivity = 0.00, and specificity = 1.00). The SWISS-MODEL tool was used to analyze stability after amino acid changes. Ramachandran plots indicated that amino acid positions were altered (Figures 3F,H). Rebuilding the molecular structure based on a 5k7l.1.A template resulted in the identification of residue changes at amino acid position 623 (Figures 3E,G). Using SWISS-MODEL protein stability prediction tools, ensemble changes among the encoded amino acids exhibited significant variance. Three types of calculation methods all demonstrated significant destabilizing changes (mCSM = −0.338 kcal/mol).

To validate the functional impairment of *KCNH2* c.1868C>A, two kinds of overexpression plasmids were established as wild type human *KCNH2* (KCNH2-wt) and c.1868C>A allele *KCNH2* (KCNH2-mut) based on the pgl3 basic vector, and both KCNH2 molecules (wt and mut) were liganded with mScarlet by P2A (pgl3-KCNH2-wt-P2A-mScarlet and pgl3-KCNH2-mut-P2A-mScarlet). Then neonatal mice ventricular myocytes (NMVMs) were isolated using the Neomyt Kit (Cellutron, NC-6031) and plated on 1% Matrigel (Corning, 354234)-coated plates in cardiomyocyte culture media (low glucose DMEM (Gibco), 5% horse serum (American Type Culture Collection, 30–2040), and 2% chicken embryo extract (VWR, 100356-958)). The following day, two plasmids were transfected into NMVMs. Protein was extracted by the RIPA lysis buffer system (Santa Cruz Biotechnology, sc-24948) with Mini Protease Inhibitor Cocktail Tablets (cOmplete, 4693124001). The expression of KNCH2 was assessed by Western Blotting of mScarlet (Figure 4A). NMVMs were harvested on the 7th culture day and fixed using paraformaldehyde. Then, immunofluorescence was performed to demonstrate the expression of transfected KCNH2 (mScarlet), while cardiomyocytes were stained with SAA (Figure 4B). Intracellular Ca^{2+} recordings were performed after loading with Fluo-4 AM (10 μM, Invitrogen, F14217) for 30 min. After loading, NMVMs were subsequently washed with a normal Tyrode solution (140 mM NaCl; 4 mM KCl; 1 mM MgCl2; 1.8 mM CaCl2; 10 mM Glucose; and 5 mM HEPES, pH 7.4, adjusted with NaOH) to remove the excess dye for 20 min. All image data were acquired using an FV3000 confocal microscope (Figure 4C), which demonstrated the prolonged duration of pgl3-KCNH2-mut-P2A-mScarlet infected NMVMs both in time to peak and decay50 (Figure 4D). Thus, this experiment validated the impaired KCNH2 function-carrying c.1868C>A allele.

Outcome and follow-up

After the neonate was transferred to the cardiac intensive care unit, a temporary pacemaker was implanted for the positive treatment. Once the genetic result of *KCNH2*

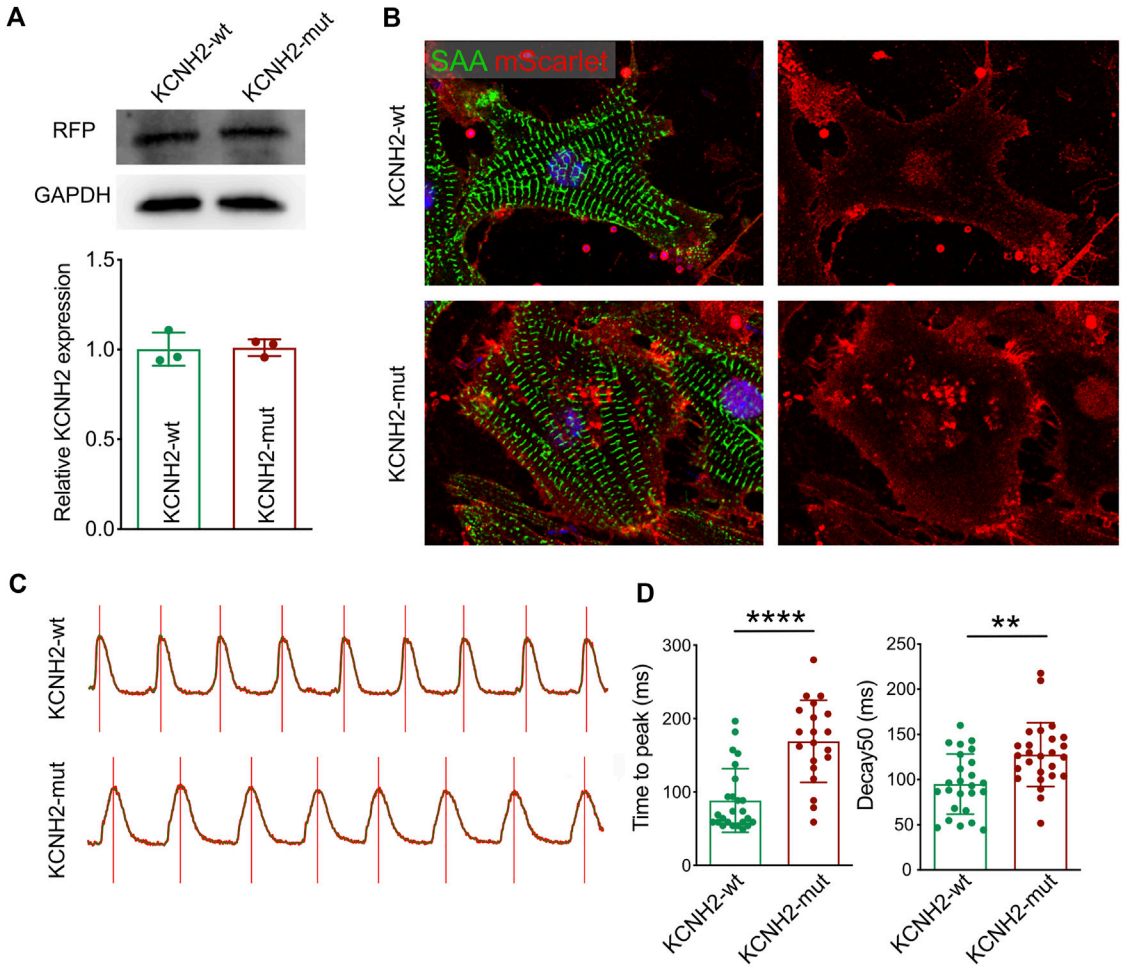

FIGURE 4
Functional validation of *KCNH2* c.1868C>A mutation on cardiomyocyte. **(A)** Western blotting demonstrated the similar expression of KCNH2 protein between wild type and mutation. **(B)** Immunofluorescence staining revealed the successful infection of KCNH2 overexpression plasmids in cardiomyocytes. **(C)** Calcium transit waves between KCNH2-wt and KCNH2-mut plasmids transfected cardiomyocytes. **(D)** The increased duration of time to peak and decay50 was identified in KCNH2-mut cardiomyocytes. RFP, red fluorescence protein; SAA, sarcomeric α-actinin. **, $p < 0.01$; ****, $p < 0.0001$.

c.1868C>A was identified, the neonate remained at an extremely high risk of SCD. Thus, a permanent pacemaker was a therapeutic alternative. The neonate's parents agreed to the implantation of a permanent pacemaker, and thus, the patient planned to receive an epicardial pacemaker implantation between 3 and 4 months. Additionally, her parents declined to have any medication administration. During two months of postnatal follow-up, the patient did not suffer from syncope or heart dysfunction. However, the body length remained approximately -3.2 SD from the reference value following prenatal long-term DEX exposure, which revealed a developmental restriction. Unfortunately, the patient died from SCD around 2.5 months of age before the scheduled date of pacemaker implantation. Suspected fatal arrhythmia, such as torsades de pointes due to LQTS, was likely the main reason for the induction of death.

Discussion

Inherit arrhythmias lead to higher risks of heart dysfunction, even SCD, in early childhood (Dai et al., 2021). However, most types of inherit arrhythmias have not been identified in fetuses, which indicates a low intrauterine penetrance. Generally, maternal autoimmune diseases impair the conduction system by transplacental transfusion of immune antibodies that attack the heart conduction system and result in localized fibrosis (Suryawanshi et al., 2020). Maternal autoimmune diseases and autoimmune antibodies, especially high-titer anti–SSB/La

antibodies and particularly when accompanied by high-titer anti–SSA/Ro antibodies, may cause congenital AVB, sinoatrial node dysfunction, ventricular and junctional tachycardias, and long QT intervals (Wainwright et al., 2020). Indeed, autoimmune factors contribute to more than half of fetal bradycardia cases. However, a large proportion of fetal bradycardia cases lack any evidence of immune involvement. The DEX administration strategy for such cases is critical and challenging.

Congenital LQTS, which is an autoimmune antibody-negative fetal bradycardia, is a cause of fetal AVB (Otsuki et al., 2020). The occurrence of AVB in concert with LQTS is not due to disease of the conduction system itself but rather due to the prolonged ventricular repolarization time that leads to atrial activation before ventricular repolarization is complete (Batra and Balaji, 2019). Generally, QT interval prolongation is responsible for bradycardia (Oka et al., 2010). In a report from Garson et al. that included a series of 287 patients with LQTS, there were 15 patients (5%) with AVB, 13 patients with 2:1 AVB, and only 2 (0.7%) patients with congenital AVB (Mendoza et al., 2010). Early awareness of LQTS is critical in preventing adverse clinical outcomes. Once AVB induced by QT prolongation occurs, it carries a high risk of TDP, which is closely associated with SCD (Rosso et al., 2014). Intrauterine LQTS-induced 2:1 transduction AVB is associated with higher mortality due to fetal hydrops and cardiac dysfunction. In such cases, postnatal genetic screening is recommended by the American Heart Association (AHA) to reach a definitive diagnosis as most conditions of congenital LQTS do not require any treatment during infancy; treatment is only recommended at the onset of ventricular tachycardia or TDP.

According to most protocols or guidelines of fetal arrhythmia management, LQTS should be highly suspected in fetal bradycardia cases, especially for the 2:1 transduction AVB (Kasar et al., 2019), and postnatal genetic screening is recommended to reach a definitive diagnosis. However, if there is no positive family history, it may be difficult to distinguish LQTS from other types of fetal bradycardia using fetal ECG. AHA guidelines recommend fetal magnetocardiography or ECG to monitor the QTc interval; however, there is still a gap in illustrating the actual QTc interval. Fetal therapy with DEX is strongly recommended for autoimmune-mediated fetal bradycardia. DEX treatment of fetuses with established CHB and without heart failure might also be considered with the goal of improving survival or reducing the incidence of dilated cardiomyopathy. The usefulness of DEX therapy in this population has not been established given that current studies have been retrospective and nonrandomized and have had an incomplete follow-up. Generally, DEX is also provided to autoimmune antibody-negative fetuses with DEX dosage reduction based on whether the fetal CHB may be terminated or unchanged after four weeks of treatment. Moreover, if the high-degree fetal AVB changed to first-degree AVB or non-threatening fetal bradycardia, a small dosage of DEX is always continuously administrated to birth. Recently, the long-term adverse effects of prenatal DEX exposure have been noted by researchers (Pal et al., 2022; Shinwell et al., 2022; Wang et al., 2022). In experimental animals, pulmonary fibrosis, osteoporosis, long bone growth impairment, and neonatal hypoglycemia were identified following prenatal DEX exposure (Rivet et al., 2022; Wu et al., 2022; Xie et al., 2022; Zhang et al., 2022). Mechanistically, circadian rhythms, insulin-like growth factor 1 signaling, angiotensin II signaling, histone modifications, and dysregulation of miRNAs were responsible for long-term adverse presentations following DEX exposure (Han et al., 2022; Liu et al., 2022; Madhavpeddi et al., 2022; Murray et al., 2022; Qiu et al., 2022). Thus, the benefits from prenatal DEX administration for autoimmune antibody-negative patients are still being debated.

LQTS is a type of inherit cardiovascular disease that induces the prolonged duration of QT interval. Besides, some cases also demonstrated that LQTS presents as AVB (Aziz et al., 2010; Oka et al., 2010; Sun et al., 2022). It has been considered that AVB could be due to LQTS as a kind of pseudo AVB. The variant of KCNH2 would lead to the loss-of-function of this molecule. The delay repolarization would cause the next beating signaling from atrioventricular node to be irresponsive, which would induce the 2:1 AVB. In this case, the fetus presented with 2:1 transduction AVB at the first fetal ECG, and no positive results had been identified for autoimmune antibodies or potential maternal-related disease screenings. However, the patient initially received DEX therapy, and the high-degree AVB regressed into a mild prolonged AV interval, indicating some positive effects of the DEX treatment. Thus, continuous small dose DEX administration was provided until delivery. After birth, LQTS was confirmed by ECG and genetic screening. Unfortunately, the neonate developed growth restriction postnatally. Subsequently, the case was brought to us to review the treatment strategy for prenatal CHB without positive evidence of autoimmune antibodies and for a critical discussion of the benefits of DEX exposure. Importantly, prenatal genetic screening should be highly recommended for autoimmune antibody-negative fetuses to exclude any genetic syndromes and channelopathies. With the rapid development of next generation sequencing technologies, the expense and duration of such methods have been significantly reduced and allow timely and convincing molecular results. Additionally, the shifted diagnostic timepoint of LQTS or other types of channelopathies may help to avoid unnecessary DEX prenatal exposure.

Conclusion

Prenatal management of fetal CHB with DEX benefits neonates with high-degree AVB and positive autoimmune antibody tests. However, genetic screening should be recommended for fetuses with autoimmune antibody-negative

high-degree AVB, especially those with 2:1 AVB and in those cases in which changes in fetal heart rhythm occur with initial DEX treatment. Genetic screening may help identify genetic variant–related channelopathies and is critical for avoiding unexpected prenatal DEX exposure and its long-term adverse postnatal complications.

Data availability statement

The original contributions presented in the study are included in the article/Supplementary Material; further inquiries can be directed to the corresponding authors.

Ethics statement

The studies involving human participants were reviewed and approved by the Ethics Committee of West China Second Hospital of Sichuan University. Written informed consent to participate in this study was provided by the participants' legal guardian/next of kin. Written informed consent was obtained from the individual(s), and minor(s)' legal guardian/next of kin, for the publication of any potentially identifiable images or data included in this article.

Author contributions

YL, LW, HY, HY, and KZ were the patient's physicians. HH and QZ reviewed the literature and contributed to manuscript drafting. YL performed the mutation analysis. SJ performed the functional validation experiments. YL, KZ, and YH conceptualized and designed the study, coordinated and supervised data collection, and critically reviewed the manuscript for important intellectual content. KZ, YL, and HY were responsible for the revision of the manuscript for important intellectual content. All authors issued final approval for the version submitted.

Funding

This work was supported by grants from the Technology Project of Sichuan Province of China (2021YFQ0061 and 2021YJ0211) and Central Government Funds of Guiding Local Scientific and Technological Development for Sichuan Province (2021ZYD0105).

Conflict of interest

The authors declare that the research was conducted in the absence of any commercial or financial relationships that could be construed as a potential conflict of interest.

Publisher's note

Supplementary material

The Supplementary Material for this article can be found online at: https://www.frontiersin.org/articles/10.3389/fgene.2022.1010078/full#supplementary-material

References

Adler, A., Novelli, V., Amin, A. S., Abiusi, E., Care, M., Nannenberg, E. A., et al. (2020). An international, multicentered, evidence-based reappraisal of genes reported to cause congenital long QT syndrome. *Circulation* 141 (6), 418–428. doi:10.1161/circulationaha.119.043132

Aziz, P. F., Tanel, R. E., Zelster, I. J., Pass, R. H., Wieand, T. S., Vetter, V. L., et al. (2010). Congenital long QT syndrome and 2:1 atrioventricular block: An optimistic outcome in the current era. *Heart rhythm.* 7 (6), 781–785. doi:10.1016/j.hrthm.2010.02.035

Batra, A. S., and Balaji, S. (2019). Fetal arrhythmias: Diagnosis and management. *Indian Pacing Electrophysiol. J.* 19 (3), 104–109. doi:10.1016/j.ipej.2019.02.007

Dai, Y., Yin, R., Yang, L., and Li, Z. H. (2021). Clinical and genetic spectrum of neonatal arrhythmia in a NICU. *Transl. Pediatr.* 10 (10), 2432–2438. doi:10.21037/tp-21-233

Han, H., Xiao, H., Wu, Z., Liu, L., Chen, M., Gu, H., et al. (2022). The miR-98-3p/JAG1/Notch1 axis mediates the multigenerational inheritance of osteopenia caused by maternal dexamethasone exposure in female rat offspring. *Exp. Mol. Med.* 54 (3), 298–308. doi:10.1038/s12276-022-00743-x

Kasar, T., Kafali, H. C., and Ergul, Y. (2019). A rare association: First degree AV block and long QT syndrome. *Cardiol. Young* 29 (5), 697–698. doi:10.1017/s1047951119000775

Liao, H., Tang, C., Qiao, L., Zhou, K., Hua, Y., Wang, C., et al. (2021). Prenatal management strategy for immune-associated congenital heart block in fetuses. *Front. Cardiovasc. Med.* 8, 644122. doi:10.3389/fcvm.2021.644122

Liu, Y., Liu, M., Liu, Y., and Wang, H. (2022). MiR-466b-3p/HDAC7 meditates transgenerational inheritance of testicular testosterone synthesis inhibition induced by prenatal dexamethasone exposure. *Biochem. Pharmacol.* 199, 115018. doi:10.1016/j.bcp.2022.115018

Madhavpeddi, L., Hammond, B., Carbone, D. L., Kang, P., Handa, R. J., and Hale, T. M. (2022). Impact of angiotensin II receptor antagonism on the sex-selective dysregulation of cardiovascular function induced by *in utero* dexamethasone exposure. *Am. J. Physiol. Heart Circ. Physiol.* 322 (4), H597–h606. doi:10.1152/ajpheart.00587.2021

Manolis, A. A., Manolis, T. A., Melita, H., and Manolis, A. S. (2020). Congenital heart block: Pace earlier (Childhood) than later (Adulthood). *Trends cardiovasc. Med.* 30 (5), 275–286. doi:10.1016/j.tcm.2019.06.006

Martínez-Barrios, E., Cesar, S., Cruzalegui, J., Hernandez, C., Arbelo, E., Fiol, V., et al. (2022). Clinical genetics of inherited arrhythmogenic disease in the pediatric population. *Biomedicines* 10 (1), 106. doi:10.3390/biomedicines10010106

Mendoza, A., Belda, S., Salguero, R., and Granados, M. A. (2010). Congenital complete atrioventricular block associated with QT prolongation: Description of a patient with an unusual outcome. *Pediatr. Cardiol.* 31 (6), 887–890. doi:10.1007/s00246-010-9725-6

Murray, A., Tharmalingam, S., Khurana, S., Lalonde, C., Nguyen, P., and Tai, T. C. (2022). Effect of prenatal glucocorticoid exposure on circadian rhythm gene expression in the brains of adult rat offspring. *Cells* 11 (10), 1613. doi:10.3390/cells11101613).

Oka, Y., Itoh, H., Ding, W. G., Shimizu, W., Makiyama, T., Ohno, S., et al. (2010). Atrioventricular block-induced Torsades de Pointes with clinical and molecular backgrounds similar to congenital long QT syndrome. *Circ. J.* 74 (12), 2562–2571. doi:10.1253/circj.cj-10-0498

Otsuki, S., Izumi, D., Hasegawa, Y., Yagihara, N., Iijima, K., and Minamino, T. (2020). Suppression of cardiac memory-related severe form of torsades de pointes by landiolol in a patient with congenital long QT syndrome type 2. *Hear. Case Rep.* 6 (7), 407–410. doi:10.1016/j.hrcr.2020.03.013

Pal, S., Sardar, S., Sarkar, N., Ghosh, M., and Chatterjee, S. (2022). Effect of antenatal dexamethasone in late preterm period on neonatal hypoglycemia: A prospective cohort study from a developing country. *J. Trop. Pediatr.* 68 (2), fmac021. doi:10.1093/tropej/fmac021

Qiu, J., Fan, X., Ding, H., Zhao, M., Xu, T., Lei, J., et al. (2022). Antenatal dexamethasone retarded fetal long bones growth and development by down-regulating of insulin-like growth factor 1 signaling in fetal rats. *Hum. Exp. Toxicol.* 41, 9603271211072870. doi:10.1177/09603271211072870

Rivet, T. R., Lalonde, C., and Tai, T. C. (2022). Gene dysregulation in the adult rat paraventricular nucleus and amygdala by prenatal exposure to dexamethasone. *Life (Basel)* 12 (7), 1077. doi:10.3390/life12071077

Rosso, R., Adler, A., Strasberg, B., Guevara-Valdivia, M. E., Somani, R., Baranchuk, A., et al. (2014). Long QT syndrome complicating atrioventricular block: Arrhythmogenic effects of cardiac memory. *Circ. Arrhythm. Electrophysiol.* 7 (6), 1129–1135. doi:10.1161/circep.114.002085

Shinwell, E. S., Gurevitz, P., and Portnov, I. (2022). Current evidence for prenatal and postnatal corticosteroids in preterm infants. *Arch. Dis. Child. Fetal Neonatal Ed.* 107 (2), 121–125. doi:10.1136/archdischild-2020-319706

Sun, H., Liu, X., Hao, X., Zhou, X., Wang, J., Han, J., et al. (2022). Case report: Characterization of a novel NONO intronic mutation in a fetus with X-linked syndromic mental retardation-34. *Front. Genet.* 13, 593688. doi:10.3389/fgene.2020.593688

Suryawanshi, H., Clancy, R., Morozov, P., Halushka, M. K., Buyon, J. P., and Tuschl, T. (2020). Cell atlas of the foetal human heart and implications for autoimmune-mediated congenital heart block. *Cardiovasc. Res.* 116 (8), 1446–1457. doi:10.1093/cvr/cvz257

Tang, C., Yu, H., Shao, S., Hua, Y., Chen, M., Zhu, Q., et al. (2021). Case report: Prenatal diagnosis and treatment of fetal autoimmune-associated first-degree atrioventricular block: First report from China. *Front. Cardiovasc. Med.* 8, 683486. doi:10.3389/fcvm.2021.683486

Wainwright, B., Bhan, R., Trad, C., Cohen, R., Saxena, A., Buyon, J., et al. (2020). Autoimmune-mediated congenital heart block. *Best. Pract. Res. Clin. Obstet. Gynaecol.* 64, 41–51. doi:10.1016/j.bpobgyn.2019.09.001

Wang, J., Chen, F., Zhu, S., Li, X., Shi, W., Dai, Z., et al. (2022). Adverse effects of prenatal dexamethasone exposure on fetal development. *J. Reprod. Immunol.* 151, 103619. doi:10.1016/j.jri.2022.103619

Wu, Z., Wen, Y., Xiao, H., Zhu, J., Li, B., Shangguan, Y., et al. (2022). 11β-Hydroxysteroid dehydrogenase 2: A key mediator of high susceptibility to osteoporosis in offspring after prenatal dexamethasone exposure. *Pharmacol. Res.* 175, 105990. doi:10.1016/j.phrs.2021.105990

Xie, L., Jiao, Z., Zhang, H., Wang, T., Qin, J., Zhang, S., et al. (2022). Altered hippocampal GR/KCC2 signaling mediates susceptibility to convulsion in male offspring following dexamethasone exposure during pregnancy in rats. *Toxicol. Lett.* 364, 12–23. doi:10.1016/j.toxlet.2022.05.004

Zhang, Z., Chen, H., Yu, P., Ge, C., Fang, M., Zhao, X., et al. (2022). Inducible factors and interaction of pulmonary fibrosis induced by prenatal dexamethasone exposure in offspring rats. *Toxicol. Lett.* 359, 65–72. doi:10.1016/j.toxlet.2022.02.001

frontiers | Frontiers in Genetics

TYPE Original Research
PUBLISHED 13 December 2022
DOI 10.3389/fgene.2022.1019283

OPEN ACCESS

EDITED BY
Francois Foulquier,
UMR8576 Unité de Glycobiologie Structurale et Fonctionnelle (UGSF), France

REVIEWED BY
Peter Witters,
University Hospitals Leuven, Belgium
Katrin Õunap,
University of Tartu, Estonia

*CORRESPONDENCE
Dariusz Rokicki,
d.rokicki@ipczd.pl

SPECIALTY SECTION
This article was submitted to Genetics of Common and Rare Diseases, a section of the journal Frontiers in Genetics

RECEIVED 14 August 2022
ACCEPTED 23 November 2022
PUBLISHED 13 December 2022

CITATION
Greczan M, Rokicki D, Wesół-Kucharska D, Kaczor M, Rawiak A and Jezela-Stanek A (2022), Perinatal manifestations of congenital disorders of glycosylation—A clue to early diagnosis.
Front. Genet. 13:1019283.
doi: 10.3389/fgene.2022.1019283

Perinatal manifestations of congenital disorders of glycosylation—A clue to early diagnosis

Milena Greczan[1], Dariusz Rokicki[1]*, Dorota Wesół-Kucharska[1], Magdalena Kaczor[1], Agata Rawiak[1] and Aleksandra Jezela-Stanek[2]

[1]Department of Pediatrics, Nutrition and Metabolic Diseases, Children's Memorial Health Institute, Warsaw, Poland, [2]Department of Genetics and Clinical Immunology, National Institute of Tuberculosis and Lung Disease, Warsaw, Poland

N-glycosylation defects—isolated or mixed with other glycosylation defects—are the most frequent congenital disorders of glycosylation and present mostly in childhood, with a specific combination of non-specific phenotypic features. The diagnosis, however, is often delayed. The aim of this study is to describe the perinatal phenotype of congenital disorders of N-glycosylation. We present an analysis of perinatal symptoms in a group of 24 one-center Polish patients with N-glycosylation defects—isolated or mixed. The paper expands the perinatal phenotype of CDGs and shows that some distinctive combinations of symptoms present in the perinatal period should raise a suspicion of CDGs in a differential diagnosis.

KEYWORDS

CDG (congenital disorders of glycosylation), glycosylation, effusion, dysmorphia, thrombocytopenia, hydrops fetalis

1 Introduction

Congenital disorders of glycosylation (CDGs) are a group of inborn monogenic errors of glycoprotein and glycolipid formation and/or assembly (Chang et al., 2018; Altassan et al., 2019). The group is numerous, heterogeneous, and is divided into four subgroups, based on the pathomechanism: congenital disorders of N-glycosylation, disorders of O-glycosylation, disorders of glycolipids and glycophosphatidylinositol anchor synthesis (GPI-CDG), and mixed disorders of glycosylation (Chang et al., 2018).

Disorders of N-glycosylation form the most prevalent CDG subgroup, and their pediatric phenotype is well described. The symptoms usually involve multiple organs, and the course of the disease may be severe, milder with relapsing episodes of exacerbations and/or slowly improving (Péanne et al., 2018; Altassan et al., 2019). The most common features of N-glycosylation are dysmorphia, like inverted nipples, upslanted palpebral fissures, and abnormal fat pads over the buttocks; cerebellar hypoplasia; hepatopathy; nephromegaly; proteinuria; hypertension; hypoalbuminemia; coagulation defects (both

TABLE 1 Clinical symptoms found in different CDG types.

Symptom	PMM2-CDG *n* = 15	MPI-CDG *n* = 1	SRD5A3-CDG *n* = 4	ATP6AP1-CDG *n* = 1	ALG1-CDG *n* = 2	DPAGT1-CDG *n* = 1	Total *n* = 24
Prenatal symptoms	in 6/14 pts; 1 pt no data	in 0 pts	in 1 pt; 3 pts no data	in 1 pt	in 1 pt	in 1 pt	in 10/20
Poor fetal movements	3	-	-	-	-	-	3
Hydrops fetalis	1	-	-	1	-	-	2
Pericardial effusion	2	-	-	-	-	-	2
Hydrocele testis	1	-	-	-	-	-	1
Impending asphyxia	1	-	-	-	-	-	1
Multi-VSD	-	-	1	-	-	-	1
Ventricular cysts	-	-	1	-	-	-	1
Shortening of the long bones	-	-	1	-	-	-	1
Polyhydramnios	-	-	-	-	1	-	1
Hypotrophy	-	-	-	-	-	1	1
Oligohydramnios	-	-	-	-	-	1	1
Suspicion of situs inversus	-	-	-	-	-	1	1
Dysmorphia	in 9/12 pts; 3 pts no data	in 0 pts	in 3 pts	in 1 pt	in 2 pts	in 1 pt	in 16/21
Inverted nipples	8	-	-	-	-	-	8
Wide-set nipples	3	-	-	-	1	-	4
Upslanted palpebral fissures	2	-	-	-	-	-	2
Gothic palate	1	-	-	-	1	-	2
Low-set ears	1	-	1	-	1	-	3
Large ears	1	-	-	-	-	-	1
Orange peel skin	1	-	-	-	-	-	1
Abnormal fat pads	3	-	-	-	-	-	3
Joint contractures	4	-	-	-	-	1	5
Cryptorchidism	3	-	-	-	-	1	4
Generalized edema	6	-	-	-	-	-	6
Thin nasal bridge	1	-	-	-	-	-	1
Hypotelorism	1	-	-	-	-	-	1
Barrel-shaped chest	1	-	-	-	-	-	1
Long fingers	1	-	-	-	-	-	1
Hypotrophy	-	-	1	-	-	1	2
Hypertelorism	-	-	1	-	1	-	2
Downslanted palpebral fissures	-	-	1	-	-	-	1
Micrognathia	-	-	1	-	1	-	2
Retrognathia	-	-	1	-	1	-	2
Not specified facial dysmorphia	2	-	3	1	-	-	6

(Continued on following page)

TABLE 1 (*Continued*) Clinical symptoms found in different CDG types.

Symptom	PMM2-CDG *n* = 15	MPI-CDG *n* = 1	SRD5A3-CDG *n* = 4	ATP6AP1-CDG *n* = 1	ALG1-CDG *n* = 2	DPAGT1-CDG *n* = 1	Total *n* = 24
Bird-like nose	-	-	-	-	1	-	1
Microcephaly	-	-	-	-	1	-	1
Cutis laxa	-	-	-	1	-	-	1
Adaptive disturbances	in 10 pts	in 0 pts	in 1 pt	in 0 pts	in 1 pt	in 1 pt	in 14/24
Hypoglycemia	5	-	1	-	-	-	6
Transient respiratory problems	9	-	-	-	1	1	11
RDS (X-ray)	2	-	-	-	1	-	3
Neurologic symptoms	in 12/12 pts; 3 pts no data	in 0 pts	in 4 pts	no data	in 2 pts	in 1 pt	in 19/20
Hypotonia	8	-	3		1	-	12
Hypertonia	3	-	1		1	1	6
Central hypertonia with peripheral hypotonia	1	-	-		-	-	1
Poor sucking	4	-	-		1	-	5
Poorly expressed neonatal reflexes	3	-	-		1	-	4
Dystonia	-	-	1		-	-	1
Absent tendon reflexes	1	-	-		-	-	1
Overexpressed tendon reflexes	-	-	-		-	1	1
Ocular symptoms	in 13/13 pts; 2 pts no data	in 0 pts	in 4 pts	in 0 pts	in 1 pt	in 1 pt	in 19/22
Nystagmus	4	-	3	-	1	-	8
Roving eye movements	6	-	-	-	-	-	6
Strabismus	3	-	-	-	-	-	3
Pale retina	7	-	-	-	-	-	7
Hypoplastic macula	1	-	-	-	-	-	1
Hypoplastic optic nerve	1	-	-	-	-	-	1
Retinal pigment clumping	-	-	1	-	-	-	1
Cataract	-	-	-	-	-	1	1
Hematological symptoms	in 10/10 pts; 5 pts no data	in 0 pts	in 1/1 pt; 3 pts no data	in 1 pt	in 1/1 pt; 1 pt no data	in 1 pt	in 14/15
Thrombocytopenia	6	-	-	-	-	-	7
Anemia	5	-	1	1	-	1	8
Neutropenia	1	-	-	-	1	-	1
Thrombocythemia	1 + 1*	-	-	-	-	-	1 + 1*
Hyperleukocytosis	4 + 2*	-	-	-	-	-	5 + 2*
Elevated INR	2	-	-	-	1	-	2
Elevated APTT	2	-	-	-	-	-	2

(Continued on following page)

TABLE 1 (*Continued*) Clinical symptoms found in different CDG types.

Symptom	PMM2-CDG *n* = 15	MPI-CDG *n* = 1	SRD5A3-CDG *n* = 4	ATP6AP1-CDG *n* = 1	ALG1-CDG *n* = 2	DPAGT1-CDG *n* = 1	Total *n* = 24
Protein S deficiency	4/4	n/a	-	n/a	-	n/a	4
Protein C deficiency	3/4	n/a	n/a	n/a	n/a	n/a	5
AT III deficiency	4/5	n/a	n/a	n/a	1	n/a	5
Bruises, petechiae	5	-	n/a	-	1	-	6
Bleeding from mucosas	2	-	-	-	1	-	2
Gastrointestinal	in 6/15 pts	in 0 pts	in 0 pts	in 0 pts	in 2/2 pts	in 1/1 pt	9/24 pts
Regurgitations	3	-	-	-	1	1	5
Food retention	2	-	-	-	-	1	3
No swallowing reflex	0	-	-	-	1	-	1
Nasogastric tube	4	-	-	-	1	1	6
Parenteral nutrition	3	-	-	-	1	1	5
Cardiac	in 12/15 pts	no data	in 1/2 pts; 2 pts n/a	no data	in 1/2 pts	no data	14/19 pts
Pericardial effusion	9		-		-		9
HCM	3		-		-		3
IVS thickening	6		-		-		6
PFO	6		1		1		8
PDA	2		-		-		2
PST	1		-		-		1
Multi-VSD	-		1		-		1
Repolarisation abnormalities	1		-		-		1
Sinus tachycardia	1		-		-		1
CNS pathology	in 10/10 pts	no data	no data	no data	in 0/2 pts	in 1/1 pt	11/13 pts
Cerebellar hypoplasia	5				-	-	5
Ventriculomegaly	2				-	-	2
IVH	6				-	1	7
Pineal cyst	1				-	-	1
Arachnoid cyst	1				-	-	1
Biochemical	10 pts	no data	in 1 pt; 3 pts no data	in 1 pt	in 2/2 pts	No data	14/14
Hypoalbuminemia	7		1	n/a	2		10
Hypertransaminasemia	3		-	1	-		4
Hypocholesterolemia	5		n/a	1	1		7
Proteinuria	7		-	n/a	1		8
Endocrine hypothyreosis	3	0	0	0	0	0	3

Pts, patients; multi-VSD, multi-ventricular septal defect; RDS, respiratory distress syndrome; INR, international normalized ratio; APTT, activated partial thromboplastin time; AT III, antithrombin III; HCM, hypertrophic cardiomyopathy; IVS, intraventricular septum; PFO, patent foramen ovale; PDA, patent ductus arteriosus; CNS, central nervous system; IVH, intraventricular hemorrhage.

pro- and anticoagulating factor deficiencies); cytopenias; and third-space effusions (Malhotra et al., 2009). All these symptoms, as well as generalized edema, cardiomyopathy, or cutis laxa, may be present also in the neonate (van de Kamp et al., 2007; Marklová and Albahri. 2008; Malhotra et al., 2009; Funke et al., 2013). Prenatally CDGs may manifest as non-immune hydros fettles, cerebellar hypoplasia, skeletal deformities, polyhydramnios or Ballantyne syndrome (Morava et al., 2012; Altassan et al., 2019; Čechová et al., 2020). Current knowledge on the perinatal manifestation is, however, still scarce. The literature claims that diagnosing CDG on the basis of clinical data during the neonatal period is not easy and requires a high index of suspicion (Edwards et al., 2006; Thong et al., 2009). Indeed, as supported by our experience, the diagnosis is usually delayed and is rarely made in the neonatal period (Funke et al., 2013; Schulte Althoff. 2016).

The aim of this study is to broaden the knowledge about the perinatal symptoms of CDGs by analyzing a group of Polish CDG patients.

2 Materials and methods

We identified 35 CDG patients hospitalized in our Institute in years 1995–2022; out of this group, 33 patients had N-glycosylation or mixed glycosylation defects. The group of 24 CDG patients, for whom perinatal data were available, was further analyzed.

3 Results

The analyzed group consisted of 24 patients: 19 with isolated N-glycosylation defects, i.e., 15 patients with PMM2-CDG, 2 with ALG1-CDG, 1 patient with DPAGT1-CDG, and 1 patient with MPI-CDG; 4 patients with the dolichol synthesis defect SRD5A3-CDG; and 1 patient with the disorder of Golgi homeostasis ATP6AP1-CDG. The detailed clinical information about the patients is summarized in Supplementary Table S1 and Table 1.

Majority of patients were delivered on term (87,5%, i.e., 21/24–21 patients of 24 for whom these data are available), with normal birth body weight (79,1%; i.e., 19/24); the median body weight was 3,000 g (15–50 percentile for the term neonate, according to WHO growth charts; range 1,360–4,180 g), median head circumference 33 cm (15–50 percentile; range 31–35 cm), and median birth body length 54 cm (>97 percentile; range 49–56 cm). The Apgar score was abnormal in 71% of patients (15/21), with abnormal results ranging from four to eight points in the first minute to five to nine points in the 10th minute and the lowest score in DPAGT1-and one ALG1-CDG patient (4–5). The delivery by cesarean section prevailed (69%, 9/13) and was caused by lack of labor progress (4), abnormal fetus position (2), premature labor (1), twin pregnancy in the systemic lupus erythematosus mother (1), and impending asphyxia in one case. The pregnancies were complicated in 8/24 cases (mother's: thrombocytopenia in the ninth month (1), severe anemia (2), massive lower limb edemas (1), hypothyroidism (1), gestational diabetes mellitus type 2 (1), and pregnancy-induced hypertension (1)).

Perinatal symptoms were present in 79% of patients (19/24).

Prenatal symptoms were described in 50% of patients (10/20) and encompassed: poor fetal movements (3), mild pericardial effusion (2), non-immune hydrops fetalis (2), polyhydramnios (1), oligohydramnios, hypotrophy and suspicion of situs inverses (one, in a DPAGT1-CDG patient), impending asphyxia (1) and a combination of multi-ventricular septal defect (mVSD), ventricular cysts, and shortening of the long bones in one SRD5A3-CDG patient.

In all patients, some symptoms of illness were seen in the first days of life. Dysmorphic features were found in 76% (16/21) and included: inverted nipples (8), wide-set nipples (4), generalized edema (6), big joint contractures (5), abnormal fat distribution (3), low-set ears (3), upslanted palpebral fissures (2), hypotrophy (2), hypertelorism (2), gothic palate (2), micrognathia (2), retrognathia (2), and single cases of downslanted palpebral fissures, bilateral cataracts, high forehead, small forehead, barrel-shaped chest, bird-like nose, and hypotelorism. In boys, urogenital malformations were found, i.e., cryptorchidism (4/16 boys), hydrocele testis (2/16 boys), micropenis (1/16 boys), and hypoplastic scrotum (1/16 boys).

Almost half of the group suffered from transient adaptive respiratory problems starting in the first minutes to hours of life (45%, 11/24), with six patients requiring nCPAP or mechanical ventilation for 1–43 days and five requiring oxygen supplementation at least for a few hours. The chest X-ray revealed features of RDS (Respiratory Distress Syndrome) in three patients, including two prematurely born (29 and 32 weeks of gestation) and pneumonia in one. Six patients also had hypoglycemia in the first 1–2 days of life and received intravenous glucose infusions. Four patients developed jaundice, requiring phototherapy.

The neurological evaluation revealed muscle tone disturbances in 90% of patients (18/20), specifically 12 patients had hypotonia, while seven had hypertonia, which was combined with dystonia in one patient. In all patients, for whom those data were available (4/4), tendon reflexes were present in the neonatal period; however, in one, they were overexpressed. Neonatal reflexes were poorly expressed in seven patients, including poor sucking in four.

Another distinctive group of abnormalities found in the study group was ocular symptoms: nystagmus (64% of patients, 14/22), most often described as roving eye movements (6) or vertical–upward–eye movements (5). Horizontal nystagmus was found only in two patients. Three patients also had strabismus. In

some patients, those symptoms were paroxysmal. Another prevalent ocular finding was pale retina (78%, 7/9), in four cases described even as "albinotic". There were also single cases of retinal pigment clumping around the optic nerve, hypoplastic macula, oval optic disc, and bilateral cataracts.

Signs of coagulopathy such as bruises, petechiae, bleeding from injection sites, or bleeding from the mucosas were found in 29% of patients (7/24).

Gastrointestinal disturbances were present in 37% of patients (9/24): regurgitations, vomiting, poor sucking, and lack of swallowing reflex. Six patients required feeding by the nasogastric tube and/or parenteral nutrition (4).

In cardiological evaluation, the most common symptom was mild pericardial effusion, found in nine patients, and patent foramen ovale, (PFO) in eight. Mild cardiomyopathy was found in five patients, and isolated thickening of the intraventricular septum (IVS), in another five. Two patients suffered from cardiac arrhythmias from the first days of life, and it was paroxysmal supraventricular tachycardia (PST) in one and significant sinus tachycardia in the other. None of the patients required pericardial drainage in the neonatal period.

Brain imaging revealed intraventricular hemorrhage (IVH) I° or II° in 72% (6/8) of patients and ventriculomegaly (2/8) in ultrasound, while MRI scan revealed cerebellar hypoplasia in 72% (6/8) of examined patients.

In laboratory tests, hematological disturbances were prevalent, which concerned 78% of patients (14/18). The most frequent were cytopenia, i.e., severe thrombocytopenia (7) (transient in one case), thrombocytosis (1) (and one in the fourth week of life), anemia (7), hyperleukocytosis (5) (and one in the fourth week of life), and leukopenia (1). Coagulation assessment revealed profound antithrombin III deficiency in 83% (5/6) of patients, protein C in 83% (5/6), and protein S in 100% (4/4) examined patients; partial antithrombin time was elongated in two of three cases, and the international normalized ratio was slightly elevated in three of four patients (range 1,1–1,78). Biochemical tests revealed normal transaminases in 67% (8/12), while in the other four patients they were only mildly elevated; hypoalbuminemia was present in 100% of diagnosed patients (10/10), proteinuria in 10, and erythrocyturia in 4 patients. Also, thyroid gland evaluation was normal in 72% (8/11) of patients, with hypothyroidism found in the remaining three.

The course of the disease in the perinatal period was mild in 11 patients; thus, they were discharged in the first week of life. Patients more severely ill (14) required hospitalization for multiple weeks. No patient demised in the neonatal period. In all patients with severe course, some distinctive symptoms were more frequent, like generalized edema, hematological disturbances (thrombocytopenia or thrombocytosis, anemia, and hyperleukocytosis), and signs of coagulopathy, respiratory failure, pericardial effusion, and intolerance of enteral feeding.

None of our patients received a proper diagnosis in their neonatal period, and the median time to recognize the disease by transferrin isofocusing was six months of age (range 1–108 months). The most frequently noted initial diagnoses were congenital CMV infection, sepsis, RDS, myocarditis, pericarditis, pylorostenosis, cerebral palsy, and Smith–Lemli–Opitz syndrome.

4 Discussion

The group of congenital disorders of N-glycosylation consists of at least 31 diseases, with different enzyme or transporter deficiencies, which lead to a similar pathophysiological effect: defect of synthesis and/or processing of glycoproteins and glycolipids (Abu Bakar et al., 2018). Some types of CDGs have their distinctive features, but there is still a pool of symptoms that are common for a majority of N-glycosylation CDGs and some of the mixed glycosylation disorders involving the N-glycosylation pathway, like psychomotor retardation, hypotonia, peripheral neuropathy, stroke-like episodes, nephrotic syndrome, failure to thrive, nystagmus, strabismus, retinitis pigmentosa, third space effusions, cardiomyopathy, liver disease, or microcystic kidneys presenting as hyperechogenic in ultrasonography (USG) (Hertz-Pannier et al., 2006; Goreta et al., 2012; Öncül et al., 2022). Dysmorphic features usually described in those patients are inverted, wide-set nipples, abnormal fat pads, orange peel skin, high forehead, large ears, or thin upper lip (Verheijen et al., 2020). CDG patients with defective N-glycosylation also share common laboratory deviations such as hypertransaminasemia (most prominent in MPI-CDG, but also in others), hypoalbuminemia, low plasma cholesterol, laboratory indices of hypothyroidism (the actual cause of which is often a deficiency of the thyroxin-binding globulin), cytopenias, proteinuria, and serum clotting factor deficiencies (such as protein S, protein C, AT III, and factors IX, XI, II, V, VII, VIII, and X) (Truin et al., 2008; Verheijen et al., 2020).

N-glycosylation deficiency symptoms, such as non-immune hydrops fetalis, polyhydramnios, cardiomyopathy, pericardial effusions, skeletal abnormalities, or mirror syndrome (Ballantyne syndrome), may also occur prenatally (van de Kamp et al., 2007; Malhotra et al., 2009; Lei et al., 2021).

The results of our study confirm that many of aforementioned symptoms are present also in the perinatal period. In the analyzed group, we found pre- and neonatal non-immune generalized edemas, cardiomyopathy, pericardial effusions, and dysmorphic features like inverted, wide-set nipples, cryptorchidism, and abnormal fat pads, although according to the

literature, the latter are rarely present in neonates (Goreta et al., 2012). In the first days of life, our patients also presented other typical symptoms, such as hypotonia, strabismus, failure to thrive, regurgitations, cerebellar hypoplasia, bleeding, coagulopathy, cytopenia (mainly thrombocytopenia or anemia), proteinuria, hypoalbuminemia, or serum clotting factor deficiencies.

Furthermore, our study also revealed some symptoms that are rarely described in the literature but were frequent in our study group and are discussed in the following paragraphs.

The interesting frequent finding (found in 45% of patients) is transient respiratory deterioration in the first minutes or hours of life, sometimes correlated with RDS features in RTG (mainly in prematurely born, but not only), requiring at least oxygen therapy or artificial ventilation for some time (range 1–43 days in the described group), and mostly not correlated with elevated inflammatory parameters. Such symptoms have been described in single cases previously, but its pathomechanism remains unknown (Schulte Althoff et al., 2016; van de Kamp et al., 2007). Hypothetically, pulmonary edema—as a part of generalized edema—might be the cause; another possibility is surfactant dysfunction due to hypoglycosylation of surfactant protein B and surfactant protein A (Taponen et al., 2013; Yang et al., 2014), but these considerations are beyond the subject of this paper.

Another finding rarely described previously is muscle hypertonia, which was present in seven patients, and a presence of tendon reflexes in all examined patients. According to the literature and personal experience, hyporeflexia is found in a majority of infants and older children with CDGs (Marklová and Albahri. 2007). Poor neonatal reflexes, including poor sucking and swallowing, were also frequent findings in the study group. This, together with enteral nutrition intolerance, manifested by typical regurgitations, vomiting, and undigested food retention, led to parenteral nutrition combined with nasogastric tube feeding in the neonatal period in a big fraction of our patients.

Not a common finding in the literature concerning CDGs, was also big joint contractures, found in 23% of patients in our study group.

An unusual type of nystagmus was prevalent in our cohort; it was described as roving eye movements or upward eye deviations and was often confused with epileptic seizures, particularly because it was paroxysmal in some patients. Another prevalent ocular finding was pale, albinotic retina, while in the literature, retinitis pigmentosa is described as the most frequent symptom (Lettice et al., 2010).

In addition to typical CDG hematological deviations, a part of our group presented transient significant hyperleukocytosis (30,144–80 × 10⁹/L) that started in the neonatal period and normalized during the next few weeks of life and was not correlated with other signs or indices of infection. In two cases, it was also accompanied by significant thrombocytosis. According to our knowledge, such a phenomenon has never been described previously.

Interestingly, some of the well-known CDG symptoms have not been noted in a majority of the study group in their perinatal age, which are hyporeflexia, hypertransaminasemia, and hypothyroidism. Abdominal ultrasound was also normal in the majority of patients in their first days of life, without typical hepatomegaly or renal ultrasound findings, such as kidney enlargement, hyperechogenicity, and altered corticomedullary differentiation (Tiwary et al., 2022). Renal ultrasound abnormalities appeared gradually in the first few weeks or months of life in the described group.

More than half of our patients presented with a severe phenotype, which was more specific and easier to recognize. Still, almost the same number of patients showed a mild neonatal phenotype, and they were discharged from the hospital in the first weeks of life, without even posing a suspicion of CDGs. One of those patients with a "mild" neonatal phenotype (No. 5) presented to our hospital at the age of three months, in order to perform diagnostics of poor body weight gain. His/her dysmorphic features were highly suggestive of CDG, so during examination, the echocardiogram was performed, revealing impending cardiac tamponade. Another patient (No. 3), presented as a neonate with intensive vomiting and food retention and was suspected of having pylorostenosis. He/she underwent pyloroplasty in the third week of life, which was complicated by dehiscence of the stomach wall and general deterioration, partially due to *Pseudomonas aeruginosa* and *Candida albicans* sepsis. In addition, this surgery did not fix the enteral feeding problem, the patient required parenteral nutrition, so venesection was performed, which was complicated by the upper limb vein thrombosis.

This paper presents and extends the perinatal phenotype of congenital N-glycosylation disorders. It is important to emphasize that although the individual CDG symptoms seem to be non-specific, the occurrence of a combination of several of them, with the involvement of different systems, should direct the differential diagnosis specifically toward congenital disorders of N-glycosylation. Despite the specific treatment being available only to a few of them, early diagnosis may influence patient's further medical care and genetic counseling for the family, concerning family planning. It may reduce a number of procedures, which are at higher risk in this group of patients, such as surgery, and monitor patients for the occurrence of potential life-threatening complications of the disease.

Data availability statement

The original contributions presented in the study are included in the article/Supplementary Materials, further inquiries can be directed to the corresponding author.

Author contributions

MG: conceptualization, methodology, investigation, resources, data curation, and writing—original draft. DR: resources and data curation. DW-K, MK, and AR: data curation. AJ-S: conceptualization. All authors agreed to be accountable for the content of the work.

Conflict of interest

The authors declare that the research was conducted in the absence of any commercial or financial relationships that could be construed as a potential conflict of interest.

Publisher's note

Supplementary material

The Supplementary Material for this article can be found online at: https://www.frontiersin.org/articles/10.3389/fgene.2022.1019283/full#supplementary-material

References

Abu Bakar, N., Lefeber, D. J., and van Scherpenzeel, M. (2018). Clinical glycomics for the diagnosis of congenital disorders of glycosylation. *J. Inherit. Metab. Dis.* 41 (3), 499–513. doi:10.1007/s10545-018-0144-9

Altassan, R., Péanne, R., Jaeken, J., Barone, R., Bidet, M., Borgel, D., et al. (2019). International clinical guidelines for the management of phosphomannomutase 2-congenital disorders of glycosylation: Diagnosis, treatment and follow upErratum in. *J. Inherit. Metab. DisJ Inherit. Metab. Dis.* 4242 (13), 5577–5628. PMID: 30740725. doi:10.1002/jimd.12024

Čechová, A., Altassan, R., Borgel, D., Bruneel, A., Correia, J., Girard, M., et al. (2020). Consensus guideline for the diagnosis and management of mannose phosphate isomerase-congenital disorder of glycosylation. *J. Inherit. Metab. Dis.* 43 (4), 671–693. doi:10.1002/jimd.12241

Chang, I. J., He, M., and Lam, C. T. (2018). Congenital disorders of glycosylation. *Ann. Transl. Med.* 6 (24), 477. PMID:30740408; PMCID: PMC6331365. doi:10.21037/atm.2018.10.45

Edwards, M., McKenzie, F., O'callaghan, S., Somerset, D., Woodford, P., Spilsbury, J., et al. (2006). Prenatal diagnosis of congenital disorder of glycosylation type Ia (CDG-Ia) by cordocentesis and transferrin isoelectric focussing of serum of a 27-week fetus with non-immune hydrops. *Prenat. Diagn.* 26, 985–988. doi:10.1002/pd.1543

Funke, S., Gardeitchik, T., Kouwenberg, D., Mohamed, M., Wortmann, S. B., Korsch, E., et al. (2013). Perinatal and early infantile symptoms in congenital disorders of glycosylation. *Am. J. Med. Genet. A* 3, 578–584. doi:10.1002/ajmg.a.35702

Goreta, S. S., Dabelic, S., and Dumic, J. (2012). Insights into complexity of congenital disorders of glycosylation. *Biochem. Med.* 22 (2), 156–170. doi:10.11613/bm.2012.019

Hertz-Pannier, L., Dechaux, M., Sinico, M., Emond, S., Cormier-Daire, V., Saudubray, J. M., et al. (2006). Congenital disorders of glycosylation type I: A rare but new cause of hyperechoic kidneys in infants and children due to early microcystic changes. *Pediatr. Radiol.* 36, 2108–2114. doi:10.1007/s00247-005-0001-5

Lei, Y-L., Zhen, L., Xu, L. L., Yang, Y. D., and Li, D. Z. (2021). Foetal phenotype of ALG1-CDG caused by paternal uniparental disomy 16. *J. Obstet. Gynaecol.* 41 (5), 828–830. doi:10.1080/01443615.2020.1786031

Léticée, N., Bessières-Grattagliano, B., Dupré, T., Vuillaumier-Barrot, S., de Lonlay, P., Razavi, F., et al. (2010). Should PMM2-deficiency (CDG Ia) be searched in every case of unexplained hydrops fetalis? *Mol. Genet. Metab.* 101 (2-3), 253–257. Epub 2010 Jun 22. PMID: 20638314. doi:10.1016/j.ymgme.2010.06.009

Malhotra, A., PatemAn, A., Coman, D., and Menahem, S. (2009). Prenatal cardiac ultrasound finding in congenital disorder of glycosylation type 1a. *Fetal diagn. Ther.* 251, 54–57. doi:10.1159/000196816

Marklová, E., and Albahri, Z. (2007). Screening and diagnosis of congenital disorders of glycosylation. *Clin. Chim. Acta.* 385 (1-2), 6–20. Epub 2007 Jul 13. PMID: 17716641. doi:10.1016/j.cca.2007.07.002

Morava, E., Vodopiutz, J., Lefeber, D. J., Janecke, A. R., Schmidt, W. M., Lechner, S., et al. (2012). Defining the phenotype in congenital disorder of glycosylation due to ALG1 mutations. *Pediatrics* 130, e1034–e1039. doi:10.1542/peds.2011-2711

Öncül, U., Kose, E., and Eminoğlu, F. T. (2022). ALG1-CDG: A patient with a mild phenotype and literature review. *Mol. Syndromol.* 13 (1), 69–74. Epub 2021 Sep 21. PMID: 35221878; PMCID: PMC8832214. doi:10.1159/000517797

Péanne, R., de Lonlay, P., Foulquier, F., Kornak, U., Lefeber, D. J., Morava, E., et al. (2018). Congenital disorders of glycosylation (CDG): Quo vadis? *Eur. J. Med. Genet.* 61, 11184–11663. doi:10.1016/j.ejmg.2017.10.012

Schulte Althoff, S., GrunebergM.Reunert, J., Park, J. H., RuSt, S., Muhlhausen, C., et al. (2016). TMEM165 deficiency: Postnatal changes in glycosylation. *JIMD Rep.* 26, 21–29. doi:10.1007/8904_2015_455

Taponen, S., Huusko, J. M., Petaja-Repo, U. E., Paananen, R., Guttentag, S. H., Hallman, M., et al. (2013). Allele-specific N-glycosylation delays human surfactant protein B secretion *in vitro* and associates with decreased protein levels *in vivo*. *Pediatr. Res.* 74 (6), 646–651. doi:10.1038/pr.2013.151

Thong, M. K., FietzM.NiCholls, C., Lee, M. H., and Asma, O. (2009). Congenital disorder of glycosylation type ia in a Malaysian family: Clinical outcome and description of a novel PMM2 mutation. *J. Inherit. Metab. Dis.* 32, S41–S44. doi:10.1007/s10545-009-1031-1

Tiwary, H., Hecht, L. E., Brucker, W. J., Berry, G. T., and Rodig, N. M. (2022). The development of end stage renal disease in two patients with PMM2-CDG. *JIMD Rep.* 63 (2), 131–136. PMCID: PMC8898725. PMID: 35281664. doi:10.1002/jmd2.12269

Truin, G., Guillard, M., Lefeber, D. J., Sykut-Cegielska, J., Adamowicz, M., Hoppenreijs, E., et al. (2008). Pericardial and abdominal fluid accumulation in congenital disorder of glycosylation type Ia. *Mol. Genet. Metab.* 94 (4), 481–484. doi:10.1016/j.ymgme.2008.05.005

van de Kamp, J. M., Ruijter, G. J. G., Steggerda, S. J., den Hollander, N. S., Willems, S. M., Matthijis, G., et al. (2007). Congenital disorder of glycosylation type Ia presenting with hydrops fetalis. *J. Med. Genet.* 44 (4), 277–280. doi:10.1136/jmg.2006.044735

Verheijen, J., Tahata, S., Kozicz, T., Witters, P., and Morava, E. (2020). Therapeutic approaches in congenital disorders of glycosylation (CDG) involving N-linked glycosylation: An update. *Genet. Med.* 22 (2), 268–279. doi:10.1038/s41436-019-0647-2

Yang, W., Shen, H., Fang, G., Li, H., Li, L., Deng, F., et al. (2014). Mutations of rat surfactant protein A have distinct effects on its glycosylation, secretion, aggregation and degradation. *Life Sci.* 117 (2), 47–55. doi:10.1016/j.lfs.2014.09.006

frontiers | Frontiers in Genetics

TYPE Original Research
PUBLISHED 13 January 2023
DOI 10.3389/fgene.2022.1020475

OPEN ACCESS

EDITED BY
Ting Hu,
Sichuan University, China

REVIEWED BY
Lila Allou,
Max Planck Institute for Molecular Genetics, Germany
Siddaramappa Patil,
Mazumdar Shaw Medical Centre, India

*CORRESPONDENCE
Lihong Fan,
fanlihong0411@163.com

†These authors have contributed equally to this work

SPECIALTY SECTION
This article was submitted to Genetics of Common and Rare Diseases, a section of the journal Frontiers in Genetics

RECEIVED 16 August 2022
ACCEPTED 28 November 2022
PUBLISHED 13 January 2023

CITATION
Shen X, Li Z, Pan X, Yao J, Shen G, Zhang S, Dong M and Fan L (2023), Prenatal diagnosis of recurrent moderate skeletal dysplasias in lamin B receptors.
Front. Genet. 13:1020475.
doi: 10.3389/fgene.2022.1020475

Prenatal diagnosis of recurrent moderate skeletal dysplasias in lamin B receptors

Xueping Shen[1†], Zhi Li[1†], Xuekui Pan[1], Juan Yao[1], Guosong Shen[1], Su Zhang[1], Minyue Dong[2,3] and Lihong Fan[1*]

[1]Center of Prenatal Diagnosis, Huzhou Maternity & Child Healthcare Hospital, Huzhou, China, [2]Women's Hospital, School of Medicine Zhejiang University, Hangzhou, China, [3]Key Laboratory of Reproductive Genetics (Zhejiang University), Ministry of Education, Hangzhou, China

The lamin B receptor (*LBR*) gene is located in chromosome 1q42.12 and encodes the lamin B receptor, an intracellular protein that binds to lamin B. *LBR* mutations are associated with a broad phenotypic spectrum ranging from non-lethal to lethal skeletal dysplasias. The typical phenotypes include the Pelger–Huet anomaly (PHA) and embryonic lethal Greenberg dysplasia (GRBGD). With the further study of this gene, other phenotypes have been found in different individuals. This retrospective study analyzed recurrent prenatal moderate skeletal dysplasias in Chinese fetuses. Nothing malformed was detected in the fetal karyotype and microarray, while the whole-exome sequencing identified a homozygous variant (NM_002296.4:c.1757G>A, NP_002287.2:p.Arg586His) in exon 14 of the *LBR* gene in both fetuses. Mutation analysis in the parents confirmed that the c.1757G>A variation is heterozygous by Sanger sequencing. Intensive analysis on bioinformatics and familial co-segregation suggest that the homozygous variation in the *LBR* gene is responsible for this recurrent prenatal moderate skeletal dysplasia. Moreover, moderate skeletal dysplasias differ from typical GRBGD phenotypes. Our findings are based on the DNA base test and the prenatal diagnosis of skeletal dysplasia, which can be helpful in proper phenotyping and contribute to a better understanding of the correlation between the phenotype and genotype.

KEYWORDS

prenatal moderate skeletal dysplasia, lamin B receptor, NM_002296.4:c.1757G>A, NP_002287.2:p.Arg586His, whole-exome sequencing, genetic counseling

Introduction

The *LBR* is a bifunctional protein encoded by the gene of the *LBR*. It has the dual function of affecting the nucleus division of neutrophils and sterol reductase activity. Mutations in this gene can affect a range of phenotypes. Variants may affect sterol reductase activity, resulting in the failure of cholesterol synthesis and elevated levels of the sterol metabolite cholesta-8, 14-dien-3-ol (accumulated in GRBGD fetuses), resulting in specific skeletal abnormalities in the developing fetus and fatal perinatal dysplasia. It can also cause defects in neutrophil differentiation characterized by a reduced number of

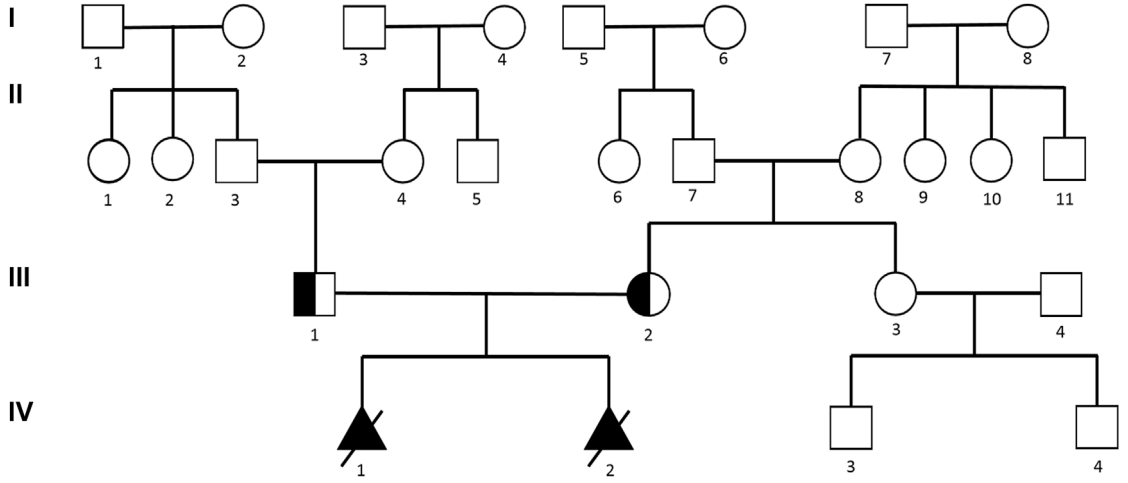

FIGURE 1
Pedigree of the fetuses.

nuclear fragments (dumbbell-shaped double-pore nuclei) and coarse aggregation of the nuclear chromatin, resulting in the Pelger–Huet anomaly (PHA) and Reynolds syndrome. There is also a mild skeletal dysplasia, the Pelger–Huet anomaly with a mild skeletal dysplasia (PHASK). The clinical features of 11 fetuses with the Greenberg dysplasia have been reported in the relevant studies, of which biallelic pathogenic variants have been identified in the *LBR* in seven cases (Greenberg et al., 1988; Chitayat et al., 1993; Horn et al., 2000; Waterham et al., 2003; Konstantinidou et al., 2008; Clayton et al., 2010; Giorgio et al., 2019). The clinical manifestations of the other four cases were similar to those of the Greenberg dysplasia, which were caused by the deficiency of the sterol metabolism (Gregersen et al., 2020). Dappled diaphyseal dysplasia in the two fetuses were described in Carty's report (Carty et al., 1989), Astley–Kendall dysplasia in another two fetuses were described in Astley and Kendall's report (Astley & Kendall, 1980), and three intermediate phenotype fetuses were described in Elçioglu's study (Elçioglu and Hall, 1998). Thus, the Greenberg dysplasia has multiple characteristics of a skeletal dysplasia, and its severity varies.

In this study, two fetuses with moderate skeletal dysplasia with homozygous variation c.1757G>A of the *LBR* gene were studied to expand the phenotypic spectrum and further guide the prenatal diagnosis of this disease.

Patients and methods

Case presentation

A 25-year-old primiparous woman (III2, Figure 1) was referred to the prenatal diagnosis center of our researching hospital due to an abnormal ultrasound at 25+1 weeks of gestation. Fetal system ultrasounds suggested that the limb long bones of the fetal are less than 2–4 standard deviations, while the thoracic cage is smaller than normal (IV1, Figure 2). After the termination of the first pregnancy, the woman had another pregnancy again after 1 year. The second fetus (IV2) was diagnosed as lethal skeletal dysplasia by prenatal ultrasound and only mild moth-eaten skeletal dysplasia by X-ray after induction at 17+3 weeks of gestation (Figure 3). Hydrops was not detected in both fetuses under ultrasound after labor induction. The patient did not have an MRI and refused to perform an autopsy on the fetus. There was no nuclear lobulation in the peripheral blood of the parents, only leaving the fetus unexamined. The woman denied any exposure to teratogenic chemicals, radiation, nicotine, or alcohol before or during the pregnancy. The relevance of the family congenital inheritance was also denied. The research was approved by the Ethics Committee of Huzhou Maternity & Child Health Care Hospital. Informed consent brief was signed by the parents for the examination of the fetus, as was done by all the other participants.

Acquisition of the amniotic fluid

Within the attendance, projected amniotic fluid was obtained through an ultrasound-guided puncture under sterile conditions at 25+1 and 17+3 weeks of gestation, respectively. A volume of 30 ml amniotic fluid was collected, of which 15 ml was used for cell culture chromosome karyotype preparation, and the other 15 ml was used for DNA extraction for subsequent experiments.

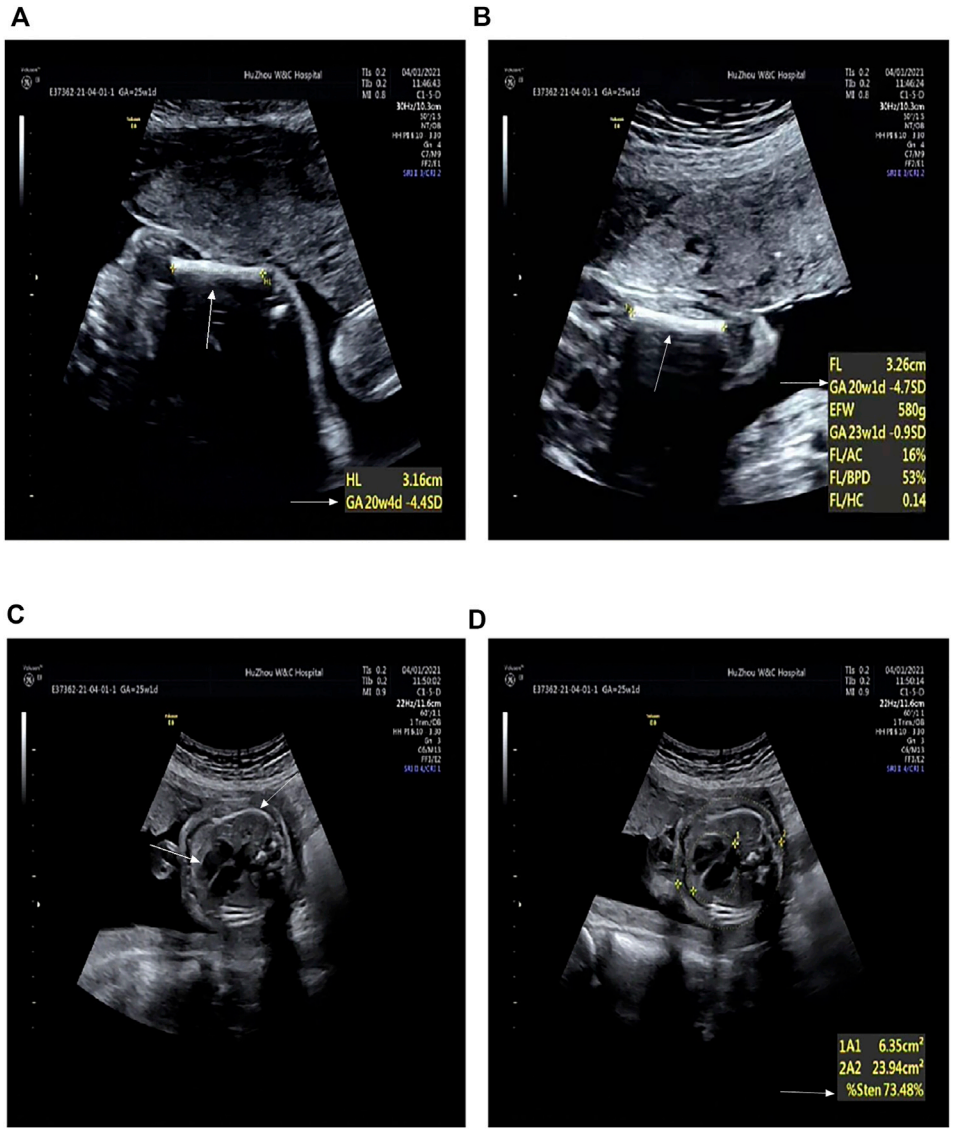

FIGURE 2
Radiographic features of the first fetus (at 25+1 weeks' gestation). **(A)** Humerus is smaller by 4.4 SD (arrows). **(B)** Femur is smaller by 4.7 SD (arrows). **(C)** Thoracic area is significantly reduced (arrows). **(D)** Enlarged cardiothoracic ratio (arrows).

Karyotype analysis

Fetal exfoliated epithelial cells in the amniotic fluid were prepared in an appropriate medium (BIO-AMF^{TM}-2) and afterward cultured at 37°C with the condition of 5% CO_2 for a week. Soon after subculturing, G-banding was performed at the 400-band level through treatment with 0.1 mg/ml colchicine and hypotonic (trisodium citrate 10%) fixation (glacial acetic acid: methanol = 1:3), with the analysis under the conditions of a microscope. On the basis of the International System for Human Cytogenomic Nomenclature (2016), 20 chromosomes were dated, meanwhile five karyotypes were analyzed as well.

Chromosomal microarray analysis

A total of 250 mg fetal DNA was extracted from the amniotic fluid, and analyzed by the CytoScan™ HD whole-genome SNP array (Affymetrix, United States), including 750,000 SNP probes and 1,950,000 CNV probes. The experiment contains quality control, enzyme digestion, PCR, purification, labeling,

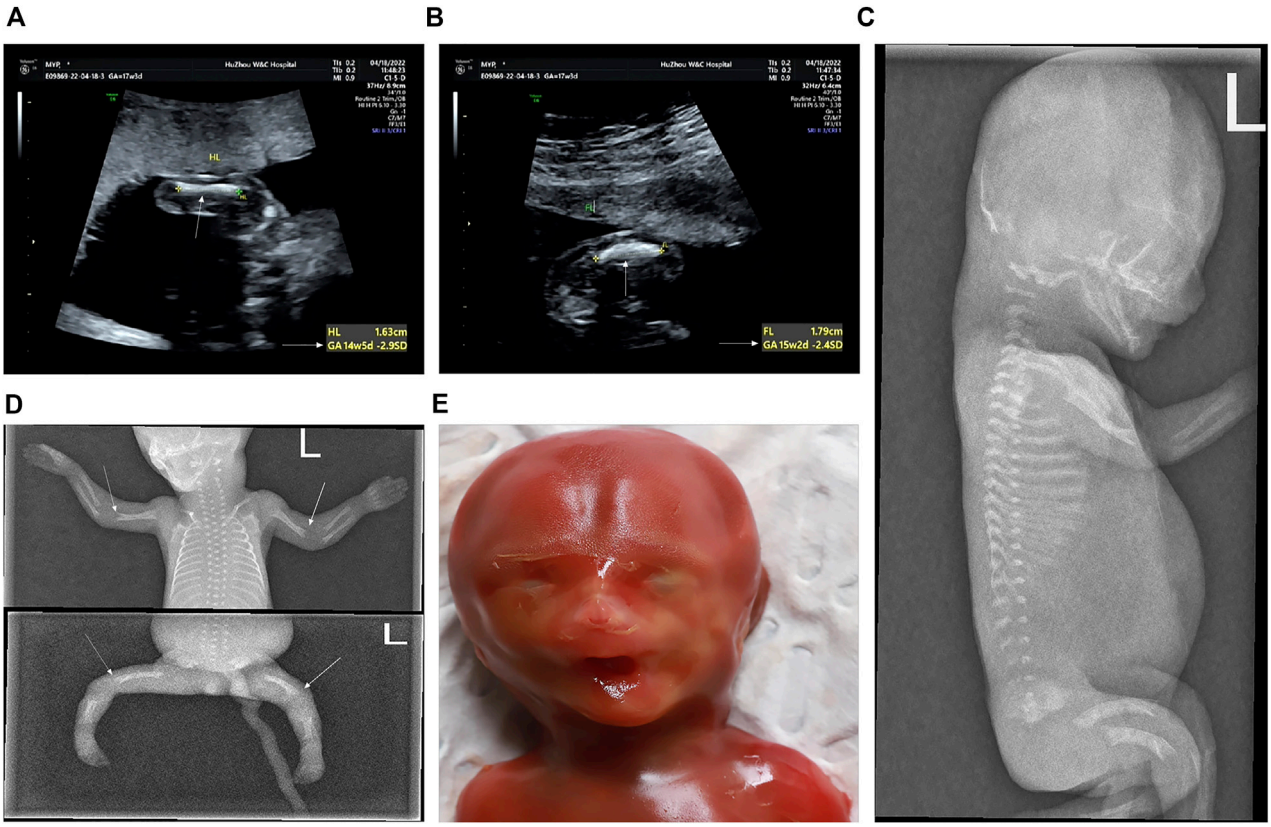

FIGURE 3
Prenatal and postnatal images of the second fetus (at 17+3 weeks' gestation). **(A)** Humerus is smaller by 2.9 SD (arrows). **(B)** Femur is smaller by 2.4 SD (arrows). **(C–E)** Features of the second fetus after induction. **(C)** Lateral view of the spine shows flattening of each vertebral body and dysplasia of the epiphysis. **(D)** Elbow joint of the long bone end was misaligned. The multiple densities at the end of the long bones of the extremities were not uniform, and the edge was irregular. Mild moth-eaten skeletal dysplasia is seen in the distal humerus and femur of both sides (arrows). **(E)** In the mugshot of the fetus after induced labor, there was no obvious special face.

hybridization, and scanning. All the data were analyzed by the Chromosome Analysis Suite 4.2 based on the conditions of the instructions of the manufacturers.

Whole-exome sequencing and Sanger sequencing

Genomic DNA was extracted from the amniotic fluid of the two fetuses and peripheral blood of the parents, which was used for the whole-exome sequencing. Exome capture was performed using the SureSelect Human All Exon V4 kit (Agilent Technologies, Santa Clara, CA, United States), followed by sequencing using the Illumina NovaSeq 6000 system (Illumina, San Diego, CA, United States). After sequencing and filtering out the low-quality reads, the high-quality reads were compared to the GRCh37/hg19 reference human genome using Sentieon BWA (Sentieon, United States) with the MEM align method, and the only variants located in the coding sequence as the only splice site regions were retained. Variant calling was performed using the Genome Analysis Tool Kit (GATK v4.0). Afterward, the candidate variants, including single-nucleotide variants (SNVs) and indels, were filtered by frequencies of specific databases, including the Human Gene Mutation Database (HGMD), ClinVar database, 1000 Genomes Project, Exome Aggregation Consortium (ExAC), Exome Sequencing Project 6500 (ESP6500), database of single-nucleotide polymorphisms (dbSNP), and Genome Aggregation Database (gnomAD). Mutation sites, known as polymorphic sites, were excluded, and the variants with allele frequency ≤1% were retained. Here, it can be predicted that the effect of variants is

TABLE 1 Primer sequences used to simplify *LBR* genomic fragments.

Name of the primer	Primer sequences (5′–3′)
Exon 14-*LBR*-F	ACCTTCTGCCACTTTCCAGT
Exon 14-*LBR*-R	CAGCTGGAATTGCAGGAGTA

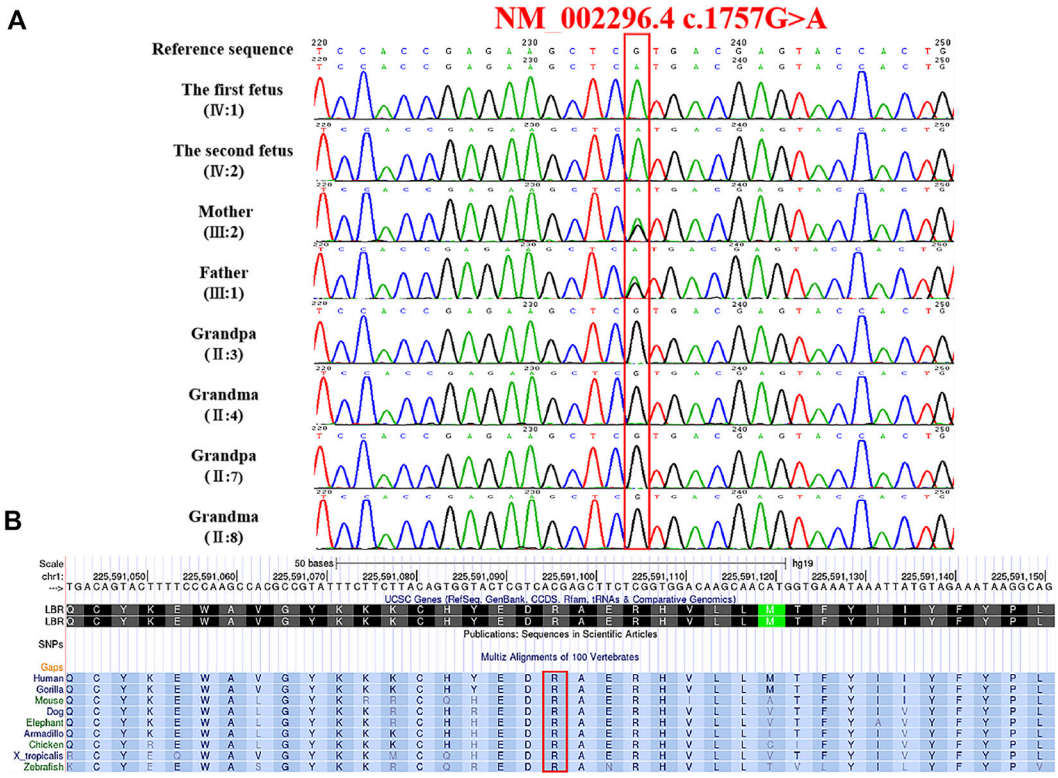

FIGURE 4
Genetic variation identified in these cases. **(A)** Variation detected in two fetuses and parents. **(B)** Conservation of the mutant amino acid (Pro586) in different species (human, gorilla, dog, mouse, elephant, armadillo, chicken, X-tropicalis, and zebrafish).

affected by SIFT, MutationTaster, and PROVEAN. The 3D-folded structure of the encoded protein was predicted, and the effects of mutations were predicted by AlphaFold (https://alphafold.ebi.ac.uk/). The interpretation of sequence variants was performed according to the American College of Medical Genetics and Genomics (ACMG). The online Clustal Omega (https://www.ebi.ac.uk/Tools/msa/clustalo/) was used to analyze the evolutionarily conserved sequences among species (human, gorilla, dog, mouse, elephant, armadillo, chicken, X-tropicalis and zebrafish). Ultimately, the variants were confirmed through Sanger sequencing and amplification of potentially mutated sequences. The primer sequences (Table 1) were designed by Primer3 (http://primer3.ut.ee/). PCR products were sequenced using the ABI 3500DX and further analyzed using DNASTAR 5.0 software (Fan et al., 2022).

Results

Identification and bioinformatics prediction of c.1757G>A in the *LBR*

Karyotype and CMA analysis showed no abnormalities. Subsequently, our group performed the whole-exome sequence to detect the presence of any mutations. Nearly 20,000 genes in the human genome were detected using the capture high-throughput chip technology for sequencing. The results showed that a homozygous mutant in the *LBR* (chr1: 225591096, NM_002296.4:c.1757G>A, NP_002287.2:p.Arg586His) in both fetuses, which were inherited from their parents; a missense mutation caused by the nucleotide G at position 1757 of the gene coding sequence was changed to A, which led to the arginine at position 586 to be changed to histidine. Sanger sequencing confirmed the variant and showed that the *LBR* variant in this family was consistent with the co-segregation of this disease (Figure 4A).

The frequency of the mutation in both the general population and the East Asian population is less than 1% in GnomAD and ExAC databases. The 1000 Genomes database showed that the frequency of the variation in the general population is < 1% and in the East Asian population is 1%. Both fetuses with a dysplasia of the bone carrying a heterozygous variant c. 1757G>A were reported in this study. This mutation is recorded in the HGMD database (CM136799). In the ClinVar database, only one record showed that the mutation is pathogenic, and the other one is of uncertain significance. It has been reported that one heterozygous variant c.1757G>A in the *LBR* gene was

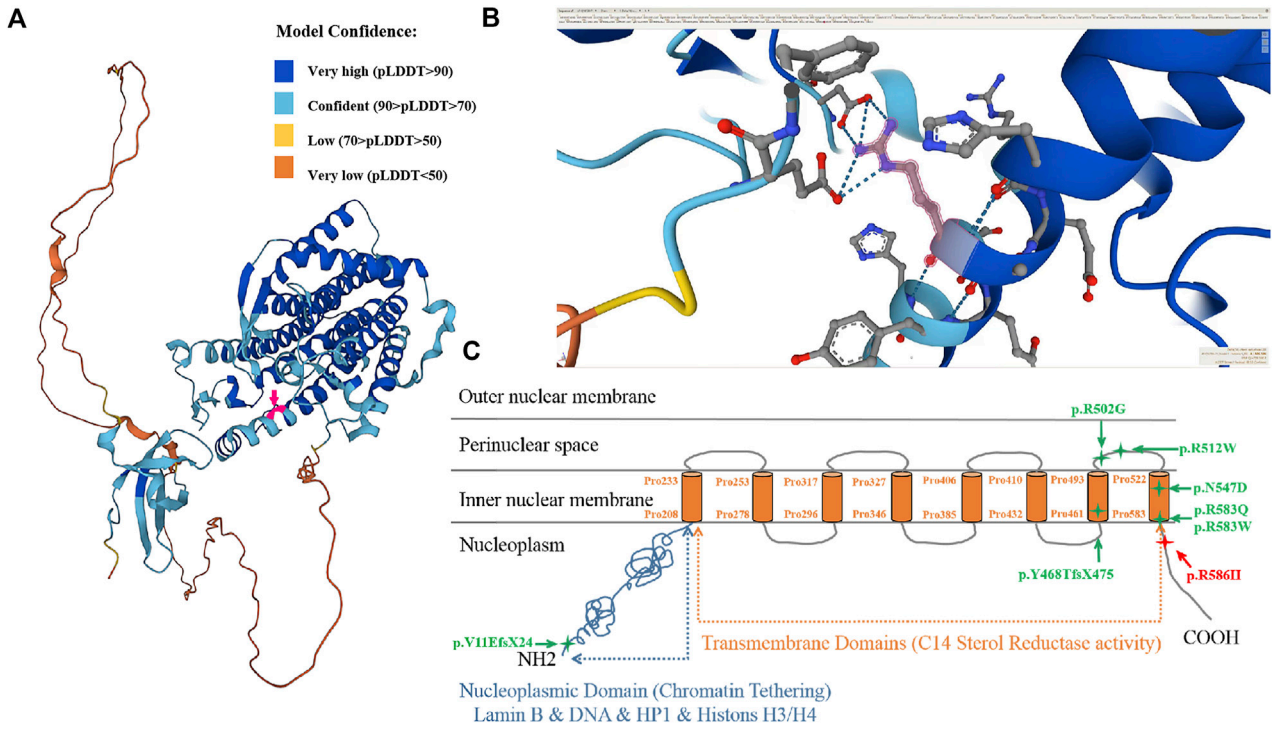

FIGURE 5
3D protein simulation of 3-beta-hydroxysterol delta 14-reductase encoded by the *LBR* in AlphaFold. **(A)** Overall structure of 3D protein simulation and the localization of the mutated amino acid (red arrow, Pro586 is confident) (model confidence: dark blue is very high, pLDDT>90; light blue is confident, 90 > pLDDT>70; yellow is low, 70 > pLDDT>50; orange is very low, pLDDT<50). **(B)** Enlarged view of the molecular structure of the mutant amino acid (Pro586, red arrow). **(C)** Schematic view of the lamin B receptor as a protein in the nuclear envelope and the location of identified mutations. The missense mutation p.R586H is located near the 8th transmembrane domain (sterol reductase domain).

TABLE 2 ***In silico*** **analysis of the** ***LBR*** **variant c.1757G>A.**

Variant	MutationTaster		PROVEAN		SIFT	
	Score	Prediction	Score	Prediction	Score	Prediction
c.1757G>A	1	Disease causing	−4.44	Damaging	0.001	Damaging

detected in a patient with bilobed neutrophil nuclei and a mild skeletal dysplasia phenotype; another heterozygous variation in the *LBR* gene was detected in the trans position (Borovik et al., 2013). The amino acid sequence alignment of multiple species confirmed that the mutation was 100% conserved (Figure 4B). According to AlphaFold, we confirmed that the Arg586 is located at a conserved site in the 3D folding of 3-β-hydroxysterol δ14-reductase and found that Arg586 is located at one of α-helix (Figure 5A). It also combines with ASP450 and GLU208 as a donor of hydrogen bonds (Figure 5B) (pLDDT score: 88.50). However, we have not scored this mutation through the DeepMind pipeline because there are several limitations in the current implementation of AlphScore. The functional prediction results of the variants by the SIFT, PROVEAN, and MutationTaster tools are shown in Table 2. According to the American College of Medical Genetics and Genomics (ACMG) guidelines for the interpretation of sequence variants, we considered this variant to be likely pathogenic (PM2_Supporting + PP3_Moderate + PM3_Strong + PP4).

Prenatal diagnosis and genetic counseling

Based on the effect of *LBR* mutations and co-segregation analysis of this disease, it was speculated that the homozygous mutation might be responsible for the cause of prenatal lethal

TABLE 3 Pathogenic variation of the *LBR* gene in the five reported cases of GRBGD.

Reports	Case	Variation information	Functional changes	Clinical features
			Zygote type	
Peter Clayton et al.	Fetus A	c.1402delT:p.Tyr468Thrfs*475	Nonsense mutation	1. Narrow thorax 2. Generalized hydrops fetalis 3. Ectopic calcification centers 4. Intrauterine growth retardation 4. Intrauterine growth retardation 5. Long bones were severely shortened and moth-eaten bones
			Homozygous	
	Fetus B	c.32_35delTGGT:p.Val11Glufs*24	Nonsense mutation	
			Heterozygous	
		c.1748G>A:p.Arg583Gln	Missense mutation	
			Heterozygous	
	Fetus C	c.1639A>G:p.Asn547Asp	Missense mutation	
			Homozygous	
Eliza Thompson et al.	Patient 1	c.1504C>G:p.Arg502Gly	Missense mutation	1. Short stature 2. Dysplasia of the metaphysis of the spine
			Heterozygous	
		c.1748G>T:p.Arg583Leu	Missense mutation	
			Heterozygous	
	Patient 2	c.1534C>T:p.Arg512Trp	Missense mutation	
			Homozygous	

bone dysplasia in this Chinese family. Eventually, the couple made the decision to terminate the pregnancy after deep consideration and planned to use pre-implantation prenatal diagnosis to have a healthy baby.

Discussion

The *LBR* gene was first reported by Schulerin in 1994. It is 35 kb in size and encodes a lamin B receptor with 615 amino acid residues. The *LBR* is a nuclear membrane protein that functions as a 3-beta-hydroxysterol delta 14-reductase and belongs to the ERG4/ERG24 family.

Exons 2–5 encode N-terminal nucleoplasmic domains that interact directly or indirectly with the chromatin, lamina, heterochromatin proteins, histones, and other nuclear components to maintain the structural integrity of lamina networks and immobilize the heterochromatin within the nuclear membrane. Pathogenic aberrance with PHA is located in nucleoplasmic domains or whole genes. Exons 6–14 encode eight C-terminal hydrophobic transmembrane domains, belonging to the sterol reductase family, which participates in cholesterol synthesis through sterol C14-reductase activity and realizes the metabolic function of the *LBR*. Pathogenic variants in the transmembrane domain of the *LBR* may affect sterol reductase activity, leading to a failure of cholesterol synthesis that increase and accumulate the sterol metabolite cholesta-8, 14-dien-3-ol *in vivo*, leading to specific skeletal abnormalities in the developing fetus and a perinatal lethal skeletal dysplasia (Borovik et al., 2013). It has been reported that the aberrance of the pathogen in some cases of skeletal dysplasia are located in hydrophobic transmembrane regions (Nikolakaki et al., 2017). Up to now, there are 38 disease-associated *LBR* gene variants in the database, but only five cases of GRBGD have been reported (Table 3; Figure 5C).

Clayton et al., 2010 collected three GRBGD fetuses with the identical clinical characteristics, all of which presented with thoracic spinal stenosis, generalized hydrops fetalis, ectopic calcification center, intrauterine growth retardation, severely shortened long bones and moth-eaten bones, and carrying nonsense or missense variants in the *LBR* gene (Clayton et al., 2010). Eliza Thompson *et al.* reported that two patients with a moderate severity of skeletal dysplasia and spontaneous continuous improvement for the first time, with clinical phenotypes of short stature and spinal metaphyseal dysplasia (Thompson et al., 2019). It can be concluded that GRBGD caused by *LBR* gene variants has a wide range of phenotypic heterogeneity, especially skeletal abnormalities. The reports about exon 14 of the *LBR* gene in the literature are very rare, including only five cases of defects (Best et al., 2003; Mchugh et al., 2011; Clayton et al., 2010; Borovik et al., 2013; Thompson et al., 2019) (Table 4). The clinical manifestations range from isolated PHA to mild skeletal dysplasia PHA and then to the Greenberg skeletal dysplasia.

In reference to multiple studies (Sobreira Net al., 2015; M.D.F. Carvalhoet al., 2017; Waterham et al., 2003), the

TABLE 4 Reported cases of the *LBR* gene exon 14 mutation.

Case	Reports	Variation information	Functional changes Zygote type	Disease	Clinical features
#1	Best et al.	**c.1706C>G:p.Pro569Arg**	Missense mutation Heterozygous	PHA	Neutrophil Pelger–Huet phenomenon
#2	Peter Clayton et al. (Fetus B)	**c.1706C>G:p.Pro569Arg**	Nonsense mutation Heterozygous	GRBGD	1. Narrow thorax 2. Generalized hydrops fetalis
		c.1748G>A:p.Arg583Gln	Missense mutation Heterozygous		3. Ectopic calcification centers 4. Intrauterine growth retardation 5. Long bones were severely shortened and moth-eaten bones
#3	Borovik L et al.	**c.1757G>A:p.Arg586His**	Missense mutation Heterozygous	PHASK	1. Short stature 2. Hyperlordosis
		c.651-653delCATins TGATGAGAAA: p.Ile218Aspfs*19	Nonsense mutation Heterozygous		3. Mild kyphosis 4. Short finger-shaped and dumbbell-shaped Pelger–Huet cells
#4	Mchugh D et al.	**c.1747C>T:p.Arg583Term**	Nonsense mutation Heterozygous	PHA	1. Neutrophil nuclei are lobed (bilobed or rod-shaped) 2. Rough chromatin
#5	Eliza Thompson et al. (patient 1)	c.1504C>G:p.Arg502Gly	Missense mutation Heterozygous	GRBGD	1. Short stature 2. Dysplasia of the metaphysis of the spine
		c.1748G>T:p.Arg583Leu	Missense mutation Heterozygous		

Bold values is exon 14 mutation.

defects in the *LBR* gene were found to be associated with mild skeletal phenotypes, including missense, nonsense, or frameshift variants, and these defects were distributed throughout the nucleoplasmic and transmembrane regions of proteins. In addition, one of the two pathogenic variants involves exons 12, 13, and 14.

A homozygous variant (c.1757G>A(p.Arg586His)) was reported in both fetuses for the first time in our study. Homozygous pathogenic variants were more common in probands born to consanguineous parents due to common ancestors. In the family, we report that the homozygous pathogenic variants came from unrelated parents, which can be explained by recessive consanguinity. In future studies, we can try to explore this mystery. Although, prenatal long bone measurements belong to the fatal skeletal dysplasia in the two fetuses. Based on prenatal USG and X-rays findings, both fetuses appeared to have a moderate skeletal dysplasia, similar to that reported by Thompson *et al*.

Although prenatal measurements of long bones are fatal for fetal skeletal dysplasias, according to the results of prenatal USG and X-ray examination, both fetuses appeared to have moderate skeletal dysplasia, which was similar to that reported by Thompson et al.

Standardized and systematic ultrasound examination is the basis for the prenatal detection of skeletal dysplasias. Although prenatal ultrasound examination of a lethal skeletal dysplasia is not a difficult task, there is an overlap in ultrasound imaging findings between different types of lethal and non-lethal skeletal dysplasias. Therefore, on the basis of strict use of standard measurement methods, the use of USG for the prediction and diagnoses of prenatal fatal and non-fatal skeletal dysplasias still have some limitations. According to AlphaFold, we can confirm that Arg586 is at a conserved residue in the 3D folding of 3-β-hydroxysterol δ14-reductase. We can not only find that Arg586 is in the α-helix, it is also found to be linked to ASP450 and GLU208 as a donor of hydrogen bonds (pLDDT score: 88.50).

Nevertheless, we have not scored this mutation through the DeepMind pipeline because there are still several limitations to the current implementation of AlphScore. Indeed, we do align the structure between the mutation and reference. Although there is no significance in the α-helix in Arg586 residues, it has an effect on the next α-helix.

The predicted mutation protein structure was constructed using AlphaFold and compared using PyMOL (https://colab.research.google.com/github/sokrypton/ColabFold/blob/main/AlphaFold2.ipynb#scrollTo=UGUBLzB3C6WN). According to the aforementioned analysis, the effect of Arg586 on the next α-helix may be related to the moderate skeletal dysplasia of both fetuses in this Chinese family.

In conclusion, the c.1757G>A(p.Arg586His) variant located at the end of the transmembrane domain 8 results in a moderate skeletal dysplasia phenotype. With the limitations of ultrasound diagnosis, whole-exome sequencing can help clinically, especially, in genetic counseling to carry out more scientific phenotyping and expanding the phenotypic spectrum of the disease.

Data availability statement

The data presented in the study are deposited in the repository of Sequence Read Archive (SRA), accession number is SUB12035353, https://submit.ncbi.nlm.nih.gov/subs/sra/SUB12035353.

Author contributions

LF designed the study and reviewed the manuscript. XS was in charge of the analysis of the data. Afterward, LF wrote the manuscript. SZ and MD participated in clinical analysis and genetic counseling. JY and GS performed the experiments and collected the data. ZL and XP analyzed the radiological results. All authors have read and confirmed the manuscript.

Funding

The work was supported by the Zhejiang Medical and Health Technology program (2023KY323).

Conflict of interest

The authors declare that the research was conducted in the absence of any commercial or financial relationships that could be construed as a potential conflict of interest.

Publisher's note

All claims expressed in this article are solely those of the authors and do not necessarily represent those of their affiliated organizations, or those of the publisher, the editors, and the reviewers. Any product that may be evaluated in this article, or claim that may be made by its manufacturer, is not guaranteed or endorsed by the publisher.

References

Astley, R., and Kendall, A. C. (1980). A bone dysplasia for diagnosis. *Ann. Radiol.* 23 (2), 121–123.

Best, S., Salvati, F., Kallo, J., Garner, C., Height, S., Thein, S. L., et al. (2003). Lamin B-receptor mutations in Pelger-Huët anomaly. *Br. J. Haematol.* 123 (3), 542–544. doi:10.1046/j.1365-2141.2003.04621.x

Borovik, L., Modaff, P., Waterham, H. R., Krentz, A. D., and Pauli, R. M. (2013). Pelger-huet anomaly and a mild skeletal phenotype secondary to mutations in *LBR*. *Am. J. Med. Genet. A* 161a (8), 2066–2073. doi:10.1002/ajmg.a.36019

Carty, H., Kozlowski, K., and Sillence, D. (1989). Dappled diaphyseal dysplasias. *Rofo* 150 (2), 228–229. doi:10.1055/s-2008-1047014

Chitayat, D., Gruber, H., Mullen, B. J., Pauzner, D., Costa, T., Lachman, R., et al. (1993). Hydrops-ectopic calcification-moth-eaten skeletal dysplasia (Greenberg dysplasia): Prenatal diagnosis and further delineation of a rare genetic disorder. *Am. J. Med. Genet.* 47 (2), 272–277. doi:10.1002/ajmg.1320470226

Clayton, P., Fischer, B., Mann, A., Mansour, S., Rossier, E., Veen, M., et al. (2010). Mutations causing Greenberg dysplasia but not Pelger anomaly uncouple enzymatic from structural functions of a nuclear membrane protein. *Nucleus* 1 (4), 354–366. doi:10.4161/nucl.1.4.12435

Elçioglu, N., and Hall, C. M. (1998). A lethal skeletal dysplasia with features of chondrodysplasia punctata and osteogenesis imperfecta: An example of astley-kendall dysplasia. Further delineation of a rare genetic disorder. *J. Med. Genet.* 35 (6), 505–507. doi:10.1136/jmg.35.6.505

Fan, L., Jin, P., Qian, Y., Shen, G., Shen, X., and Dong, M. (2022). Case report: Prenatal diagnosis of postaxial polydactyly with Bi-allelic variants in smoothened (SMO). *Front. Genet.* 13, 887082. doi:10.3389/fgene.2022.887082

Giorgio, E., Sirchia, F., Bosco, M., Sobreira, N. L. M., Grosso, E., Brussino, A., et al. (2019). A novel case of Greenberg dysplasia and genotype-phenotype correlation analysis for *LBR* pathogenic variants: An instructive example of one gene-multiple phenotypes. *Am. J. Med. Genet. A* 179 (2), 306–311. doi:10.1002/ajmg.a.61000

Greenberg, C. R., Rimoin, D. L., Gruber, H. E., DeSa, D. J., Reed, M., and Lachman, R. S. (1988). A new autosomal recessive lethal chondrodystrophy with congenital hydrops. *Am. J. Med. Genet.* 29 (3), 623–632. doi:10.1002/ajmg.1320290321

Gregersen, P. A., McKay, V., Walsh, M., Brown, E., McGillivray, G., and Savarirayan, R. (2020). A new case of Greenberg dysplasia and literature review suggest that Greenberg dysplasia, dappled diaphyseal dysplasia, and Astley-Kendall dysplasia are allelic disorders. *Mol. Genet. Genomic Med.* 8 (6), e1173. doi:10.1002/mgg3.1173

Horn, L. C., Faber, R., Meiner, A., Piskazeck, U., Spranger, J., and Piskazeck, U. (2000). Greenberg dysplasia: First reported case with additional non-skeletal malformations and without consanguinity. *Prenat. Diagn.* 20 (12), 1008–1011. doi:10.1002/1097-0223(200012)20:12<1008:aid-pd954>3.0.co;2-s

Konstantinidou, A., Karadimas, C., Waterham, H. R., Superti-Furga, A., Kaminopetros, P., Grigoriadou, M., et al. (2008). Pathologic, radiographic and molecular findings in three fetuses diagnosed with HEM/Greenberg skeletal dysplasia. *Prenat. Diagn.* 28 (4), 309–312. doi:10.1002/pd.1976

Mchugh, D., Cameron, C. A., Abdenur, J. E., Abdulrahman, M., Adair, O., and Al Nuaimi, S. A. (2011). *Genetics in medicine : Official journal of the american college of medical genetics*. Berlin, Germany: Nature Publishing Group.

Nikolakaki, E., Mylonis, I., and Giannakouros, T. (2017). Lamin B receptor: Interplay between structure, function and localization. *Cells* 6 (3), 28. doi:10.3390/cells6030028

Thompson, E., Abdalla, E., Superti-Furga, A., McAlister, W., Kratz, L., Unger, S., et al. (2019). Lamin B receptor-related disorder is associated with a spectrum of skeletal dysplasia phenotypes. *Bone* 120, 354–363. doi:10.1016/j.bone.2018.11.006

Waterham, H. R., Koster, J., Mooyer, P., Noort Gv, G., Kelley, R. I., Wilcox, W. R., et al. (2003). Autosomal recessive HEM/Greenberg skeletal dysplasia is caused by 3 beta-hydroxysterol delta 14-reductase deficiency due to mutations in the lamin B receptor gene. *Am. J. Hum. Genet.* 72 (4), 1013–1017. doi:10.1086/373938

Frontiers in Genetics

Highlights genetic and genomic inquiry relating to all domains of life

The most cited genetics and heredity journal, which advances our understanding of genes from humans to plants and other model organisms. It highlights developments in the function and variability of the genome, and the use of genomic tools.

Discover the latest Research Topics

See more →

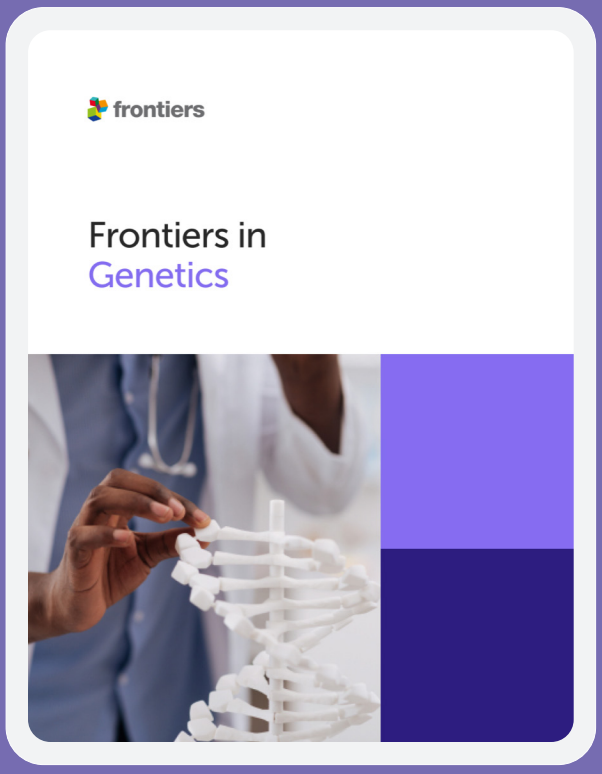

Frontiers

Avenue du Tribunal-Fédéral 34
1005 Lausanne, Switzerland
frontiersin.org

Contact us

+41 (0)21 510 17 00
frontiersin.org/about/contact